FEMS Microbiology Reviews, fuab051, 46, 2022, 1–35

https://doi.org/10.1093/femsre/fuab051
Advance Access Publication Date: 11 October 2021
Review Article

REVIEW ARTICLE

Weaving of bacterial cellulose by the Bcs secretion systems

Wiem Abidi[1,2,3,†,#], Lucía Torres-Sánchez[1,2,3,†,‡], Axel Siroy[1,2,†,$] and Petya Violinova Krasteva[1,2,*,§]

[1]Structural Biology of Biofilms group, European Institute of Chemistry and Biology (IECB), F-33600 Pessac, France, [2]Université de Bordeaux, CNRS, Bordeaux INP, CBMN, UMR 5248, F-33600 Pessac, France and [3]École doctorale 'Innovation thérapeutique: du fundamental à l'appliqué' (ITFA), Université Paris-Saclay, F-92296 Chatenay-Malabry, France

*Corresponding author: Structural Biology of Biofilms group, IECB, 2 Rue Robert Escarpit, F-33600 Pessac, France. Tel: +33 5 40 00 31 01; E-mail: pv.krasteva@iecb.u-bordeaux.fr

One sentence summary: This review describes the current mechanistic knowledge on bacterial cellulose secretion with focus on the structure, assembly and cooperativity of Bcs secretion system components.

†These authors contributed equally. Author order was determined based on seniority within the SBB group.

Editor: Jan Roelof van der Meer

#Wiem Abidi, https://orcid.org/0000-0001-7378-9653
‡Lucía Torres-Sánchez, https://orcid.org/0000-0001-8486-0005
$Axel Siroy, https://orcid.org/0000-0002-8013-3596
§Petya Violinova Krasteva, https://orcid.org/0000-0002-1858-8127

ABSTRACT

Cellulose is the most abundant biological compound on Earth and while it is the predominant building constituent of plants, it is also a key extracellular matrix component in many diverse bacterial species. While bacterial cellulose was first described in the 19th century, it was not until this last decade that a string of structural works provided insights into how the cellulose synthase BcsA, assisted by its inner-membrane partner BcsB, senses c-di-GMP to simultaneously polymerize its substrate and extrude the nascent polysaccharide across the inner bacterial membrane. It is now established that bacterial cellulose can be produced by several distinct types of cellulose secretion systems and that in addition to BcsAB, they can feature multiple accessory subunits, often indispensable for polysaccharide production. Importantly, the last years mark significant progress in our understanding not only of cellulose polymerization *per se* but also of the bigger picture of bacterial signaling, secretion system assembly, biofilm formation and host tissue colonization, as well as of structural and functional parallels of this dominant biosynthetic process between the bacterial and eukaryotic domains of life. Here, we review current mechanistic knowledge on bacterial cellulose secretion with focus on the structure, assembly and cooperativity of Bcs secretion system components.

Keywords: biofilm formation; matrix exopolysaccharides; bacterial cellulose secretion (Bcs); c-di-GMP signaling; synthase-dependent systems

Received: 2 June 2021; **Accepted:** 8 October 2021

INTRODUCTION

Cellulose, an unbranched homopolysaccharide of β-1,4-linked D-glucose molecules, is the most abundant biopolymer on Earth. It is the main constituent of the plant cell wall and as such represents a crucial sink for Earth's atmospheric carbon. For millennia, humanity has used the polymer with its exceptional tensile strength; resistance to chemical, thermal or mechanical challenges; and excellent calorific value as a material for building, clothing or energy provision. Despite its ubiquitous spread in the plant kingdom, cellulose biosynthesis is not at all limited to plants and has been reported in a vast range of bacteria (Canale-Parola, Borasky and Wolfe 1961; Nobles, Romanovicz and Brown 2001; Römling and Galperin 2015; Trivedi *et al.* 2016), protists (Grimson, Haigler and Blanton 1996; Blanton *et al.* 2000), fungi (Grenville-Briggs *et al.* 2008), algae (Domozych *et al.* 2012) and animals (Kimura *et al.* 2001; Matthysse *et al.* 2004). Even some giant viruses, such as members of the *Pandoravirus* genus, incorporate cellulose in their tegument, likely through hijacking their host's biosynthetic machinery during the viral replication cycle (Brahim Belhaouari *et al.* 2019). The membrane-embedded cellulose synthases responsible for glucose polymerization share remarkably conserved features among studied pro- and eukaryotes—from protein sequence, through tertiary fold to likely enzymatic mechanism (McNamara, Morgan and Zimmer 2015; Little *et al.* 2018; Purushotham, Ho and Zimmer 2020). It is therefore commonly held that the widespread counterparts in present-day vascular plants have evolved from cyanobacterial genes via multiple lateral gene transfers during ancient endosymbiotic events (Nobles, Romanovicz and Brown 2001; Little *et al.* 2018). Being among the oldest organisms on Earth, cyanobacteria could thus be both the first cellulose producers to emerge, and the last common ancestors between plants and prokaryotes (Nobles, Romanovicz and Brown 2001; Nobles and Brown 2004).

A common feature among cellulose biosynthetic machineries is the coupling of the glucose polymerization reaction with secretion of the polymer either to the cell's envelope or the extracellular matrix (Fig. 1A). The synthase activity is processive and the resultant polymers can be thousands of glucose units long (Brown 2004). Within the linear polysaccharide, each glucose moiety is flipped by 180° relative to its neighbors due to the β-configuration of the C1 carbon. Overall, the polymer adopts a hydrogen bond-stabilized extended conformation with a reducing end that would exit the synthase and, by extension, the cell surface first, and a non-reducing end, at which polymerization occurs in the nascent polysaccharide (McNamara, Morgan and Zimmer 2015). The secreted polymer is intrinsically amphipathic and cellulose strands can associate with each other through a combination of hydrogen bonding involving the lateral hydroxyl groups and hydrophobic van der Waals forces between the glucopyranose rings (Blackwell 1982; Notley, Pettersson and Wågberg 2004) (Fig. 1B). Although such aggregation could be random and lead to an amorphous extracellular matrix, some bacterial species (e.g. *Gluconacetobacter xylinus*) and most plants are able to secrete cellulose with high degree of crystallinity (Fig. 1C). In it, individual cellulose strands pack into ordered fibrils, sheets or ribbons, which can interact with additional extracellular polysaccharides or even glycoproteins (Brown 2004; Keegstra 2010). Most commonly, natural crystalline cellulose exists as the cellulose I allomorph, in which the individual strands pack parallel to each other in the higher-order crystalline lattice, but antiparallel cellulose II structures have also been observed in some algae, as well as bacteria (Brown 2004).

In the bacterial world, cellulose secretion often goes hand in hand with biofilm formation or the growth of extracellular matrix-embedded, collaborative, multicellular communities. Within the biofilm, cells are protected from noxious stimuli or host immune responses, exchange substances and genetic information, and cooperate in surface colonization and resource capture (O'Toole, Kaplan and Kolter 2000; Hall-Stoodley, Costerton and Stoodley 2004; Serra, Richter and Hengge 2013; Flemming *et al.* 2016). Cellulose's exceptional water retention capacity, porosity, mechanical resistance and chemical simplicity, combined with its low antigenicity and ability to interact with additional saccharidic or proteinaceous components from the bacteria or their hosts, makes the polymer a preferred architectural element for the biofilms of many and highly diverse prokaryotic species (Römling and Galperin 2015).

Here, we provide a detailed overview of the bacterial biosynthetic pathways leading to the secretion of nanocellulose as a widespread biofilm matrix component. In the following pages, we discuss the current knowledge of the structure, function, assembly and interactions of the different Bcs subunits that act in a concerted fashion to secure the initiation, polymerization, extrusion, crystallinity and/or chemical modifications of the exopolysaccharide. We summarize proposed molecular mechanisms concerning the separate roles of prevalent Bcs proteins; however, we underscore that the ensemble of Bcs subunits in any cellulose-reliant bacterial species should be viewed as a highly cooperative, envelope-spanning secretion system. We further present this information in relation to other bacterial exopolysaccharide-producing systems, as well as recent advances in our understanding of plant cellulose biogenesis. To conclude, we briefly review the role of bacterial cellulose not only in its physiological context but also in a number of biotechnological applications and underscore the importance of ongoing and future mechanistic studies for fundamental research, human health and biotechnology.

METABOLIC REQUIREMENTS FOR CELLULOSE BIOSYNTHESIS

Cellulose synthases use a single type of preactivated substrate, UDP-glucose, to incorporate the sugar moiety into the nascent polysaccharide and release UDP back in the cytosol (Fig. 1A). The substrate is made available by a dedicated enzyme—UDP-glucose pyrophosphorylase, UDPGP or GalU—which is essential for cellulose secretion *in vivo* but is otherwise dispensable in bacterial physiology (Valla *et al.* 1989). Substrates for UDPGP are UTP and glucose-1-phosphate, respectively. UTP is energetically equivalent to ATP and can be synthesized from recycled UDP by the enzyme nucleoside diphosphate kinase (Ndk), a housekeeping enzyme that balances cellular NTP levels and is involved in multiple physiological and virulence pathways (Yu, Rao and Zhang 2017). Glucose-1-phosphate, on the other hand, is converted from glucose-6-phosphate by a second dedicated enzyme, phosphoglucomutase or Pgm (Krystynowicz *et al.* 2005) (Fig. 1A). Given the central role of the UDPGP, Ndk and Pgm enzymes in synthase substrate generation, fine-tuning their expression levels and activities has been a key strategy in the quest of engineered cellulose superproducers (Huang *et al.* 2020; Hur *et al.* 2020).

Glucose-6-phosphate is a key metabolic product that can be synthesized through various pathways and from a variety of carbon sources such as glucose and fructose, as well as intermediates of the pentose-phosphate (PP) pathway, Krebs cycle, glycolysis, gluconeogenesis and alcohol dissimilation reactions.

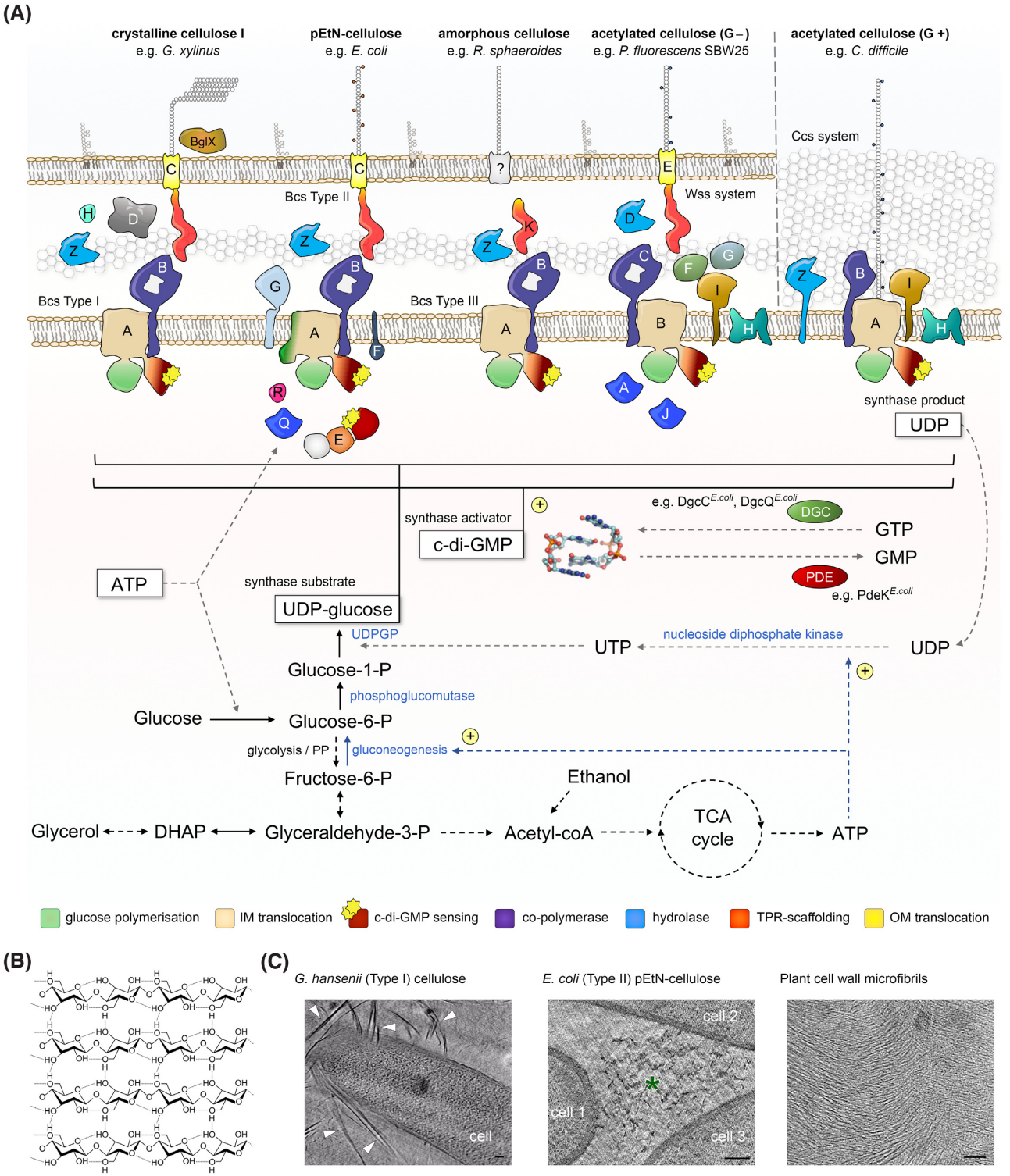

Figure 1. Bacterial cellulose secretion. **(A)** Prevalent types of bacterial cellulose secretion systems and associated metabolic processes. UDPGP: UDP-glucose pyrophosphorylase, also called UTP–glucose-1-phosphate uridylyl transferase or GalU; UDP: uridine diphosphate; ATP: adenosine triphosphate; PP: pentose-phosphate pathway; DHAP: dihydroxyacetone phosphate; TCA cycle: tricarboxylic acid cycle; c-di-GMP: cyclic diguanosine monophosphate; PDE: phosphodiesterase; DGC: diguanylate cyclase. **(B)** Inter- and intrastrand hydrogen bonding in crystalline cellulose I. Image by Luca Laghi, reproduced under license CC BY-SA 3.0 (https://creativecommons.org/licenses/by-sa/3.0/legalcode). **(C)** Cryo-electron micrographs of secreted bacterial and plant cellulose. Data: courtesy of William J. Nicolas, partially reported in (Nicolas *et al.* 2021) and reproduced under the CC BY 4.0 license (https://creativecommons.org/licenses/by/4.0/legalcode). Left: a biofilm-embedded *Gluconacetobacter hansenii* cell surrounded by crystalline cellulose ribbons (marked by white arrowheads); middle: amorphous phosphoethanolamine (pEtN)-cellulose (marked by an asterisk), secreted by the commensal *Escherichia coli* 1094 strain; right: plant cellulose microfibrils observed as electron-dense filaments in onion cell wall *in situ*. Scale bars: 100 nm.

Given that cellulose secretion is an energetically and metabolically costly process, it is more typically associated with prevalent anabolic processes such as gluconeogenesis (Ross, Mayer and Benziman 1991; White *et al.* 2010) (Fig. 1A). In *G. xylinus*, which lacks the glycolysis enzyme phosphofructokinase and therefore cannot catabolize glucose anaerobically (Gromet, Schramm and Hestrin 1957), addition of noncarbohydrate carbon sources such as ethanol can have the indirect benefit of entering the central metabolic flux and increasing the overall levels of cellular ATP, all the while inhibiting the requirement for glucose assimilation via the pentose-phosphate pathway (Naritomi *et al.* 1998; Yunoki *et al.* 2004) (Fig. 1A). In addition, at least in some bacteria alternative carbon sources can be more efficiently incorporated into cellulose biogenesis than direct utilization of glucose itself. For example, analyses of the central carbon flux in *G. xylinus* have further shown that only about a fifth of the metabolic carbon gets incorporated into cellulose polymers when glucose is used as the carbon source, whereas this value increases to ∼48% for glycerol utilization (Zhong *et al.* 2013). Finally, while some cellulose-secreting bacteria (e.g. *G. xylinus*) are obligatory aerobes, others (e.g. *Enterobacter* sp. FY-07) are highly efficient cellulose producers in both aerobic and anaerobic conditions (Ma *et al.* 2012). The efficiency of cellulose secretion thus depends on a plethora of factors among which media composition, carbon source, growth conditions, and bacterial species or strain, whereas the engineering of cost-effective approaches for bacterial cellulose production remains a longstanding priority for an increasingly diverse array of biotechnological applications.

TYPES OF CELLULOSE SECRETION SYSTEMS

It is now well established that bacterial cellulose can be produced by several distinct types of cellulose secretion systems that have been best studied in Gram-negative Proteobacteria (Römling and Galperin 2015) (Fig. 1A). A recent review and classification of proteobacterial *bcs* operons proposed a standardized nomenclature for *bcs* gene products and highlighted both the high mosaicity of the coding operons, as well as the three most prevalent types of bacterial cellulose secretion systems as determined by accessory to the synthase Bcs subunits (Römling and Galperin 2015). In most bacteria the catalytic core of the secretory assembly is represented by the BcsAB tandem, of which BcsA is the inner-membrane synthase incorporating a cytosolic glycosyltransferase domain, a transmembrane module for cellulose export and a C-terminal c-di-GMP-sensing PilZ domain (Morgan, Strumillo and Zimmer 2013; Morgan, McNamara and Zimmer 2014). Its partner BcsB, which is sometimes encoded in a single polypeptide chain with the synthase, is a tail-anchored protein with carbohydrate-binding domains in the periplasm proposed to guide the nascent polysaccharide on its way toward the outer membrane secretory components (Morgan, Strumillo and Zimmer 2013; Morgan, McNamara and Zimmer 2014; Abidi *et al.* 2021) (Figs 1–3). Interestingly, *in vitro* studies on purified BcsAB complexes from two different Gram-negative species, *E. coli* and *Rhodobacter sphaeroides*, have demonstrated that the C-terminal BcsB tail—composed of the transmembrane anchor and a short amphipathic helix immediately preceding it—is indispensable for cellulose polymerization, thus making BcsB a co-catalytic subunit, or co-polymerase (Omadjela *et al.* 2013). In addition to the biosynthetic BcsAB tandem, most proteobacterial *bcs* operons also encode periplasmic homologs of the cellulase BcsZ and a tetratricopeptide repeat (TPR)-rich outer membrane exporter BcsC (Römling and Galperin 2015) (Fig. 1A).

In particular, type I cellulose secretion systems are found among certain α-, β-, and γ-Proteobacteria and include biotechnologically and medically relevant species from the *Gluconacetobacter*, *Dickeya* and *Burkholderia* lineages (Römling and Galperin 2015). The characteristic feature of this group is the presence of the *bcsD* gene in addition to the core *bcsABZC* components, whose product is proposed to localize in the periplasm and to contribute to the regular packing of glucan chains in species secreting crystalline cellulose (Saxena *et al.* 1994; Römling and Galperin 2015) (Fig. 1A). Additional Bcs components, such as BcsH, BcsO, BcsP, BcsQ, BcsS or BglX can also be encoded. The second, or *E. coli*-like, type of *bcs* operons is widespread among β- and γ-Proteobacteria, including many enterobacterial pathogens (Römling and Galperin 2015) (Fig. 1A). Its distinguishing components are the BcsE and BcsG subunits, a cytosolic c-di-GMP-binding protein and a membrane-anchored periplasmic pEtN transferase, respectively (Fang *et al.* 2014; Thongsomboon *et al.* 2018; Zouhir *et al.* 2020). In addition, the BcsR, BcsQ and BcsF components are often found in these systems, whereas *bcsP* and *bcsO* genes can be present occasionally. The third major type of cellulose secretion systems are limited to certain cyano- and α-proteobacterial species. They lack all three BcsD, BcsE and BcsG subunits, and are often devoid of the TPR-rich outer membrane porin BcsC but instead encode a different TPR-based scaffolding protein, BcsK (Römling and Galperin 2015) (Fig. 1A).

In addition to these major groups of cellulose biosynthesis systems, there are also multiple examples for alternative secretory assemblies. In many cases, loci for specific Bcs components can be lost or duplicated and many systems feature a hybrid operon architecture, where both BcsD and BcsE(F)G subunits are encoded (Römling and Galperin 2015; Bundalovic-Torma *et al.* 2020). In others, however, the likely cellulose secretion machineries differ drastically from the prevalent types described above. Some cyanobacteria for example, such as *Thermosynechococcus vulcanus*, contain functional BcsA and BcsZ homologs; however, BcsB and BcsC are substituted by an efflux pump-like tandem composed of an inner-membrane HlyD-like subunit and an outer-membrane TolC-like exporter (Maeda *et al.* 2018). While *E. coli*-like cellulose secretion systems were recently shown to secrete a pEtN-modified polymer (Thongsomboon *et al.* 2018), other bacteria are known to secrete acetylated cellulose (Spiers *et al.* 2003; Bundalovic-Torma *et al.* 2020; Scott *et al.* 2020). In *Pseudomonas fluorescens* SBW25 and a few other bacteria, such chemically modified polysaccharide is synthesized by products of the hybrid *wss* operon, which encodes homologs of BcsQ and the BcsABZC core on one hand, as well as a polysaccharide acetylation complex homologous to the alginate secretion system's, on the other (Spiers *et al.* 2003; Riley *et al.* 2013). Acetylated cellulose is also secreted by Gram-positive clostridia featuring a yet distinct operon organization with BcsA, BcsB and BcsZ functional homologs, as well as a pair of envelope-embedded acyltransferases (Scott *et al.* 2020) (Fig. 1A). Another example for an unusual cellulose secretion system can be found in Gram-positive actinomycetes. Studies on *Streptomyces coelicolor* have shown that its secreted cellulose plays key roles in aerial growth, mycelium development, resistance to osmotic stress, cell wall morphology, and surface attachment via amyloid fimbriae by anchoring the latter to the cell surface (Xu *et al.* 2008; de Jong *et al.* 2009; Liman *et al.* 2013). The cellulose synthase gene, *cslA*, is found in a *cslA-glxA-cslZ* gene cluster, where the *cslZ* encodes a BscZ-like endoglucanase, while GlxA is a galactose oxidase-like membrane-anchored protein, likely acquired by horizontal gene transfer from fungi (Liman *et al.* 2013). GlxA is essential for cellulose secretion in the bacterium, displays three predominantly

β-sheet domains including a large β-propeller in the periplasm and its *in vivo* maturation depends on copper exposure, suggesting coupling between copper utilization, cellulose biosynthesis and multicellular, fungus-like hyphae development (Liman *et al.* 2013; Chaplin *et al.* 2015; Petrus *et al.* 2016).

Finally, there are bacteria that are known to secrete functionally important cellulose; however, the dedicated secretion machineries have not been identified to date. For example, pathogenic *Mycobacterium tuberculosis* (Mtb) has been shown to secrete biofilm-promoting cellulose both *in vitro* and in granulomatous lesions in lungs of infected hosts *in vivo* (Trivedi *et al.* 2016; Chakraborty *et al.* 2021). Whereas *M. tuberculosis* strains deficient in biofilm formation were also attenuated for survival and establishment of infection in mice, administration of nebulized cellulase to hosts with established Mtb infection was found to potentiate the effects of antibiotics (Chakraborty *et al.* 2021). Together, these data suggest that the cellulose-rich extracellular matrix contributes to mycobacterial drug tolerance, while simultaneously protecting the pathogen from triggering immune responses in the host. Mycobacteria are a special clade within Gram-positive actinobacteria in that they have a complex bacterial envelope with a low-fluidity, low-permeability asymmetric outer membrane—or 'mycomembrane'—whose inner leaflet is composed of exceptionally long-chain mycolic acids that are covalently linked to the cell wall peptidoglycan through a polysaccharide network of arabinogalactan (Chiaradia *et al.* 2017). This complex and waxy structure makes the cells practically impervious to Gram-staining, and they can be therefore viewed as Gram-negative-like diderms. To date, no mycobacterial *bcsA* homolog has been reliably identified in the pathogen; however, cellulose-dependent biofilm formation would likely require a multicomponent pan-envelope secretion machinery to produce and translocate the nascent polysaccharide through the exceptionally complex mycobacterial coating.

THE CATALYTIC BcsAB TANDEM

In most characterized cellulose secreting bacteria, the *bcsA* gene is found in tandem with *bcsB* which, as mentioned earlier, encodes a tail-anchored co-catalytic subunit (Omadjela *et al.* 2013; Römling and Galperin 2015) (Fig. 1A). The structure and functional mechanism of the BcsAB tandem have been best studied on the homologs from *R. sphaeroides*, a bacterium featuring a Type III cellulose secretion system (Morgan, Strumillo and Zimmer 2013; Morgan, McNamara and Zimmer 2014; Morgan *et al.* 2016) (Fig. 2). BcsA is an ~100 kDa protein whose domain architecture features an α-helical transmembrane cellulose export domain ($BcsA^{TMD}$). Two functional cytosolic insertions break the domain's amino acid sequence: the catalytic glycosyl transferase domain ($BcsA^{GT}$ between $TM4^{Rs}$ and $TM5^{Rs}$) and a core interface helix (IF) followed by an active site-gating loop (between $TM6^{Rs}$ and $TM7^{Rs}$) (Morgan, Strumillo and Zimmer 2013). At its C-terminal end, $BcsA^{TMD}$ is followed by a c-di-GMP-sensing PilZ β-barrel domain ($BcsA^{PilZ}$), which points away from $BcsA^{GT}$ at ~90°, and the polypeptide ends with a C-terminal interface helix (IF-CT), likely interacting with the inner leaflet of the cytosolic membrane, as well as with TM3, IF and TM8. TM3-8 form a tilted, narrow transmembrane channel (~8 by 33 Å), which in all crystallized states accommodates a non-hydrated translocating polysaccharide that is spontaneously co-purified with the BcsAB tandem and not added during the purification steps (Morgan, Strumillo and Zimmer 2013; Morgan, McNamara and Zimmer 2014; Morgan *et al.* 2016). The polysaccharide emerges from the channel and kinks along the membrane-proximal surface of $BcsB^{D3}$, a carbohydrate-binding jellyroll module, which is proposed to aid periplasmic translocation of the nascent polysaccharide (see later). The channel accommodates ~10 glucose units, whose glucopyranose rings interact through CH-π stacking interactions with multiple hydrophobic residues (Met^{300}, Phe^{301}, Phe^{316}, Trp^{383}, Phe^{419}, Phe^{426}, Tyr^{433}, Phe^{441}, Val^{551}, Val^{555}, Trp^{558}), whereas the equatorial hydroxyl groups hydrogen-bond with Tyr^{80}, Asn^{118}, His^{276}, Asn^{412}, Arg^{423}, Glu^{439}, Tyr^{455}, Ser^{476} and Glu^{477} (Morgan, Strumillo and Zimmer 2013).

The purified BcsAB tandem is catalytically active *in vitro* upon addition of activating c-di-GMP, the substrate UDP-glucose and Mg^{++} ions mediating the sugar addition onto the non-reducing end of the polymer (Morgan, Strumillo and Zimmer 2013). Nevertheless, the default presence of translocating polysaccharide in all crystallized states, and consequently purified BcsAB samples, precludes the identification of the polymerization initiation mechanism. Whereas direct polymerization onto a single glucose molecule has been proposed based on structural similarities between the coordination of the acceptor glucose unit in BcsA and that of galactose by the sodium-dependent sugar transporter (SGLT) (Faham *et al.* 2008; Morgan, McNamara and Zimmer 2014), other studies have suggested that at least some bacterial and plant cellulose synthases can utilize lipid-linked oligosaccharidic primers to initiate catalysis. For example, studies on *Agrobacterium tumefaciens* following the incorporation of UDP–^{14}C-glucose into cellulose upon mixing of extracts derived from various *bcs* gene mutants, suggested the direct involvement of a lipid-linked intermediate in cellulose biogenesis (Matthysse, Thomas and White 1995). Similarly, studies on *Gossypium hirsutum* (cotton) CesA1 identified sitosterol-β-glucosides as primers for cellulose synthesis by the synthase and proposed that the enzymes UDP-glucose–sterol glucosyltransferase (SGT) and the KORRIGAN cellulase are responsible for primer synthesis and cleavage from the nascent polysaccharide, respectively (Peng *et al.* 2002).

The structures of the $BcsA^{GT}$ domain provide direct insights in substrate coordination, catalysis and translocation. The domain carries the conserved D,D,D, Q(Q/R)xRW motif that is common in processive β-glycosyl transferases and consists of three variably spaced Asp residues, as well as the linear Q(Q/R)xRW sequence (Morgan, Strumillo and Zimmer 2013; Morgan, McNamara and Zimmer 2014; Morgan *et al.* 2016). The first two Asp residues (Asp^{179} and Asp^{246} in *R. sphaeroides*) are involved in UDP coordination, whereas the third one is the catalytic base and is part of the strictly conserved TED motif at the tip of the so-called 'finger helix', whose movements are coupled with gating loop relaxation and polysaccharide translocation (Morgan, Strumillo and Zimmer 2013). The Q^{379}RGRW motif on the other hand is part of a membrane-proximal horizontal helix above the finger helix and the Arg^{382} and Trp^{383} residues participate in stacking interactions with the terminal or preterminal sugar unit of the polysaccharide. In the crystallized c-di-GMP-free state the so-called gating loop is partly occluding the substrate-binding pocket due to tethering salt bridge formation between Arg^{580} and Glu^{371} and additional interactions with T^{511} from the gating loop (Morgan, Strumillo and Zimmer 2013). The polysaccharide is found in a pre-translocated state with the finger helix in an 'out' conformation contacting the terminal glucose moiety of the polysaccharide. The effects of c-di-GMP binding and finger helix-assisted polysaccharide translocation on the gating loop conformation and substrate re-entry are discussed in detail later (Fig. 2B).

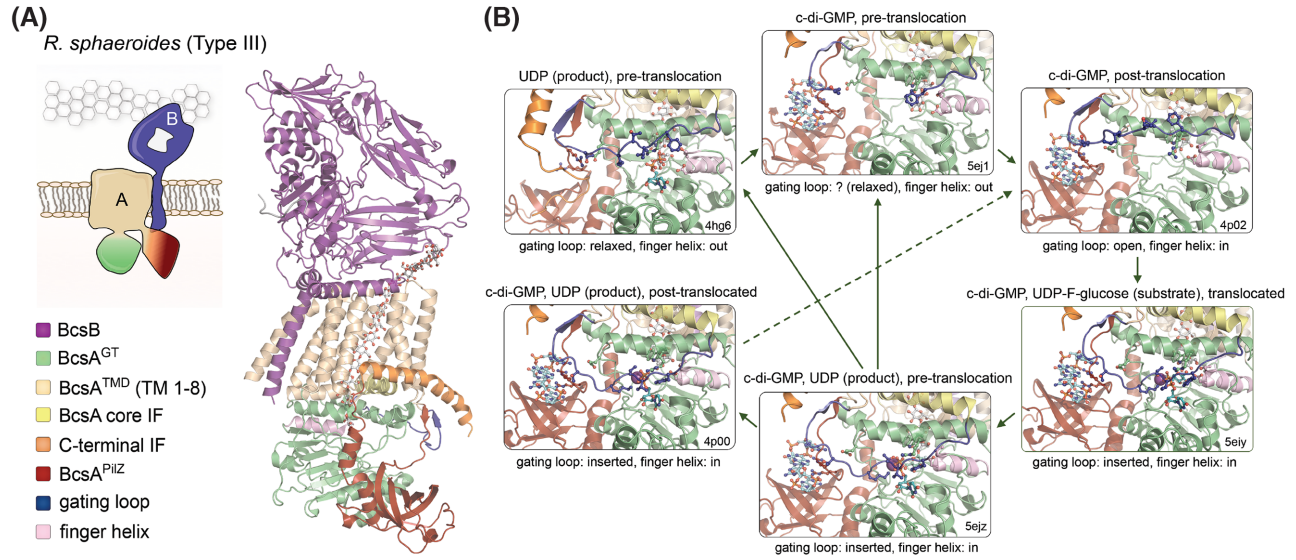

Figure 2. The BcsAB catalytic complex. **(A)** Thumbnail representation and crystal structure of the 1:1 BcsAB tandem from *R. sphaeroides*. A co-purified cellulose polymer is shown in sticks (pdb 4p02) (Morgan, McNamara and Zimmer 2014). TMD: transmembrane export domain; IF: interface helix; GT: glycosyltransferase domain. **(B)** Zoom-in of the synthase active site as captured in the crystal structures of the *R. sphaeroides* BcsAB tandem from crystals grown or incubated with different ligands. Color coding as in panel (A). Protein data bank accession numbers, as well as the presence of substrate homologs, products, c-di-GMP, translocation state of the polymer and gating loop conformation are indicated for each state (Morgan, Strumillo and Zimmer 2013; Morgan, McNamara and Zimmer 2014; Morgan *et al.* 2016). Green arrows indicate putative conformation transition pathways integrating all captured conformational states. Alternative pathways would depend on local c-di-GMP, product and substrate concentrations, as well as finger helix-mediated or spontaneous translocation. The cellulose polymer, substrate homolog, UDP product, c-di-GMP and key residues from the gating loop, c-di-GMP coordinating PilZ-proximal linker, finger helix and conserved QRGRW motif are shown as sticks.

As mentioned earlier, BcsA functions in tandem with its intraoperon partner BcsB. The latter's primary structure carries a cleavable N-terminal signal peptide for export from the cytosol, followed by a four-domain periplasmic architecture composed of alternating carbohydrate binding jellyrolls (D1 and D3) and flavodoxin-like α-β-α modules (D2 and D4) that lead to the required for catalysis C-terminal amphipathic helix and inner-membrane anchor (Morgan, Strumillo and Zimmer 2013; Omadjela *et al.* 2013). The monomeric crystal structures of the BcsAB$^{R.sphaeroides}$ tandem show that BcsA and BcsB interact in an equimolar ratio (Fig. 2), where the BcsB C-terminal anchor tightly associates with and completes the inner-membrane transport domain of BcsA by fitting in a groove between TM1-3 (Morgan, Strumillo and Zimmer 2013; Morgan, McNamara and Zimmer 2014; Morgan *et al.* 2016). This, together with the fact that BcsB is sometimes encoded by the same *bcsAB* gene in certain *bcs* operons, had long supported a model of equimolar BcsAB biosynthetic assemblies across the bacterial kingdom.

Our recent works on the enterobacterial Type II cellulose secretion system from the commensal strain *E. coli* 1094 revealed a surprising architecture with the formation of a stable, catalytically active, multi-subunit secretory assembly, which encompasses most of the inner-membrane and periplasmic subunits (BcsRQABEF or referred to as the Bcs macrocomplex herein) and includes a multimeric periplasmic crown of up to six BcsB protomers in a fan-like arrangement (Krasteva *et al.* 2017; Abidi *et al.* 2021) (Fig. 3 and Fig. 4A). Using cryo-EM we resolved the structure of the assembled Bcs macrocomplex, which revealed the polymeric BcsB$^{E.coli}$ crown at nearly atomic resolution (Abidi *et al.* 2021). As revealed by our work and confirmed by a subsequent lower-resolution study (Acheson *et al.* 2021), BcsB$^{E.coli}$ adopts an overall similar 4-domain fold as the *R. sphaeroides* homolog with several crucial exceptions. In particular, BcsB^{D2} features a C-proximal β-strand insertion that extends the domain's central β-sheet, whereas BcsB^{D4} lacks a large amphipathic helix found in the *R. sphaeroides* counterpart and instead presents an additional 3-stranded β-sheet that interacts with both BcsB^{D2} and BcsB^{D4} to assemble a continuous 9-stranded β-sheet shared between neighboring protomers in the crown (Abidi *et al.* 2021) (Fig. 3E–G). This secondary structure-mediated polymerization mechanism between the peripheral flavodoxin-like domains is functionally complemented by intersubunit stacking of β-sheet-connecting loops from the D3 jellyroll at the center of the crown, which likely guide the nascent polymer in an outward-bound ratchet-like mechanism during cellulose secretion (Abidi *et al.* 2021). Importantly, the observed superhelical BcsB oligomerization is self-driven as confirmed by the cryo-EM structure of purified full-length BcsB$^{E.coli}$ and the presence of a C-terminal membrane anchor is bound to both limit the number of BcsB copies in the crown, and introduce significant tension and/or deformation in the underlying membrane (Abidi *et al.* 2021) (Fig. 3D). The latter can have important functional roles in cellulose biosynthesis such as secretion system targeting to the pole (Le Quéré and Ghigo 2009), facilitating a functional synthase assembly (Krasteva *et al.* 2017; Abidi *et al.* 2021) or determining interactions with additional regulatory components such as the BcsG pEtN-transferase (Krasteva *et al.* 2017; Thongsomboon *et al.* 2018; Acheson *et al.* 2021), or the c-di-GMP metabolizing enzymes DgcC, DgcQ and PdeK (Da Re and Ghigo 2006; Richter *et al.* 2020) (see later).

An unexpected result from the recent cryo-EM structures of the Bcs macrocomplex is the noncanonical BcsA:BcsB stoichiometry where a single BcsA interacts with the membrane-proximal BcsB protomer of the crown, as determined by the relative position of the stacked D3 luminal loops (Abidi *et al.* 2021) (Fig. 3B and F; Fig. 4A). The rest of the synthase shows a highly conserved fold for its transmembrane and cytosolic modules; however, its PilZ domain is tightly buttressed by an apical BcsRQ regulatory complex (Abidi *et al.* 2021) (Fig. 3B and C; Fig. 4A). The N-terminal ~140 residues of the synthase that

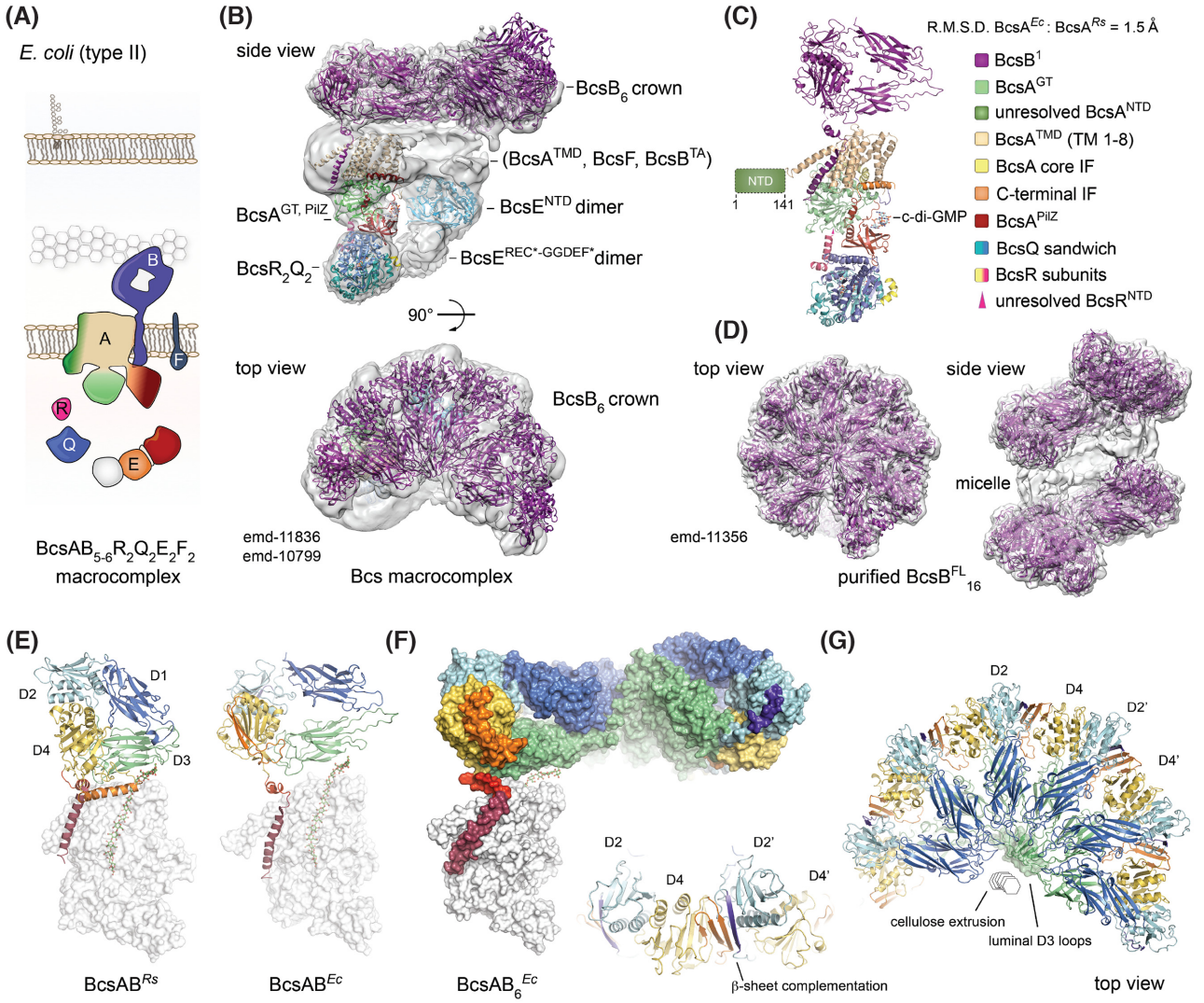

Figure 3. **(A)** Thumbnail representation of the Bcs secretion macrocomplex components in *E. coli*-like (Type II) cellulose secretion systems (Krasteva *et al.* 2017; Zouhir *et al.* 2020; Abidi *et al.* 2021). **(B)** Cryo-EM structure of the assembled BcsRQABEF macrocomplex (emd-11836) showing hexameric BcsB in the crown (based on local refinement of pentameric $BcsB^{peri}$; average resolution 2.9 Å; accessions pdb-6yg8 and emd-10799) (Abidi *et al.* 2021). The BcsA subunit was modeled in Robetta and refined in the experimental BcsRQAB electron density following local refinement (emd-11836). The crystal structure of a BcsRQ complex was rigid-body fitted in the apical density. A predicted model for a dimer of BcsE's N-terminal domains (NTD, in cyan) was fitted in the bilobal membrane-proximal densities opposite BcsA based on fold prediction in Robetta, reported head-to-tail $BcsE^{NTD}$ oligomerization and interactions with inner-membrane BcsF (Zouhir *et al.* 2020; Abidi *et al.* 2021). **(C)** A locally refined atomic model of the BcsRQAB assembly as found in the BcsRQABEF macrocomplex (emd-11836). An ~140-residue-long N-terminal BcsA domain remains unresolved in the structure (Abidi *et al.* 2021). **(D)** Cryo-EM structure of purified full-length *E. coli* $BcsB^{His}$ (emd-11356) with two octamers of BcsB's periplasmic domains refined in the experimental electron density (Abidi *et al.* 2021). Comparison of the *E. coli* and *R. sphaeroides* BcsB in the context of the BcsAB complex. **(E)** 1:1 BcsAB assemblies are shown with BcsA in white surface representation. Co-crystallized or modeled cellulose is shown as sticks. BcsB homologs are presented in cartoons with separate domains color-coded as follows: D1, blue; D2, cyan; D3, green; D4, yellow; C-terminal amphipathic and transmembrane helices, red and bordeaux, respectively. The *R. sphaeroides* D4 amphipathic helix insertion, substituted by an intersubunit 3-stranded β-sheet in *E. coli* $BcsB^{D4}$, is colored in orange. **(F)** Atomic model in surface representation of the *E. coli* $BcsAB_6$ assembly as found in the BcsRQABEF macrocomplex. Inset, β-sheet complementation between the D2′ and D4 flavodoxin-like modules from neighboring BcsB protomers, with the D2′ β-strand extension in dark blue and the D4 3-stranded β-sheet in orange. **(G)** Top view of the BcsB crown hexamer; domain color coding as in panel (E). Stacked D3 luminal loops are shown in transparent surface representation. Nascent cellulose (illustrated as stacked hexagons) is proposed to be extruded along the crown lumen with D3 luminal loops providing a ratchet-like structural support (Abidi *et al.* 2021).

have been proposed to interact with the pEtN transferase BcsG (Krasteva *et al.* 2017) remain unresolved in the structure. The BcsRQ complex is recruited and stabilized within the secretory assembly by BcsQ–BcsE–BcsF interactions to form a cytosolic vestibule around the PilZ domain (Figs 3 and 4), likely facilitating processive substrate recycling and synthase activation by c-di-GMP (see later) (Zouhir *et al.* 2020; Abidi *et al.* 2021). In addition, BcsR's N-terminal region appears to extend onto the glycosyl transferase module and likely has a direct role in catalysis as demonstrated by its essentiality for cellulose secretion *in vivo* (Abidi *et al.* 2021) and by the stimulatory effects of BcsRQ addition in *in vitro* cellulose synthesis assays (Acheson *et al.* 2021).

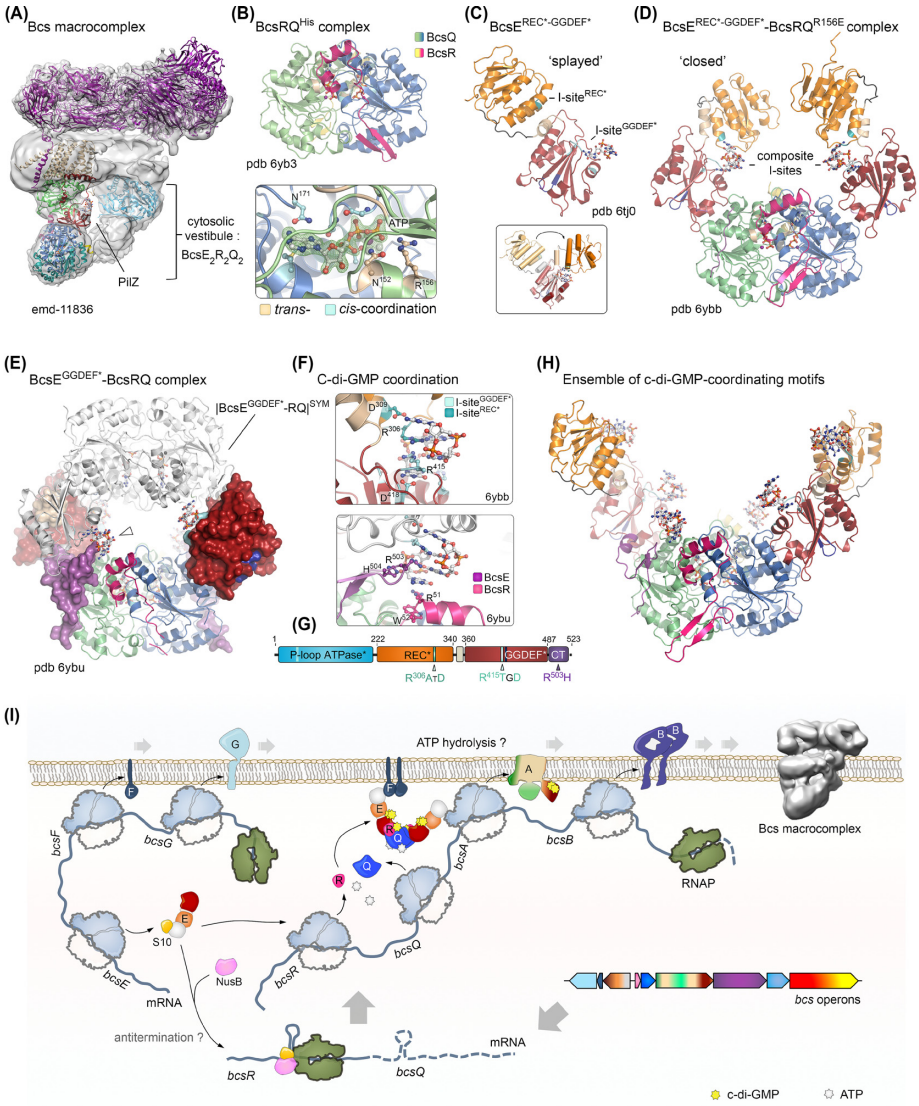

Figure 4. Nucleotide-sensing regulatory components of the *E. coli* Bcs cellulose secretion macrocomplex. Adapted from (Zouhir *et al.* 2020; Abidi *et al.* 2021) **(A)** Bcs macrocomplex assembly as in Fig. 3 highlighting the central position of c-di-GMP-bound $BcsA^{PilZ}$ within the $BcsE_2R_2Q_2$ cytosolic vestibule. Densities corresponding to the $BcsE^{REC*-GGDEF*}$ modules are not well resolved, likely due to conformational heterogeneity. **(B)** Top, crystal structure of a purified $BcsRQ^{His}$ complex. Bottom, zoom-in on one of the two ATP ligands co-purified and co-crystallized with $BcsRQ^{His}$ (pdb 6yb3). Magnesium-coordinating water molecules are also shown as gray spheres. An |Fo|-|Fc| partial electron density map calculated from a model prior to inclusion of the ATP, Mg++ and coordinating water molecules is shown as a green mesh. *Trans*- and *cis*-coordinating residues are colored in wheat and cyan, respectively (Abidi *et al.* 2021). **(C)** Crystal structure of the isolated $BcsB^{REC*-GGDEF*}$ domain showing a splayed conformation where a single c-di-GMP molecule is bound to the GGDEF* domain's I-site (pdb 6tj0). The two I-site motifs are colored in teal (REC* I-site) and cyan (GGDEF* I-site); the degenerate receiver domain (REC*) is colored in orange; and the degenerate diguanylate cyclase domain (GGDEF*) is colored in deep red. Inset, BcsE conformational changes between the splayed and closed conformations, showing movement of the receiver domain relative to the overlaid GGDEF* module. **(D)** Crystal structure of the $BcsE^{REC*-GGDEF*}$–$BcsRQ^{R156E}$ complex (pdb 6ybb), featuring a closed $BcsE^{REC*-GGDEF*}$ conformation, in which each domain contributes an I-site RxxD motif to coordinate a c-di-GMP moiety from the intercalated dimeric ligand. **(E)** Structure and crystal packing of a $BcsE^{GGDEF*}$–BcsRQ complex (pdb 6byu), with the $BcsE^{GGDEF*}$ domain shown in surface representation and the BcsQ-wrapping C-terminal tail of the protein colored in purple. A symmetry-related $BcsE^{GGDEF*}$–BcsRQ complex is shown in white and a third c-di-GMP coordinating motif is evident at the $BcsE^{C\text{-}tail}$–BcsR interface. **(F)** C-di-GMP binding motifs within the crystallized BcsERQ complexes. Top, dimeric c-di-GMP coordination by the composite I-sites with RxxD motif contributions from the REC* and GGDEF* domains in the closed BcsE conformation. The contributions of both sites in c-di-GMP binding have been experimentally confirmed and characterized (Zouhir *et al.* 2020; Abidi *et al.* 2021). Bottom, c-di-GMP coordination at the third, crystallographic binding motif shown in panel (E). **(G)** Domain architecture of full-length BcsE, showing the position and sequence of c-di-GMP binding motifs. **(H)** A composite structural model of the $BcsE^{REC*-GGDEF*}{}_2$–$BcsR_2Q_2$ complex with c-di-GMP bound at all six coordinating motifs. Although such conformation is unlikely within the assembled Bcs macrocomplex, c-di-GMP-binding motifs in the vestibule are proposed to dynamically contribute to intercalated c-di-GMP retention and recycling for processive synthase activation. **(I)** Integrated model for *E. coli* Bcs secretion system assembly: *bcsEFG* and *bcsRQABZC* operons are expressed separately as polycistronic mRNAs. BcsE forms a stable equimolar complex with the small ribosomal protein S10, which is also a component of the conserved transcription antitermination machinery (TAC). A second TAC component, NusB, competes with BcsE for S10 binding; however, the physiological role of these BcsE-S10–NusB interactions *in vivo* remains elusive. Detection of putative intrinsic terminators in the 5′-proximal regions of the *bcsRQABZC* mRNA has led to an as-yet untested hypothesis of *bcsRQABZC* expression regulation at the transcription-elongation level (Zouhir *et al.* 2020). Expressed BcsR and BcsQ stimulate each other's folding and stability to form ATP-bound 'sandwich' assemblies, which bind available BcsE and are recruited to the inner membrane via BcsE–BcsF interactions (Zouhir *et al.* 2020). While ATP hydrolysis is inhibited in the cytosolic BcsERQ complex, it is likely essential at the membrane level, where it could lead to efficient BcsA sorting, assembly and stability within the macrocomplex (Abidi *et al.* 2021). In addition, the BcsERQ complex directly affects processive glucose polymerization through synthase-proximal c-di-GMP retention and direct structural interaction with the cytosolic BcsA modules (Abidi *et al.* 2021; Acheson *et al.* 2021).

NUCLEOTIDE-DEPENDENT REGULATION OF CELLULOSE SYNTHESIS

ATP-dependent regulation and role of the BcsRQ tandem

As mentioned earlier, cellulose biogenesis is an energetically expensive process that requires high levels of cellular ATP, both for phosphorylation of the precursor sugar moieties (e.g. glucose or fructose phosphorylation by hexokinases), as well as for recycling of the UDP product into UTP by the essential enzyme nucleoside diphosphate kinase (Fig. 1A). However, glucose polymerization and extrusion at the membrane level are proposed to be powered directly by the high-energy phosphoanhydride bonds of the preactivated synthase substrate, UDP-glucose, and *in vitro* cellulose synthesis using purified BcsAB complexes does not require the addition of ATP (Omadjela *et al.* 2013).

Nevertheless, many cellulose secretion systems, including Type I, Type II and Wss secretory assemblies, encode for homologs of a SIMIBI-like (Signal-recognition particle, MinD and BioD) ATPase, BcsQ (also WssA and WssJ), often co-expressed with a short polypeptide, BcsR, as separate or fused subunits (Römling and Galperin 2015). In *E. coli* and related enterobacteria, *bcsR* encodes a 7 kDa polypeptide and leads the *bcsRQABZC* operon, whereas BcsQ is a 28 kDa cytosolic protein featuring a deviant Walker A motif (G^8VRGGVGTTT) and a preferential localization at the bacterial cell pole (Le Quéré and Ghigo 2009). We showed recently that both BcsR and BcsQ subunits are essential for cellulose secretion *in vivo* and that the two proteins exhibit chaperone-like function toward each other, where BcsQ plays a role in the folding and stability of BcsR, while the latter stabilizes BcsQ into monodisperse $BcsR_2Q_2$ heterotetramers in solution (Krasteva *et al.* 2017; Zouhir *et al.* 2020). Via the BcsQ subunit, the BcsRQ complex partakes in nanomolar affinity interactions with the third cytosolic regulator, BcsE, which in turn recruits the complex to the inner membrane through high-affinity interactions with the transmembrane polypeptide BcsF (Zouhir *et al.* 2020) (Fig. 4I).

Crystal structures of the $BcsRQ^{His}$ complex crystallized in different conditions showed that BcsQ adopts a classical α-β-α SIMIBI fold with a 7-stranded β-sheet sandwiched between flanking α-helices (Abidi *et al.* 2021). Surprisingly, $BcsRQ^{His}$ crystallized invariably as an ATP-bound 'sandwich' dimer of heterodimers, where extensive parts of the dimerization interface are mediated by the two ATP ligands stabilized by both *cis*- and *trans*-interactions with BcsQ, as well as by multiple water molecules and coordinated Mg^{++} ions stabilized and resolved in the nucleotide-binding pocket. In particular, ATP's adenine base is coordinated primarily by side-chain interactions with N^{171} in *cis*, whereas its triphosphate moiety interacts with P-loop residues in *cis*, as well as the side chains of N^{152} and R^{156} in *trans* (Fig. 4B). On the periphery, the BcsQ homodimer is effectively stitched together by extensive hydrophilic and hydrophobic interactions of both BcsQ subunits with each of the C-terminal α-helical domains of BcsR. Importantly, the essential role of 'sandwich' ATP coordination *in vivo* is demonstrated by the progressive abolishment of cellulose secretion in the $BcsQ^{N152D}$, $BcsQ^{N152D\text{-}R156E}$ and $BcsQ^{N152A\text{-}R156A\text{-}N171A}$ mutants demonstrating for the first time a direct role for ATP within the cellulose secretion system (Abidi *et al.* 2021).

Interestingly, the overall conformation of the $BcsRQ^{His}$ heterotetramer, including the ATP-bound 'sandwich' dimerization and/or the BcsR–BcsQ interface, is reminiscent of the activated, pre-catalytic conformation of conserved SIMIBI NTPases, such as the Get3-Get1 complex involved in tail-anchored protein sorting in eukaryotes, the SRP54-SR complex responsible for signal peptide-dependent protein delivery to the SEC translocon in both pro- and eukaryotes, the FlhG-FlhF tandem responsible for positioning of the flagellar Type III secretion machinery, as well as the MinD-MinE tandem preventing divisome assembly at the bacterial cell poles (Bange and Sinning 2013; Shan 2016; Abidi *et al.* 2021). A key feature of these SIMIBI proteins is the uncoupling of NTP-dependent sandwich dimerization from NTP hydrolysis, which secures important steps of the proteins' spatiotemporal cycle such as cargo loading, interaction with additional partners, and recruitment or detachment from the cell membrane among others (Bange and Sinning 2013; Shan 2016).

Consistently, BcsRQ sandwich dimer formation appears uncoupled from membrane targeting and ATP hydrolysis. In particular, whereas $BcsRQ^{His}$ crystallizes exclusively ATP-bound even after treatment with chelating agents or prolonged incubations with ADP, purified $Bcs^{His}RQ$ shows weak ATPase activity *in vitro*, which is enhanced by BcsQ mutations that are characterized by increased cellulose secretion *in vivo* (e.g. $Bcs^{His}RQ^{R156E}$). The same $Bcs^{His}RQ^{R156E}$ complex is characterized by partial disassembly in solution, likely due to spontaneous hydrolysis of the sandwiched ATP in the heterotetramers. Surprisingly, binding of BcsE to the $Bcs^{His}RQ^{R156E}$ or $Bcs^{His}RQ$ complexes both recovers the stability of stoichiometric $BcsE_2R_2Q_2$ assemblies and inhibits the ATPase activity *in vitro*, suggesting BcsE-driven stabilization of the pre-catalytic 'sandwich' dimer, similar to the presence of C-terminal hexahistidine tags in the $BcsRQ^{His}$ crystal structures. Nevertheless, sandwich dimer formation is not sufficient by itself for cellulose secretion *in vivo*, as demonstrated by the lack of cellulose secretion in the very stable, dimerization-competent but catalytically inactive $BcsQ^{T15K}$ mutant (Abidi *et al.* 2021). Finally, a $BcsQ^{C39D}$ mutant designed to carry a SIMIBI consensus aspartate at the catalytic water-activating amino acid position does not feature significantly higher ATPase activity *in vitro* but shows drastic enhancement of cellulose secretion *in vivo*, further supporting a role for uncoupled ATP hydrolysis occurring downstream of BcsERQ complex formation (Abidi *et al.* 2021) (Fig. 4I).

The role of ATP hydrolysis *in vivo* has so far eluded direct characterization. One hypothesis, based on the drastically lower levels of detectable BcsA in certain *bcsQ* or *bcsR* mutant backgrounds incompetent for cellulose secretion (Krasteva *et al.* 2017; Abidi *et al.* 2021) is that the BcsF-mediated membrane recruitment of ATP-bound BcsERQ is followed by ATP hydrolysis directly affecting BcsA membrane protein sorting and the positioning of the inner-membrane catalytic complex, in a role similar to that of other SIMIBI-like protein sortases (e.g. SRP54-SR, Get3 or FlhF-FlgG) (Abidi *et al.* 2021). Such a hypothesis can explain both why 'sandwich' ATP-dependent dimerization has been preserved in evolution and why by itself it is not sufficient for cellulose secretion *in vivo*. In addition, the encoding of the BcsRQ tandem by the Bcs system itself would confer secretion-system specific mechanisms for assembly regulation and would abolish the requirement for BcsRQ and nucleotide recycling as observed in other SIMIBI sortases (Bange and Sinning 2013; Shan 2016; Abidi *et al.* 2021). Indeed, as mentioned earlier, BcsRQ remain an integral part of the Bcs macrocomplex where the two proteins likely directly regulate the catalytic activity of the synthase by direct interactions of BcsQ and BcsR with the $BcsA^{PilZ}$ and $BcsA^{GT}$ modules, respectively, as well as by stabilizing the cytosolic BcsERQ vestibule involved in synthase-proximal c-di-GMP enrichment (see later) (Abidi *et al.* 2021).

C-di-GMP: a common signaling input across synthase-dependent EPS secretion

Much of the seminal research on bacterial cellulose secretion started on *Gluconacetobacter xylinus* in the 1980s, when it was shown that membrane preparations from the bacterium have *in vitro* cellulose synthase activity that was greatly stimulated by the presence of GTP, a GTP-converting protein factor that associates with but is not integral to the membrane, and Ca^{2+} ions (Aloni, Delmer and Benziman 1982; Aloni *et al.* 1983). Interestingly, the stimulatory effects on the synthase activity were even greater in the presence of GTP-γ-S—that can yield GMP but not GDP—suggesting pyrophosphate release by the activating protein factor (Aloni, Delmer and Benziman 1982). Shortly after, the GTP-converting enzyme was isolated using agarose-conjugated GTP as an affinity matrix and its synthase-activating product identified as *bis*(3′,5′)-cyclic diguanylic acid, or c-di-GMP (Ross *et al.* 1985; Ross *et al.* 1987). It was also shown that a c-di-GMP-degrading phosphodiesterase is also present in the *Gluconacetobacter* membrane; however, its activity is strongly inhibited by Ca^{2+} ions, thus drawing a picture of complex, reversible, c-di-GMP-dependent regulatory inputs into cellulose secretion (Ross *et al.* 1985, 1987).

With the revolution of DNA sequencing and genome assemblies in the beginning of the 21st century, c-di-GMP metabolizing enzymes were discovered—often in multiple and diverse forms—in most characterized bacterial species, and what was once a cellulose-centric observation evolved into one of the most dynamic fields of contemporary microbiology (Galperin, Nikolskaya and Koonin 2001; Simm *et al.* 2004). Importantly, the cyclic dinucleotide revealed itself as a master regulator of bacterial biofilm formation, often through direct control not only of cellulose biosynthesis, but also of other functionally homologous albeit structurally diverse synthase-dependent systems for exopolysaccharide secretion (Jenal, Reinders and Lori 2017; Krasteva and Sondermann 2017; Low and Howell 2018).

Interestingly, the c-di-GMP-independent regulatory mechanisms are markedly different across characterized exopolysaccharide (EPS)-producing biosynthetic machineries (Krasteva and Sondermann 2017; Low and Howell 2018). In the *E. coli* poly-*N*-acetylglucosamine (PNAG) secretion system, counterparts of BcsA's glycosyl transferase and inner-membrane transport modules are part of the PgaC protein; however, the protein lacks an associated PilZ domain or other integral c-di-GMP binding modules. Instead, the cyclic dinucleotide is likely sensed by a two-protein composite interface comprising PgaC and a small, inner-membrane protein—PgaD—which is essential for PNAG production (Steiner *et al.* 2013). At low c-di-GMP levels, the PgaC–PgaD interaction is likely destabilized and the latter protein is rapidly degraded, thus inhibiting exopolysaccharide secretion. Although structural information on the c-di-GMP complexation is currently lacking, the dinucleotide is proposed to coordinate between membrane-proximal arginine residues from both protein partners, thereby stabilizing PgaD within a functional synthase complex (Steiner *et al.* 2013).

In *Pseudomonas aeruginosa*, both synthase-dependent systems—for alginate and Pel secretion—employ c-di-GMP as an activating signaling input. In the Pel system, all three modules—for the glycosyl transferase reaction, inner-membrane transport and c-di-GMP sensing—are carried out by separate protein subunits (PelF, PelG and PelD, respectively), which together with a fourth protein (PelE) are proposed to form a functional inner-membrane synthase complex (Franklin *et al.* 2011; Whitfield *et al.* 2020). PelD is anchored in the inner membrane via several transmembrane helices at its N-terminus, whereas the remaining ~two thirds of the amino acid sequence fold into a GAF-GGDEF domain tandem (Li *et al.* 2012b; Whitney *et al.* 2012). Whereas the C-terminal GGDEF module features a highly degenerate primary structure and is catalytically incompetent for c-di-GMP synthesis, it has an intact RXXD I-site motif for dinucleotide binding (Lee *et al.* 2007), which—when found on active diguanylate cyclases—can serve as an autoinhibitory, product-sensing regulatory motif (R^{367}GLD in full-length *P. aeruginosa* PelD). To date, only structures of the GAF-GGDEF domain tandem have been resolved and show one or two U-shaped dinucleotide molecules bound to the I-site, with only minor rotation of the GAF domain relative to the GGDEF module observed upon c-di-GMP complexation (Li *et al.* 2012b; Whitney *et al.* 2012). Whereas the protein has been proposed to oligomerize *in vivo* (Low and Howell 2018), further investigation is necessary to uncover the mechanisms of functional PelDEFG synthase complex assembly and c-di-GMP-dependent regulation.

Synthesis of the mucoid alginate polymer involves a yet distinct c-di-GMP sensing mechanism. Similar to the PNAG system, the glycosyl transferase and inner-membrane transport domains are fused in a single subunit, Alg8 (Franklin *et al.* 2011; Krasteva and Sondermann 2017; Low and Howell 2018). C-di-GMP sensing is carried out by a second membrane protein, which is predicted to fold into an N-terminal cytosolic, c-di-GMP-binding PilZ domain followed by a single transmembrane α-helix and a C-terminal periplasmic domain showing similarities to the extracytosolic regions of the MexA and HlyD export proteins (Franklin *et al.* 2011). Crystal structures of the cytosolic regions show that the dinucleotide binds between the extended N-terminus and the PilZ β-barrel, with contributions from several conserved sequence motifs, including R^{17}xxxR from the N-terminal tail, as well as a D^{44}xSxxG motif and R^{95} from the PilZ module (Whitney *et al.* 2015). Interestingly, the protein dimerizes in a seemingly c-di-GMP-independent manner through the opposite end of the PilZ β-barrel with the formation of an extended interprotomer β-sheet (Whitney *et al.* 2015). Whereas experimental data suggests that the unusual Alg44 oligomerization is preserved *in vivo* (Moradali *et al.* 2015), further investigation is necessary to uncover the mechanisms of c-di-GMP-dependent synthase activation.

Dinucleotide sensing by BcsA and implications in catalysis

As opposed to the PNAG, Pel and alginate secretion systems, the cellulose synthase BcsA carries all three modules for sugar transfer, polymer translocation and c-di-GMP sensing in a single polypeptide chain. Similarly to Alg44, an intercalated c-di-GMP dimer is coordinated by a PilZ domain—the C-terminal $BcsA^{PilZ}$ carrying a conserved DxSxxG motif in its β-barrel—as well as the preceding linker residues containing the typical RxxxR sequence involved in π-stacking interactions with the ligand (D^{609}ASTSG and R^{580}AAPR in the *R. sphaeroides* homolog, respectively; Morgan, McNamara and Zimmer 2014). The c-di-GMP coordination at the synthase level also appears conserved in the recently characterized *E. coli* homolog; however, the bacterium uses multiple additional c-di-GMP coordinating motifs for intercalated dinucleotide binding within the assembled Bcs secretion system (Zouhir *et al.* 2020; Abidi *et al.* 2021). Importantly, neither in *R. sphaeroides*, nor in *E. coli*, does the $BcsA^{PilZ}$ domain dimerize as observed for the alginate system's Alg44 (Whitney *et al.* 2015).

Crystal structures of c-di-GMP-free and c-di-GMP-bound $BcsA^{R.sphaeroides}$ show a highly similar synthase fold with R.M.S.D. of ∼1 Å over all atoms. In the dinucleotide-bound state the PilZ β-barrel rotates by ∼20° around the so-called 'hinge' helix: a short α-helix that follows the last β-sheet of the barrel and packs between the PilZ domain and the glycosyl transferase module. The most consequential conformational change, however, involves the conserved R^{580} residue from the canonical RxxxR motif preceding the PilZ module. In the c-di-GMP-free state, the residue is flipped toward the $BcsA^{GT}$ domain where it is stabilized by a salt bridge with E^{371}, as well as interactions with T^{511} positioned at the C-terminal end of the active site-capping gating loop. Upon c-di-GMP complexation, R^{580} rotates by ∼180° to stack with the dinucleotide, which liberates the gating loop to pivot around R^{499} and E^{514} and toward the membrane interface. This movement creates a large, 22.5 × 12.4 Å-wide entry to the active site to allow substrate access (Fig. 2B).

Interestingly, all c-di-GMP-bound crystal structures containing UDP-glucose (substrate) or UDP (product) in the active site show an inward orientation of the finger helix and a gating loop conformation deeply inserted into the substrate-binding pocket, where many of the loop's residues, and in particular the conserved FXVTXK motif, directly coordinate the uracil base and the pyrophosphate of the UDP moiety regardless of the translocation state of the co-crystallized oligosaccharide (Morgan, McNamara and Zimmer 2014; Morgan *et al.* 2016) (Fig. 2B). In addition, a low-resolution crystal structure of a proposed pre-translocation state that is c-di-GMP-bound and contains no UDP-based moiety, shows a largely disordered gating loop with an overall trajectory similar to that of the UDP-bound but c-di-GMP-free state (Morgan, Strumillo and Zimmer 2013; Morgan *et al.* 2016) (Fig. 2B). The finger helix ('in') and oligosaccharide positions (pre-translocated) are also similar between the two structures. Together, these observations suggest that either release of c-di-GMP or UDP can initiate relaxing of the gating loop and finger helix-assisted polysaccharide translocation and that alternative paths for substrate reentry are possible depending on the local concentrations in substrate, c-di-GMP and freed UDP (Fig. 2B). One should not forget that all of the crystallographically captured states are stabilized by lattice contacts and prolonged incubations with saturating concentrations of the observed ligands. In fact, although c-di-GMP binds to a well-defined cleft onto the BcsA surface, its complexation buries an overall small surface area (<800 $Å^2$) and BcsA can be rapidly inactivated by c-di-GMP-degrading phosphodiesterases, suggesting dinucleotide accessibility (Ross *et al.* 1987). Furthermore, although reported BcsA–c-di-GMP binding affinities differ significantly across accounts in the literature, they are likely in the micromolar, rather than nanomolar ranges (Weinhouse *et al.* 1997; Ryjenkov *et al.* 2006; Omadjela *et al.* 2013). This suggests that c-di-GMP binding to the PilZ domain is likely highly dynamic and perhaps its release from the PilZ domain is even required between catalytic cycles, to allow for efficient gating loop relaxation, product release and polymer translocation prior to c-di-GMP-mediated active site reopening (Fig. 2B).

BcsE and synthase-proximal c-di-GMP enrichment in *E. coli*-like cellulose secretion systems

As mentioned earlier, *E. coli*-like cellulose secretion systems comprise a specific set of accessory subunits, one of which is the cytosolic BcsE regulator (Römling and Galperin 2015). Although not absolutely required for cellulose secretion *per se*, BcsE has been shown to significantly boost cellulose production *in vivo* via a c-di-GMP-binding motif, R^{415}TGD, similar to the canonical RXXD I-site motif on GGDEF domain-containing diguanylate cyclases (Chan *et al.* 2004; De *et al.* 2008; Fang *et al.* 2014; Krasteva *et al.* 2017). Consequently, the conserved C-terminal part of the protein was defined as a novel c-di-GMP-sensing domain called GIL, for GGDEF I-site–Like domain (Fang *et al.* 2014). Based on crystallographic and functional data, we showed recently that BcsE actually features a tripartite architecture (Fig. 4). In it, an N-terminal catalytically incompetent ATPase-like domain mediates BcsE dimerization, participates in BcsF-mediated membrane recruitment and interacts with conserved transcription antitermination complex (TAC) components suggesting additional regulatory roles at the gene expression level (Zouhir *et al.* 2020). The postulated GIL domain, on the other hand, is actually a degenerate receiver–GGDEF domain tandem ($BcsE^{REC*\text{-}GGDEF*}$), where the divergent diguanylate cyclase module binds both c-di-GMP and BcsQ through mutually independent interfaces (Zouhir *et al.* 2020) (Fig. 4C–H). Disparate degrees of sequence conservation between the N-terminal module and the REC*-GGDEF* tandem, as well as the identification of organisms where the corresponding BcsE parts are encoded by separate genes, point toward multidomain BcsE evolution and function integration via separate gene fusion events (Zouhir *et al.* 2020).

Interestingly, whereas the $BcsE^{REC*\text{-}GGDEF*}$ tandem crystalizes as a protein dimer sharing a single splayed c-di-GMP moiety, solution thermodynamic characterization of the protein–ligand interaction pointed toward complexation of an intercalated c-di-GMP dimer to each molecule of BcsE (Zouhir *et al.* 2020). Complexation of c-di-GMP in its synthase-activating intercalated form was subsequently confirmed by the crystal structures of two different BcsE*-BcsRQ complexes, namely $BcsR_2$–$BcsQ^{R156E}{}_2$–ATP_2–$BcsE^{REC*\text{-}GGDEF*}{}_2$–c-di-$GMP_4$ (or, $BcsE^{REC*\text{-}GGDEF*}$–$BcsRQ^{R156E}$ for short) and $BcsR_2$–$BcsQ_2$–ATP_2–$BcsE^{GGDEF*}{}_2$–c-di-GMP_4 (or $BcsE^{GGDEF*}$–BcsRQ) (Abidi *et al.* 2021) (Fig. 4C–E). Surprisingly, in the c-di-GMP-bound $BcsE^{REC*\text{-}GGDEF*}$–$BcsRQ^{R156E}$ complex, the BcsE variant adopts a markedly different conformation from the structure of c-di-GMP-bound $BcsE^{REC*\text{-}GGDEF*}$ alone (Zouhir *et al.* 2020; Abidi *et al.* 2021) (Fig. 4C and D). Whereas the canonical I-site motif on the catalytically incompetent diguanylate cyclase module coordinates a c-di-GMP moiety as expected, the degenerate receiver domain and the so-called 'interstitial helix', linking it to the GGDEF* module, undergo a 144° rotation and 45 Å displacement to contribute a distinct conserved RXXD motif (R^{306}ATD) from the REC* domain and coordinate a second, intercalated with the first one, dinucleotide molecule via virtually identical arginine/aspartate-dependent interactions (Abidi *et al.* 2021) (Fig. 3D and F). BcsE's conformational flexibility is further evidenced by changes in the REC* domain orientation relative to the GGDEF* module not only between the different crystal structures but also between different $BcsE^{REC*\text{-}GGDEF*}$ protomers in the BcsRQ-bound structure (pdb 6ybb). The importance of the REC* domain I-site in dimeric c-di-GMP complexation was further confirmed by solution-based isothermal titration calorimetry experiments, where truncated ($BcsE^{GGDEF*}$) or point-mutant BcsE ($BcsE^{REC*\text{-}GGDEF*}$•$A^{306}$ATA) variants exhibited drastically altered thermodynamic profiles of the ligand-binding reactions (Abidi *et al.* 2021). Finally, the crystal structure of the $BcsE^{GGDEF*}$–BcsRQ complex showed an additional, crystallographic c-di-GMP-binding interface involving multiple π-stacking and polar interactions with residues from cognate BcsE ($R^{503}H^{504}$), BcsR ($R^{51}W^{52}$) and BcsQ (R^{219}) protomers and stabilized by a symmetry-related GGDEF* module in the crystals (Abidi *et al.* 2021) (Fig. 4). Although, the biological relevance of

this third dinucleotide binding site remains untested, it is possible that it contributes additional weak interactions within the assembled cellulose secretion machinery.

In summary, the assembled Bcs secretion macrocomplex contains a periplasmic crown of up to 6 BcsB copies, a single BcsA synthase, and a $BcsR_2Q_2E_2$ cytosolic regulatory complex that buttresses the synthase through BcsRQ–$BcsA^{PilZ}$ interactions on one side and is anchored to the inner membrane through $BcsE^{NTD}$–BcsF interactions on the other (Zouhir *et al.* 2020; Abidi *et al.* 2021) (Figs 3 and 4). In addition, one or two copies of the pEtN-transferase BcsG likely associate dynamically with the core biosynthetic machinery to introduce post-synthetic chemical modifications (see later), whereas interactions with the periplasmic and outer-membrane components BcsZ and BcsC remain to be experimentally characterized. The cryo-EM structure of the assembled Bcs macrocomplex confirms the high conformational variability of the $BcsE^{REC*\text{-}GGDEF*}$ tandem observed in the crystal structures as the corresponding electron densities could not be reliably resolved even upon focused refinement (Abidi *et al.* 2021). Importantly, such variability between the two modules and, by extension, in the composite c-di-GMP-binding site formed by the REC* and GGDEF* RXXD motifs could translate into conformation-dependent c-di-GMP binding affinities. The overall organization of the Bcs macrocomplex in the cryo-EM structure visualizes the formation of a multicomponent cytosolic vestibule, in which the BcsRQE subunits enclose the c-di-GMP-sensing $BcsA^{PilZ}$ module in its center and which would thus provide multiple c-di-GMP binding sites in immediate proximity to the processive cellulose synthase (Fig. 4). In a functional model where dimeric c-di-GMP can migrate out and in the $BcsA^{PilZ}$ cleft to allow gating loop relaxation and substrate entry between cycles of glucose-to-cellulose incorporation, the BcsRQE regulatory complex could thus secure a synthase-proximal pool of activating intercalated c-di-GMP that is recycled through only minor conformational changes (Abidi *et al.* 2021) (Fig. 3).

DGC specificity and synthase-proximal c-di-GMP synthesis and degradation

Regulation of cellulose synthesis by c-di-GMP is not only limited to its complexation at the $BcsA^{PilZ}$ cleft or even within the assembled Bcs secretion machinery. Studies on *E. coli* have shown that under physiological conditions the actual c-di-GMP levels in the cytosol are quite low, mainly due to efficient degradation of the dinucleotide by the phosphodiesterase PdeH. In particular cellular c-di-GMP concentrations were estimated to be in the low nanomolar range (Sarenko *et al.* 2017), which would prevent efficient complexation by the BcsA synthase. Whereas the formation of a multisite c-di-GMP-binding cytosolic complex around the $BcsA^{PilZ}$ module would secure retention of the activating dinucleotide in proximity to the synthase (Zouhir *et al.* 2020; Abidi *et al.* 2021), colocalization of system-specific c-di-GMP metabolizing enzymes with the Bcs system is likely to play key roles in cellulose biogenesis. Indeed, recent work showed that despite the simultaneous presence of multiple GGDEF and EAL domain-containing proteins in *E. coli* K-12, a single diguanylate cyclase—DgcC—is specifically required for pEtN-cellulose secretion (Richter *et al.* 2020). Furthermore, bacterial two-hybrid assays showed that DgcC interacts with a specific phosphodiesterase encoded by a gene proximal to the *bcs* operons—PdeK—and that both proteins interact with the BcsB co-catalytic subunit (Richter *et al.* 2020). This supports a model where few c-di-GMP molecules produced locally by the DgcC enzyme can dramatically increase the probability of c-di-GMP capture by the Bcs secretion machinery and thus lead to cellulose secretion activation *in vivo*. Furthermore, colocalization of the DgcC, PdeK and Bcs assemblies can secure not only efficient biosynthetic activity in an otherwise dinucleotide-poor environment, but also a built-in shut-down mechanism by a system-specific phosphodiesterase, when needed. Interestingly, expression of DgcC and its homologs (e.g. AdrA in *Salmonella*) is also subject to complex upstream regulation by c-di-GMP. It involves multistep transcription activation of the *csgD* gene whose product in turn activates the expression of both *dgcC/adrA* and the rest of the *csg* genes involved in curli secretion (Römling *et al.* 1998; Römling *et al.* 2000). In particular, *csgD* transcription is activated by the MlrA transcription activator upon interaction of the latter with the diguanylate cyclase DgcM, which in turn has to be released from inhibitory interactions with a specific 'trigger' phosphodiesterase, PdeR, by the stationary phase-induced diguanylate cyclase DgcE (Lindenberg *et al.* 2013; Sarenko *et al.* 2017; Pfiffer *et al.* 2019).

CsgD-dependent, DgcC-dependent cellulose secretion activation is likely not the only mechanism for Bcs system-specific c-di-GMP targeting among bacteria. Indeed, a study of multiple *E. coli* isolates revealed additional regulatory mechanisms including CsgD-independent pathways, as well as specific roles for alternative diguanylate cyclases (Da Re and Ghigo 2006). For example, in the commensal cellulose-secreting strain *E. coli* 1094, DgcC is only weakly expressed and cellulose secretion is instead activated in a CsgD-independent manner by the constitutively active diguanylate cyclase DgcQ (Da Re and Ghigo 2006). This, together with the widespread requirement for c-di-GMP-dependent activation across EPS-secretion systems in general, highlights further both the universality of c-di-GMP as a master regulator of biofilm formation, as well as the extraordinary versatility of its specific mechanisms of action (Jenal, Reinders and Lori 2017; Krasteva and Sondermann 2017; Low and Howell 2018). In addition, the multilevel structural and functional interactions among enterobacterial Bcs components and coupled c-di-GMP metabolizing enzymes described earlier represents a paradigm of remarkable secretion system cooperativity at the genomic, transcriptional, translational and posttranslational levels.

PROTEINS AND FEATURES INVOLVED IN CELLULOSE CRYSTALLINITY

BcsD and BcsH

BcsD is a small, ~17 kDa protein, which is hallmark for Type I Bcs operons that are found in certain alpha, beta and gamma-Proteobacteria, including *G. xylinus* (Römling and Galperin 2015). Although BcsD is not essential for cellulose secretion, disruption of the BcsD-coding gene in the latter led to significant defects in the quantity and crystallinity of the secreted polysaccharide (Saxena *et al.* 1994). As opposed to the rugose colonies of the wild-type *G. xylinus* cells, the *bcsD* mutant exhibited phenotypic variation of large and small smooth colonies, where the former were characterized by complete and irreversible loss of cellulose secretion. Interestingly, however, membrane preparations of both small and large colony variants had preserved *in vitro* cellulose synthase activities, indicating that the BcsD-dependent effects were downstream of the cellulose polymerization itself. In addition, the *bcsD* mutant produced a combination of crystalline cellulose I ribbons, as well as irregular rodlets of

the cellulose II allomorph, strongly suggesting that the protein contributes to the rate-limiting step of cellulose crystallization (Benziman *et al.* 1980; Saxena *et al.* 1994).

Although BcsD does not have a detectable signal peptide or other type of export signal (Almagro Armenteros *et al.* 2019), fractionation experiments on *G. xylinus* cells showed that the protein partitions in the periplasm, consistent with its role downstream of BcsAB-dependent cellulose polymerization and inner-membrane extrusion (Iyer *et al.* 2011) (Fig. 5A). Crystal structures of the $BcsD^{G.xylinus}$ protein showed that it assembles in a cylinder-shaped head-to-tail tetramer of head-to-head dimers with a large central pore harboring the extended N-termini of the 8 protomers (Hu *et al.* 2010) (Fig. 5B). Interestingly, cellopentaose-soaked crystals show that four oligosaccharide molecules bind within the lumen of the octamer; however, each is guided through an individual passageway formed by the inward-protruding BcsD N-termini. Furthermore, plasmid-based expression of BcsD variants carrying N-terminal deletions missing the Lys^6 residue or beyond failed to complement the cellulose secretion defect in a Δ*bcdD* deletion strain (Hu *et al.* 2010). Together, these data are consistent with a model where BcsD acts in the periplasm to guide the outgoing polysaccharide chains toward the outer-membrane BcsC; however, it remains to be determined whether BcsD primes the cellulose toward structured bundling before exiting the cell or, conversely, prevents non-specific aggregation and secretion abortion. Overall, the broader BcsD distribution across multiple species secreting amorphous cellulose (Römling and Galperin 2015) indicates that BcsD function alone is generally not sufficient for crystalline cellulose secretion.

Whereas BcsD is not limited to the *Gluconacetobacter* lineage, it has been shown to directly interact with a *Gluconacetobacter*-specific protein—BcsH or CcpA—that is essential for cellulose secretion in both *G. xylinus* and *G. hansenii* (Standal *et al.* 1994; Deng *et al.* 2013; Sunagawa *et al.* 2013). Fluorescence microscopy imaging in *G. xylinus* showed that both BcsD and BcsH feature the longitudinal linear localization pattern characteristic for the so-called cellulose synthase terminal complexes (TC) and that BcsD localization was severely disrupted in a *bcsH*-knockout background (Sunagawa *et al.* 2013) (Fig. 5C).

The proposed *bcsH* open reading frame encodes a ∼37 kDa protein, which similarly to BcsD does not feature a detectable signal peptide for periplasmic sorting. Remarkably, the primary structure of the protein features very high content of proline (∼18–21%) and other small neutral amino acids suggesting an intrinsically disordered tertiary fold. Proline-rich regions in general can play important roles in signaling and scaffolding proteins and, in bacteria, can act as peptidoglycan-spanning structural or functional modules (Williamson 1994). Nevertheless, expression constructs encoding full-length and N-terminally truncated BcsH-EGFP variants based on alternative translation initiating codons within the *bcsH* gene invariably led to the expression of a fluorescently tagged ∼8 kDa protein corresponding to the C-terminal region of the annotated amino acid sequence (Sunagawa *et al.* 2013). Moreover, the truncated BcsH variant recovered to a greater extent cellulose secretion activities in the Δ*bcsH* mutant, raising the possibility that the actual essential BcsH subunit is indeed a short periplasmic polypeptide capable to tether BcsD and thus stabilize the linear TC nanoarray for crystalline cellulose secretion. However, the exact molecular mechanisms through which the BcsD and BcsH subunits cooperate to yield high-quality crystalline cellulose *in vivo* remain to be further examined.

Linear TC arrays, cortical belt and role of the cellulose ribbon

Over the last half century, multiple studies have examined the factors affecting crystalline cellulose secretion. Some of the earliest observations involved negative-stain and freeze-fracture electron microscopy experiments, that visualized the lengthwise linear arrangement of *G. xylinus* cellulose synthase TCs, coinciding with points of microfibril secretion and bundling into a crystalline cellulose ribbon (Brown, Willison and Richardson 1976). Recent *in vitro* studies on the *Rhodobacter sphaeroides* BcsAB tandem, known to secrete amorphous cellulose in nature, showed that simple nickel-film immobilization of the purified $BcsA^{His}$–$BcsB^{R.sphaeroides}$ complex can already lead to formation of crystalline cellulose II microfibrils (Basu *et al.* 2016), further supporting a model where cellulose crystallinity in nature is predetermined by the spatial organization of cellulose synthase complexes.

Interestingly, the observed *G. xylinus* TC topology was found to be sensitive to mechanical stress (such as culture agitation or centrifugation), culture media (such as pellicle formation on liquid media vs colony growth on agar) or cellulase treatment. Specifically, only conditions leading to or preserving cellulose crystallinity—i.e. static growth of air–liquid pellicles in the absence of cellulase—correlated with linear TC arrangement (Saxena *et al.* 1994), suggesting an outside-in reinforcement of the TC nanoarray and crystallinity itself by the nascent cellulose ribbon.

In addition, a recent *in situ* cryo-electron tomography study on *G. xylinus* and *G. hansenii* (Nicolas *et al.* 2021) identified a novel cytosolic structure—the cortical belt—that spatially correlates with the extracellular cellulose ribbon (Fig. 5A, D and E). Although the protein content of the cortical belt remains to be determined, it is morphologically reminiscent of belt-like cytoskeletal structures formed by bactofilins or the CTP synthase (Ingerson-Mahar *et al.* 2010; Kühn *et al.* 2010; Deng *et al.* 2019). The structure, tens of nanometers wide and hundreds of nanometers long, was found to be resistant to cellulase treatment and to localize at a fixed distance of ∼24 nm from the inner membrane, most often in several stacked sheets spaced by ∼15 nm. Moreover, it appeared to be specific for the *Gluconacetobacter* lineage, as it was not observed neither in amorphous cellulose-secreting *E. coli* 1094 cells, nor in *A. tumefaciens*, which secretes crystalline cellulose I microfibrils at the cell pole but not higher order organized cellulose ribbons (Nicolas *et al.* 2021). The similarity of the cortical belt with cytoskeletal elements and its spatial correlation with the nascent cellulose ribbon led the authors to propose that indeed it could be a *Gluconacetobacter*-specific cytoskeletal element that similarly to the cortical microtubules in plants organizes the membrane-embedded cellulose synthase complexes (Paredez, Somerville and Ehrhardt 2006; Li *et al.* 2012a; Purushotham, Ho and Zimmer 2020; Nicolas *et al.* 2021). If such a model is correct, it remains to be determined how the large space between the inner membrane and the cortical belt is bridged, given that the known intracellular domains of BcsA only protrude ∼4–5 nm inward from the inner-membrane plane, and whether additional *Gluconacetobacter* proteins could serve as counterparts of the plant Cellulose Synthase Interactive (CSI) proteins that secure the physical and

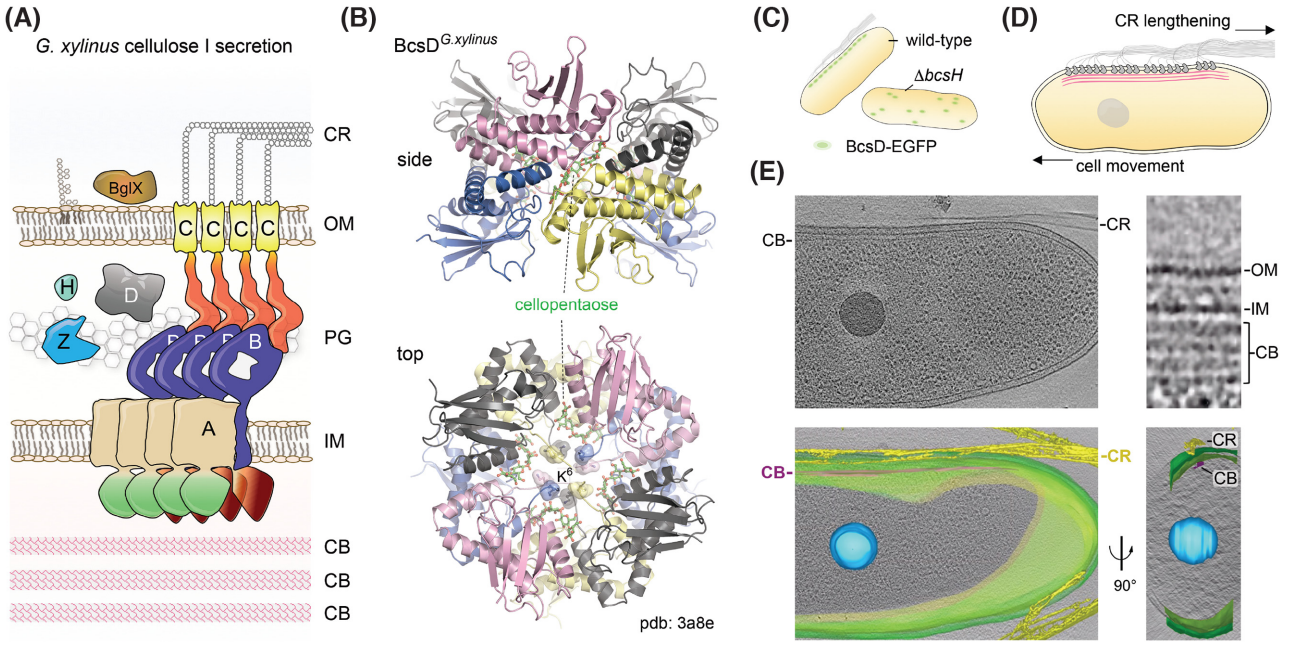

Figure 5. Crystalline cellulose secretion. **(A)** Thumbnail representation of the *G. xylinus*/*G. hansenii* type I cellulose secretion system. CB, cortical belt; IM, inner membrane; PG, peptidoglycan; OM, outer membrane; CR, crystalline cellulose ribbon. **(B)** Crystal structure of cellopentaose-bound BcsD octamers from *G. xylinus* (pdb 3a8e) (Hu *et al.* 2010). The BcsD octamer is organized as a head-to-tail tetramer of head-to-head dimers. The N-proximal K^6 residues are shown as sticks and transparent surface. The oligosaccharides occupy four independent passageways along each dimer–dimer interface and are separated by the protein N-termini in the central cavity. **(C)** Schematic representation of BcsH-dependent BcsD localization and cellulose secretion *in vivo*, based on Sunagawa *et al.* (2013). **(D)** Schematic representation of linear *G. xylinus*/*G. hansenii* terminal complex (TC) organization and crystalline ribbon secretion via interactions with the underlying cortical belt cytoskeleton. Upon crystalline cellulose ribbon elongation, the cortical belt-tethered TCs would lead to proportional cell displacement in the opposite direction. Based on Brown *et al.* (1976) and Nicolas *et al.* (2021). **(E)** Cryo-electron tomography visualization of the cellulose ribbon and cortical belt. Data from Nicolas *et al.* (2021), reproduced under the CC BY 4.0 license (https://creativecommons.org/licenses/by/4.0/legalcode). Top left, a snapshot of a vitreous ice-embedded *Gluconacetobacter* cell showing longitudinal cellulose ribbon (CR) and cortical belt (CB) polymers. Bottom left, representation of the same cell with reconstructed storage granule (blue), cell membranes (green), cortical belt (purple) and extracellular cellulose ribbon (yellow). Bottom right, the same segmentation rotated by ∼90° showing the tape-like organization of the cortical belt and its spatial colocalization with the secreted cellulose ribbon. Top right, a zoom-in of the cell envelope showing electron densities for the outer membrane (OM), inner membrane (IM) and stacked cortical belt (CB) layers.

functional crosstalk between the cellulose synthase rosettes and the cortical cytoskeleton (Li *et al.*2012a).

POST-SYNTHETIC CHEMICAL MODIFICATIONS OF THE SECRETED CELLULOSE

BcsG and pEtN-cellulose

Together with BcsE and BcsF, BcsG is a hallmark protein for the *E. coli*-like type of cellulose secretion systems and the three proteins are often found encoded by a separate operon next to the BcsRQABZC-encoding *bcs* gene cluster (Römling and Galperin 2015). BcsG is a ∼60 kDa protein and is essential for cellulose secretion in some, but not all, cellulose-producing strains (Krasteva *et al.* 2017; Sun *et al.* 2018; Thongsomboon *et al.* 2018). *In cellulo* bacterial two hybrid assays showed consistently that the protein interacts with BcsA, likely through an N-terminal extension characteristic for *E. coli*-like homologs of the synthase, as well as with its intraoperon partner BcsF (Krasteva *et al.* 2017; Thongsomboon *et al.* 2018). Structurally, the protein comprises a membrane-anchored N-terminal domain predicted to fold into five transmembrane and two short, periplasm-exposed amphipathic α-helices, a likely disordered ∼30-residue-long linker and a C-terminal alkaline phosphatase-like domain (Kim, Chivian and Baker 2004) (Fig. 6A and B). Recent works demonstrated that BcsG is responsible for decorating the nascent polysaccharide with zwitterionic pEtN residues—likely sourced from inner-membrane phosphatidylethanolamine lipids—to provide specific architecture and tensile strength of the mature biofilms via interactions with secreted amyloid curli (Hollenbeck *et al.* 2018; Thongsomboon *et al.* 2018). BcsG's native interactions with BcsA also appear to assist the assembly of the synthase within the inner-membrane biosynthetic complex, as a *bcsG* deletion in *Salmonella typhimurium* severely decreased not only the efficiency of cellulose secretion, but also the total amount of detectable BcsA in the mutant (Sun *et al.* 2018). The same study also showed that while the BcsG N-terminal transmembrane domain was necessary for proper BcsA sorting and integrity, a catalytically active C-terminal domain determined the efficiency of cellulose secretion regardless of the BcsA levels.

Two recent reports presented high-resolution crystal structures of the C-terminal catalytic domains of $BcsG^{S.typhimurium}$ (Sun *et al.* 2018) and $BcsG^{E.coli}$ (Anderson *et al.* 2020). The two proteins feature only a few amino acid substitutions in their primary structures and as expected are virtually identical in 3D (R.M.S.D. of ∼0.4 Å over all atoms) (Fig. 6B). As expected, the protein adopts a conserved alkaline phosphatase-like fold. Although sharing only limited sequence identity (11–13%), the 3D fold of $BcsG^{CTD}$ showed high structural homology with other pEtN- and phosphoglycerol (PG)-transferases, such as the mobile colistin resistance factor (MCR-1) from *E. coli* (Stojanoski *et al.* 2016),

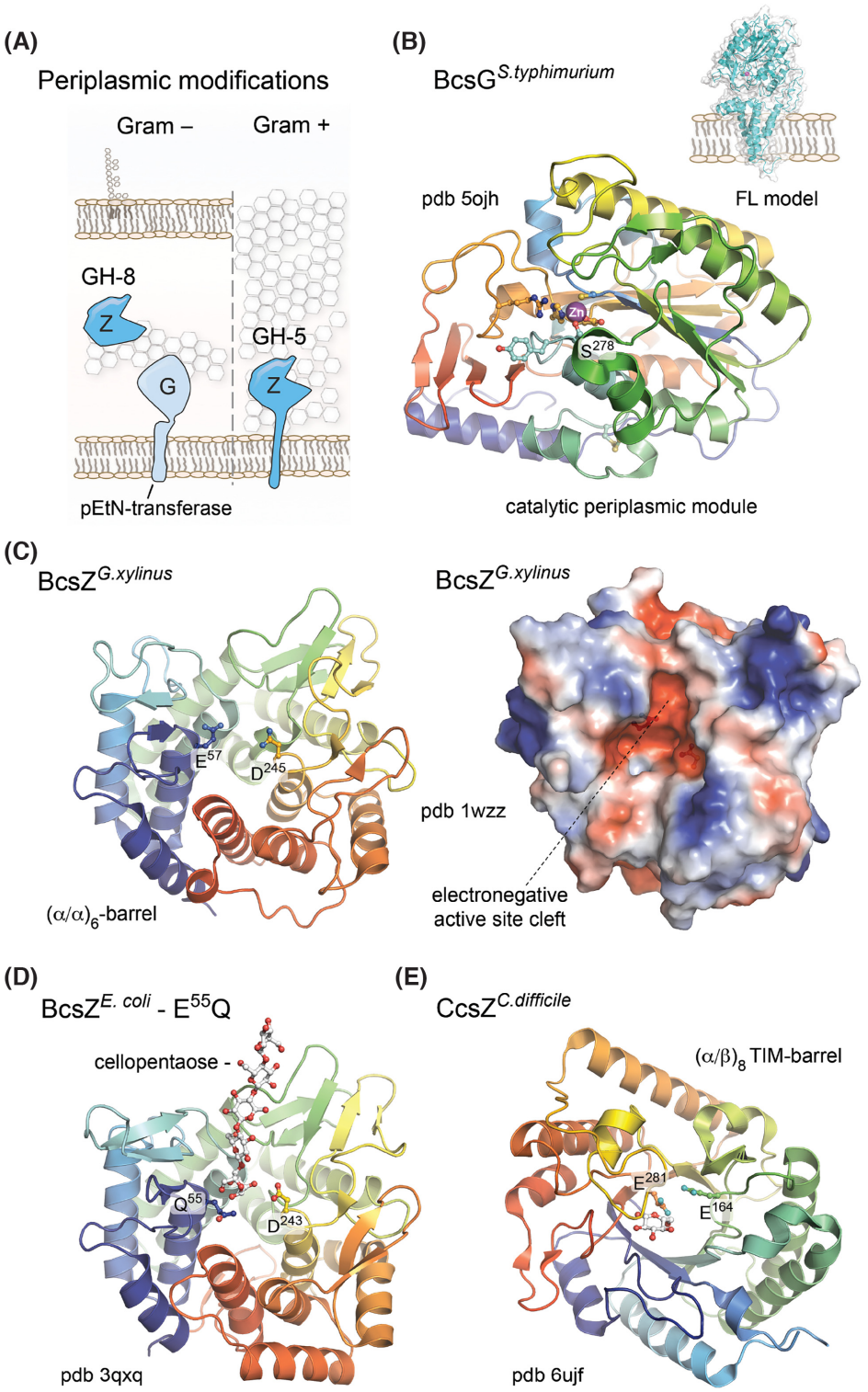

Figure 6. Prevalent periplasmic modifications. **(A)** Thumbnail representation of the BcsG pEtN-transferase and BcsZ functional homologs in Gram-negative and Gram-positive species. **(B)** Crystal structure of the BcsG periplasmic domain showing the overall fold of the catalytic module and Zn++ coordination in the active site. Key residues involved in cation coordination and/or essential for the pEtN modification are shown as sticks. Based on Sun *et al.* (2018) and Anderson *et al.* (2020). Inset, Robetta-modeled full-length BcsG. **(C)** Crystal structure of the *G. xylinus* BcsZ homolog (Yasutake *et al.* 2006). Left, cartoon representation showing the conserved $(\alpha/\alpha)_6$-barrel fold and the catalytic dyad of acidic (D/E) amino acids as sticks. Right, surface electrostatic potential shown as a red (negative)–blue (positive) gradient. **(D)** Crystal structure of a cellopentaose-bound catalytically inactive mutant of *E. coli* BcsZ (Mazur and Zimmer 2011). The oligosaccharide and catalytic dyad are shown as sticks. **(E)** Crystal structure of the *C. difficile* CcsZ, showing the $(\alpha/\beta)_6$ TIM-barrel fold in cartoon and the catalytic dyad as sticks. A single glucose molecule is also seen bound to the protein.

its homolog from *Neisseria meningitidis*—the lipooligosaccharide pEtN-transferase *Nm*EptA (Anandan *et al.* 2017), the PG transferase LtaS involved in lipoteichoic acid synthesis in *Listeria monocytogenes* and other Gram-positive pathogens (Lu *et al.* 2009; Campeotto *et al.* 2014), as well as the enterobacterial lipopolysaccharide (LPS) biogenesis factor PbgA (Clairfeuille *et al.* 2020). The core of the domain adopts a seven-stranded mixed β-sheet sandwiched between several α-helices. A second β-sheet of four short antiparallel β-strands forms at the very C-terminus of the protein and stacks between active site-proximal regions the central core and the N-terminal helix of the crystallized module (Fig. 6B). Both structures identify a single Zn ion at the active site, coordinated by a structural water molecule and the side chains of Cys^{243}, Ser^{278}, Glu^{442}, and His^{443}, all of which are essential for the protein's function (Sun *et al.* 2018; Anderson *et al.* 2020). The protein also features a conserved and functionally important intramolecular disulfide bond between residues Cys^{290} and Cys^{306}, which is proposed to orient the catalytic nucleophile, Ser^{278}, toward the active-site Zn ion (Anderson *et al.* 2020). Additional residues lining the active site pocket and specific for BcsG homologs, such as Arg^{458} and Tyr^{277}, were found to be key to the protein's function, possibly through interaction with the glucan substrate. Finally, the purified monomeric $BcsG^{CTD}$ modules were shown to be able to both cleave specifically phosphatidylethanolamine lipids (Sun *et al.* 2018) and to transfer pEtN moieties onto cellulose-like oligosaccharides from a chromogenic substrate analog (Anderson *et al.* 2020).

We showed previously that BcsG does not co-purify stably with the BcsRQABEF macrocomplex upon co-expression of all seven subunits and purification through epitope tags on BcsA, and high-resolution cryo-EM data confirmed that the periplasmic crown of the purified assembly is composed exclusively of a superhelical arrangement of BcsB periplasmic domains (Krasteva *et al.* 2017; Abidi *et al.* 2021). A subsequent, lower-resolution cryo-EM study on a similar Bcs assembly pinpointed that at low visualization thresholds of the electron density reconstruction, a featureless blob appears within the periplasmic regions opposite the BcsB crown, whereas streaks of density in the detergent micelle reminiscent of transmembrane helices were attributed to two copies of BcsG's transmembrane domains. Based on this, the authors proposed that a dimer of BcsG is an integral part of the inner-membrane biosynthetic platform (Acheson *et al.* 2021).

Such a model should be treated with caution, however, as density artifacts are common at the low reconstruction resolutions and visualization thresholds presented in the study. Although conformational heterogeneity can lead to specific densities being averaged out during 3D reconstruction, no BcsG-attributable densities in the well-resolved periplasmic crown were evident in representative molecular views, or 2D class averages, in either of the two recent cryo-EM studies (Abidi *et al.* 2021; Acheson *et al.* 2021), nor in the original report on the Bcs macrocomplex assembly, which used mildly crosslinked sample in high-contrast negative-stain (Krasteva *et al.* 2017). In fact, while streaks of electron density within the micelle region are interpreted as two copies of the putative BcsG transmembrane domains, almost half of the membrane-associated protein content in the purified complex (e.g. unresolved N-terminal regions of BcsA, the transmembrane helices of BcsF, the majority of BcsB tail anchors and any peripheral density contributions from BcsE upon its membrane recruitment) remains unaccounted for in the structural model (Acheson *et al.* 2021). In addition, BcsG's catalytic domain purifies and is catalytically active as a monomer, and crystallographic packing analyses of the deposited $BcsG^{CTD}$ structures do not consistently identify a putative dimerization interface (Krissinel and Henrick 2007; Sun *et al.* 2018; Anderson *et al.* 2020). Similarly, while some distantly homologous alkaline phosphatase-like proteins have been proposed to oligomerize (Dalebroux *et al.* 2015; Hu *et al.* 2016), most of the reported mechanistic studies on active pEtN-transferases or other structural homologs present monomeric structures and no substrate- or product-determined prerequisite for oligomerization (Lu *et al.* 2009; Schirner *et al.* 2009; Campeotto *et al.* 2014; Anandan *et al.* 2017; Clairfeuille *et al.* 2020; Fan *et al.* 2020). Finally, no binary BcsG–BcsG interactions were detected in bacterial two-hybrid assays *in cellulo* neither in our original report on the system (Krasteva *et al.* 2017), nor in the subsequent study that revealed the functional role of the BcsG subunit (Thongsomboon *et al.* 2018).

Important aspects of BcsG function that have not yet been investigated are the substrate and byproduct of the enzymatic reaction itself, namely the need for a significant flux of phosphatidylethanolamine (PE) toward the outer leaflet of the inner membrane, as well as the release of a diacylglycerol (DAG) moiety for each pEtN addition onto the nascent polysaccharide. Zwitterionic PE is the major phospholipid in bacteria, comprising ~75% of the phospholipid content in *E. coli* (Sohlenkamp and Geiger 2016). About half of it is found in the inner membrane, with a significant asymmetry between its inner and outer leaflets (75% vs 25%, respectively, in rod-shaped bacteria) (Bogdanov *et al.* 2020). This asymmetric distribution is determined by the relatively small headgroup of the phospholipid and its preference for negative membrane curvature; however, PE distribution is highly dynamic and can be affected by multiple factors such as the metabolic state, cell shape and biosynthetic needs of the bacterium (Bogdanov *et al.* 2020). DAG, on the other hand, is a minor lipid in the bacterial envelope and generally a precursor for the synthesis of various phospholipids (Sohlenkamp and Geiger 2016). It has an even smaller head group than PE and a propensity to introduce localized hotspots of negative curvature and phase separations in the membrane, and in higher organisms can act as an important second messenger in a variety of cellular processes (Carrasco and Mérida 2007). It is therefore intriguing that BcsG both uses and produces lipids that are not normally enriched in the outer leaflet of the inner membrane. It remains to be determined if the enzyme's activity and the ensuing localized changes in the membrane's lipidic content can affect the asymmetric assembly of the Bcs biosynthetic complex as a whole. As we showed recently (Abidi *et al.* 2021), Bcs macrocomplex assembly and specifically the superhelical crown polymerization of tail-anchored BcsB would likely introduce significant tension or localized deformation in the underlying membrane. While purified, detergent-solubilized BcsB is able to spontaneously oligomerize to even higher order assemblies than the hexamer typically observed in the crown (Abidi *et al.* 2021) (Fig. 3D); *in vivo* crown polymerization could be dependent not only on its interactions with the rest of the Bcs subunits but also on specific membrane microdomains resulting from the pEtN-transferase enzymatic activity.

Natural cellulose acetylation

Although reported as such recently (Thongsomboon *et al.* 2018), pEtN-cellulose is neither the first described, nor the only chemically modified cellulose found in nature. *Pseudomonas fluorescens* SBW25 is an important biocontrol organism that lives in close association with plants and can promote plant growth

and prevent pathogen invasion by nutrient exchange, biosynthesis of phytohormones and secretion of antimicrobial compounds (Couillerot *et al.* 2009). The ecological success of the bacterium—and especially of efficient surface-colonizing and biofilm-secreting isolates such as the 'wrinkly spreader' (WS) variant—was found to depend on the expression of a 10-gene operon—*wssABCDEFGHIJ*—which leads to the overproduction of a cellulose-like extracellular polymer (Spiers *et al.* 2002; Gal *et al.* 2003; Spiers *et al.* 2003) (Fig. 1A). Chemical composition and linkage analyses of the secreted polysaccharide, conducted almost two decades ago, showed that it is in fact acetylated cellulose, in which ∼14% of the glucose units are acetylated at the C2, C4 or C6 positions (Spiers *et al.* 2003).

Equivalents of the *wss* locus are found in only a few species (Bundalovic-Torma *et al.* 2020) and include a typical Bcs operon core encoding homologs of BcsA (WssB), BcsB (WssC), BcsZ (WssD) and BcsC (WssE), as well as one or two BcsQ counterparts (WssA and WssJ). The remaining Wss proteins are proposed to assemble into a cellulose O-acetylation complex and, based on sequence homology and predicted tertiary folds, likely share structural and functional features with the AlgX (WssF), AlgF (WssG), AlgI (WssH) and AlgJ (WssI) components of the *P. aeruginosa* alginate acetylation machinery (Spiers *et al.* 2002; Riley *et al.* 2013). As *P. fluorescens* has a separate and more conserved gene cluster for the synthesis and chemical modification of alginate (Spiers *et al.* 2003), it is possible that the emergent *wssFGHI* locus has been hijacked by the cellulose secretion system for polysaccharide-specific O-acetylation.

Acetylated capsular or secreted polysaccharides are a recurrent feature across the bacterial kingdom and several synthase-dependent systems, such as the widespread PNAG or Pel secretion assemblies (Bundalovic-Torma *et al.* 2020), are dedicated to secrete *N*-acetylated polysaccharides where the chemical modifications occur onto the sugar precursors prior to polymerization and inner-membrane extrusion (Franklin *et al.* 2011; Low and Howell 2018). In contrast, O-acetylation of cellulose, alginate and, likely, other extracellular polysaccharides, employs an alternative strategy similar to the pEtN addition, in that chemical modifications are introduced onto the polymeric substrate only after its exit from the inner-membrane synthase. This process requires transfer of each acetyl moiety from a cytosolic donor (e.g. an acyl-carrier protein or metabolic acetyl-CoA) through the inner membrane by a polytopic membrane-bound O-acyltransferase (MBOAT) and onto a periplasmic set of polysaccharide-specific acyltransferases for O-acetylation at the polymer level (Franklin *et al.* 2011).

In *P. aeruginosa* alginate secretion, the MBOAT function is carried out by AlgI, with which WssH shares 42% identity and 64% similarity at the sequence level. Although structural information for both proteins is currently lacking, several structures of MBOAT-family acyltransferases were recently reported, including crystal structures of the *Streptococcus thermophilus* DltB, whose homologs are involved in O-alanylation of surface lipoteichoic acids in Gram-positive bacteria (Ma *et al.* 2018). WssF shares 22% sequence identity and overall 47% similarity with DltB and is predicted to adopt a similar transmembrane fold with the addition of a C-terminal 2-helix extension (Kim, Chivian and Baker 2004; Kelley *et al.* 2015). In DltB, a ring of peripheral transmembrane helices encloses a highly conserved extracellular funnel that extends inward to the middle of the lipid bilayer and connects to the cytosol via a narrow passage for entry of the carrier-linked substrate. The catalytic histidine residue, which is strictly preserved among MBOAT family members (His^{336} in $DltB^{S.thermophillus}$ and His^{322} in $WssH^{P.fluorescens SWB25}$), is positioned at the bottom of the funnel and at the end of the putative substrate passage where the central protein core is significantly thinner. This central thinning is achieved through the protein folding into several short horizontal helices partially exposed to the cytosol and leads to an overall biconcave cross-section that could facilitate cross-membrane catalysis (Ma *et al.* 2018).

In the periplasm, the acetyl moieties are transferred from AlgI/WssH onto the nascent polysaccharides by the periplasmic acyltransferases AlgJ/WssI and AlgX/WssF (Franklin *et al.* 2011; Riley *et al.* 2013). All four proteins belong to the SGNH (Ser-Gly-Asn-His) hydrolase superfamily and likely use a set of conserved Gly residues and Ser-His-Asp catalytic triads for acetyl transfer (Riley *et al.* 2013; Baker *et al.* 2014). Whereas the protein folds and catalytic residues involved in sugar modification have been fairly well characterized for the alginate homologs, it is unclear how and in what form the acetyl moieties are transferred from the core of the AlgI/WssH MBOAT domain to the active sites of these periplasmic enzymes. AlgJ and WssI are single-domain, N-terminally membrane-anchored proteins that share 28% identity and 47% similarity in primary structure. AlgX and WssF, on the other hand, are found in the periplasm, do not share significant sequence homology and AlgX contains a C-terminal carbohydrate binding module in addition to its acyltransferase domain, whereas WssF is predicted to adopt a minimal SGNH hydrolase-like fold (Riley *et al.* 2013; Kelley *et al.* 2015). Finally, the periplasmic AlgF/WssG subunits, which share 22% sequence identity and 40% similarity, are predicted to fold in a tandem of immunoglobulin-like modules (Kelley *et al.* 2015) that likely act as structural adaptor proteins within the O-acetylation complex.

Disruption of the O-acetylation components in the WS *P. fluorescens* genetic background led to overall preserved cellulose secretion; however, the non-acetylated biofilm pellicles were characterized by reduced thickness and strength, whereas colony growth on agar showed loss of the characteristic rapid and wrinkly expansion and instead yielded a relatively compact and smooth colony morphotype (Spiers *et al.* 2003). Interestingly, similar pellicle fragility, as well as significantly altered colony morphology were observed upon BcsG disruption in pEtN-cellulose-secreting *E. coli* (Thongsomboon *et al.* 2018). Moreover, mature WS *P. fluorescens* biofilms were found to contain not only acetylated cellulose, but also significant amounts of a proteinaceous Congo Red-binding extracellular matrix component, likely similar to the pEtN-cellulose-interacting amyloid curli of enterobacteria (Spiers *et al.* 2003; Hollenbeck *et al.* 2018). This, together with the lack of a BcsG homolog encoded in the *wss* gene cluster, suggests that cellulose acetylation might have evolved as an alternative to the pEtN-transfer strategy for polymer modification, to provide similar tensile strength and interaction propensities within the mature extracellular matrix.

Although the *wss* gene cluster is only found in a few species (Bundalovic-Torma *et al.* 2020), secretion of acetylated cellulose might be more widespread in nature. For example, some *Gluconacetobacter* strains encode two additional Bcs genes—BcsX and BcsY—of which the former is essentially a WssF homolog, whereas the latter is predicted to be a polytopic inner-membrane acyltransferase (Spiers *et al.* 2002; Römling and Galperin 2015). In addition, recent work identified putative Bcs-like operons among cellulose-secreting Gram-positive Clostridia, which—besides functional homologs of the BcsA, BcsB and BcsZ core subunits—also encode putative counterparts of the WssI and WssH O-acetylation components (Scott *et al.* 2020) (Fig. 1A). Separate studies have also directly reported secretion of acetylated glucose-based polymers in different clostridial

species (Häggström and Förberg 1986; Dannheim *et al.* 2017). Nevertheless, how these bacteria secrete acetylated cellulose and what are the specific physiological roles of the polymer in nature, remains to be further examined.

Periplasmic and extracellular glucan hydrolysis

Bacterial cellulose and exopolysaccharides in general are often substrate for secretion-system specific EPS-degrading enzymes encoded within the same gene clusters as the rest of the biogenesis components (Römling and Galperin 2015; Low and Howell 2018). Examples include the PgaB and PelA proteins, which integrate both hydrolase and deacetylase activities and are each involved in PNAG or Pel biosynthesis, as well as AlgL and BcsZ, which are an alginate exolyase and an endocellulase in their respective EPS secretion systems (Low and Howell 2018). Even higher plants utilize a membrane-anchored endoglucanase named Korrigan (KOR) for cellulose secretion and correct assembly of the primary cell wall (Nicol *et al.* 1998).

The ubiquitous presence of EPS-degrading enzymes across the various biosynthetic machineries appears paradoxical and their roles remain enigmatic. On one hand, exogenously added hydrolases can disrupt and prevent biofilm formation thus making them potential therapeutic agents in biofilm-related diseases (Baker *et al.* 2016); on the other, endogenously expressed EPS hydrolases, such as *S. typhimurium* BcsZ, can act as virulence-promoting factors (Ahmad *et al.* 2016). In yet other cases, the enzymes can be beneficial for both colonizing bacteria and the host, as is the case with the white clover microsymbiont *Rhizobium leguminosarum*: Its BcsZ homolog is required for eroding the noncrystalline tips of the root-hair wall in the host, thus allowing bacterial penetration and establishment of canonical symbiotic infection (Robledo *et al.* 2008).

Interestingly, both BcsZ overexpression and *bcsZ* deletion can have deleterious effect on the actual cellulose production. Whereas the overexpression phenotypes can typically be explained with overdigestion of the secreted polysaccharide, the stimulatory effects at wild-type BcsZ levels are more subtle. Disruption of the *bcsZ* gene in *G. xylinus*, for example, has been shown to inhibit cellulose secretion by inducing irregular packing and hypertwisting of *de novo* synthesized fibrils (Nakai *et al.* 2013), suggesting that the protein can relieve fiber torque to promote microfiber alignment and crystalline cellulose biogenesis. Conversely, it has been proposed that limited BcsZ activity can increase the rate of cellulose secretion by actually yielding more disperse microfibrils and thus minimizing the rate-limiting step of cellulose crystallization (Benziman *et al.* 1980; Kawano *et al.* 2002). As the protein is required for optimal cellulose secretion not only in crystalline, but also in amorphous cellulose-secreting bacteria (Koo *et al.* 1998; Ahmad *et al.* 2016) and actually exhibits significantly higher activity toward noncrystalline cellulose as a substrate (Mazur and Zimmer 2011; Omadjela *et al.* 2013), it is possible that it has more general roles such as minimizing abortive secretion and glucan aggregation in the periplasm or even releasing the exopolysaccharide from the cell surface and into the biofilm matrix.

The *G. xylinus* and *E. coli* BcsZ homologs are ~40 kDa, single-domain proteins from the GH-8 family of enzymes. Most secretion system models localize BcsZ to the periplasm, although certain reports on the *Gluconacetobacter* protein suggest it may perform its functions extracellularly (Koo *et al.* 1998; Yasutake *et al.* 2006). Crystal structures of the two homologs revealed the typical for GH-8 family enzymes $(\alpha/\alpha)_6$-barrel fold, in which 12 α-helices, with different degrees of distortion, alternate consecutively to form an outer and inner ring around the proteins' center (Yasutake *et al.* 2006; Mazur and Zimmer 2011) (Fig. 6C). The connecting loops feature extended conformations on one side of the barrel, forming a set of three or more short, antiparallel β-sheets that enclose a deep groove serving as the substrate binding pocket and carrying the putative pair of catalytic residues, D^{243} and E^{55} in $BcsZ^{E.coli}$, at its center (Fig. 6C). Analyses of the substrate-binding pocket of the two proteins and additional GH-8 family enzymes indicate that the saccharidic moieties are coordinated by a combination of side-chain and backbone hydrogen bonds, as well as stacking interactions with a set of conserved aromatic residues along the central cleft (Yasutake *et al.* 2006; Mazur and Zimmer 2011). $BcsZ^{G.xylinus}$ needs cellopentaose or longer polysaccharides for activity, whereas $BcsZ^{E.coli}$ appears to require at least a hexasaccharide (Kawano *et al.* 2002; Mazur and Zimmer 2011). In particular, the structure of a catalytically inactive, cellopentaose-bound $BcsZ^{E.coli}$ variant revealed that the protein contacts four of the five glucan moieties exclusively on the non-reducing end of its catalytic center in a conformation proposed to represent the post-hydrolysis state, where the newly formed nonreducing end has already left the substrate binding pocket (Mazur and Zimmer 2011) (Fig. 6D). Importantly, these structural analyses were performed before the recent discovery of the pEtN modification, so the binding and cleavage mechanisms of chemically modified enterobacterial cellulose require further investigation.

In addition to BcsZ homologs from the GH-8 family of endoglucanases, some bacteria and many fungi also encode a distinct cellulose-digesting enzyme, the secreted β-glucosidase BglX (Römling and Galperin 2015) (Fig. 1A). BglX homologs are ~80 kDa, typically dimeric proteins that contain at least one fibronectin type III-like domain, as well as a tandem of GH-3 N- and C-terminal domains involved in sugar hydrolysis. Although its role is less well studied, and in some organisms homologs can have specificities for saccharidic substrates other than cellulose (Mahasenan *et al.* 2020), BglX likely plays a similar role to that of BcsZ in quality control of the secreted polysaccharide and/or carving exogenous polymers found in the natural ecological niche (Römling and Galperin 2015). Finally, recent identification of putative clostridial cellulose synthase (*ccs*) operons demonstrated that the BcsZ functional homolog—CcsZ—is in fact a membrane-tethered β-(1,4)-endoglucanase belonging to the GH-5 family of enzymes (Scott *et al.* 2020) (Fig. 6A and E). The crystal structure revealed a typical for the family $(\alpha/\beta)_8$ TIM-barrel fold consisting of eight parallel β-strands forming a central barrel, and eight partially distorted α-helices that alternate with and pack against the core β-strands (Scott *et al.* 2020). The connecting loops C-terminal to each of the central β-strands extend to form a deep cleft accommodating the substrate and enzyme's active site. Although the enzyme shows high sequence and structure similarity to other GH-5 family enzymes with broad substrate specificities (e.g. *Thermotoga maritima* Cel5A; Wu *et al.* 2011), CcsZ displayed specificity for cellulosic materials (Scott *et al.* 2020). This, together with the presence of putative functional homologs of BcsA, BcsB and polysaccharide-specific acyltransferases (see earlier), further validates the proposed role for the *ccs* gene cluster in secretion of biofilm-promoting, acetylated clostridial cellulose (Scott *et al.* 2020).

BcsC AND BcsK: PERIPLASMIC SCAFFOLDS AND OUTER MEMBRANE EXTRUSION

In many, if not most cellulose-secreting Gram-negative bacteria, extrusion through the outer membrane is secured by homologs of the BcsC protein (Fig. 1A). Although its presence is not necessary for *in vitro* cellulose synthesis, disruption of the *bcsC* gene effectively abolishes cellulose secretion in the various species examined so far (Saxena *et al.* 1994; Matthysse, White and Lightfoot 1995; Omadjela *et al.* 2013; Krasteva *et al.* 2017). BcsC is a large, extracytosolic, ∼130 kDa protein, which after signal peptide cleavage assembles into an N-terminal periplasmic domain with multiple tetratricopeptide repeats (19 TPRs for the $BcsC^{E.coli}$) and a C-terminal β-barrel of ∼400 residues embedded as a porin in the outer membrane (Fig. 7). A minimal TPR motif contains two short α-helices and multiple such repeats are frequently found together in superhelical, or solenoid, assemblies (Zeytuni and Zarivach 2012). BcsC-like architectures are a recurrent theme among exopolysaccharide secretion systems, where TPR-rich periplasmic modules are thought to interact with the peptidoglycan, secure polysaccharide guidance and protection *en route* to the outer membrane, and act as docking platforms for additional secretion system components, whereas the porin domain secures processive passage through the lipidic bilayer of the outer membrane. Examples include PgaA from the PNAG secretion system, containing similar N-terminal TPR-rich and C-terminal porin domains; the PelE-PelB tandem from the Pel system where both proteins contribute periplasmic TPR modules and the latter also integrates a C-terminal porin domain; as well as the AlgK-AlgE duo from the alginate system serving as the TPR scaffold and outer membrane export protein, respectively (Franklin *et al.* 2011; Krasteva and Sondermann 2017; Low and Howell 2018).

The crystal structure of the last periplasmic TPR motif and C-terminal porin domain of the *E. coli* BcsC homolog ($BcsC^{E.coli}$•TPR^{19}–CTD) revealed a 16-stranded β-barrel with a large, ∼15 Å-wide, electronegative interior, which likely facilitates the insertion of hydrated zwitterionic pEtN-cellulose (Acheson, Derewenda and Zimmer 2019) (Fig. 7A and B). The eight extracellular loops (EL) connecting the barrel's β-strand pairs form a dome-like structure that shields approximately half of the extracellular channel opening (Acheson, Derewenda and Zimmer 2019). Channel permeability is likely controlled by a single constriction along the transmembrane lumen, close to the extracellular surface. This constriction is secured by the extracellular loop connecting β-strands 15 and 16 (EL^8, also dubbed 'gating loop'), which tilts inward and packs against conserved tyrosine residues from EL^6 (Y^{1025} and Y^{1030}) to prevent permeation of solutes in the visualized resting state (Acheson, Derewenda and Zimmer 2019) (Fig. 7A and B). The channel's lumen is lined with conserved polar and aromatic residues proposed to guide the secreted polysaccharide through both aromatic stacking and hydrogen bonding interactions; however, structural information of a translocating polymer is currently lacking. An interesting feature of the crystallized construct is the conformation of the extreme C-terminal tail of the protein. Namely, the last ∼15 residues fold back and penetrate the channel, where they are stabilized by a network of interactions to position the conserved C-terminal Y^{1157} midway across the lumen (Acheson, Derewenda and Zimmer 2019) (Fig. 7A). The stable conformation of the BcsC tail, its conservation among pEtN-cellulose-secreting species and absence among crystalline cellulose producers, as well as the conspicuous position of the C-terminal aromatic residue in the channel suggest that this peculiar BcsC feature might have functionally evolved for translocation of pEtN-modified cellulose (Fig. 7A and C).

In addition to the abovementioned studies, the structure of the periplasmic TPR-rich domain has also been examined experimentally. Size-exclusion chromatography-coupled, small angle X-ray scattering (SEC-SAXS) experiments on a construct covering most of the periplasmic TPR repeats from an enterobacterial BcsC homolog (*Enterobacter* CJF-002 $BcsC^{24\text{-}664}$; $TPR^{1\text{-}17}$) revealed an overall extended solenoid architecture typical for TPR-rich periplasmic scaffolds (Nojima *et al.* 2017) (Fig. 7D and E). Interestingly, a crystal structure of the six N-terminal repeats of the same protein (*Enterobacter* CJF-002 $BcsC^{24\text{-}272}$; $TPR^{1\text{-}6}$) carrying five protomers in the asymmetric unit revealed three distinct conformations that varied at the C-proximal hinge of a single α-helix insertion (α_5) between TPR2 and TPR3 (Nojima *et al.* 2017). Given that the inner-to-outer membrane distances and peptidoglycan thickness can vary significantly along the cell envelope, such conformational flexibility can provide additional adaptability of the system for efficient polymer protection and outer membrane extrusion.

A significant proportion of Gram-negative cellulose-secreting bacteria lack a BcsC homolog in their cellulose biosynthesis operons, but instead encode a distinct TPR-rich periplasmic protein, BcsK (Römling and Galperin 2015) (Fig. 1A). Unlike BcsC, BcsK does not contain a C-terminal porin domain, nor are genes in the immediate vicinity likely to compensate the porin function. It is therefore likely that the assembled Bcs secretion system uses an alternative mechanism for exopolysaccharide export. It is possible that the mature BcsK protein undergoes conformational changes and/or oligomerizes to assemble a multimeric OM porin domain similar to the strategy used by the Wza or CsgD proteins involved in *E. coli* capsular polysaccharide or curli secretion respectively (Dong *et al.* 2006; Goyal *et al.* 2014). Alternatively, the TPR-rich BcsK could interact with other outer membrane export machineries to guide cellulose extrusion in these species; however, the specific protein actors and involved mechanisms remain to be experimentally determined.

Overall, while the synthase-dependent cellulose polymerization and transport appear to be highly conserved among bacteria and even across kingdoms (Römling and Galperin 2015; Purushotham, Ho and Zimmer 2020), the mechanisms for outer membrane secretion are likely highly diverse in nature. Apart from the best-characterized BcsB/TPR-dependent periplasmic guidance, some prokaryotic cellulose secretion systems lack homologs of BcsB, BcsC or BcsK altogether (Römling and Galperin 2015). For example, in some cyanobacteria the Bcs secretion system is composed of an inner-membrane synthase and a HlyD-like protein partner, whereas periplasmic guidance and outer membrane extrusion are likely secured by a TolC-like multimeric exporter (Maeda *et al.* 2018). This, together with the presence of many additional Bcs subunits with uncharacterized structures or functional roles across organisms and putative secretory assemblies (Römling and Galperin 2015), paints an intricate picture in which—despite half a century of extensive and multidisciplinary research—our mechanistic understanding of bacterial cellulose secretion is still only incipient.

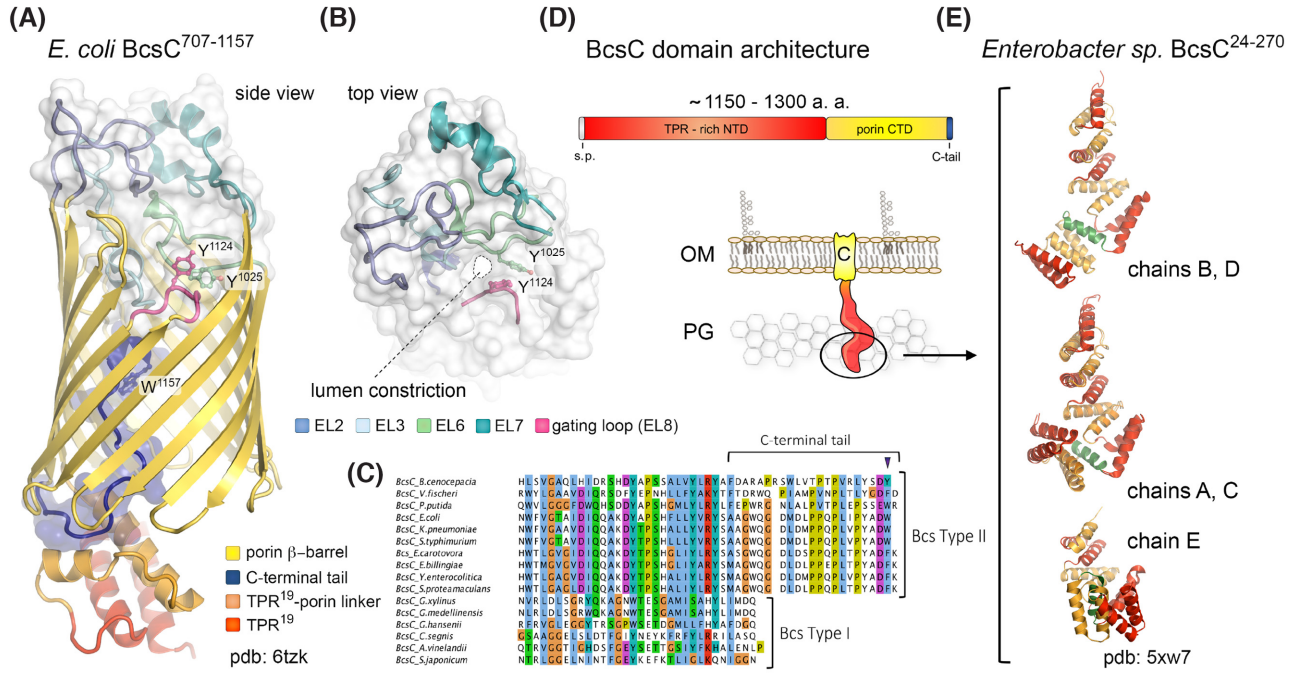

Figure 7. BcsC and outer membrane cellulose extrusion. **(A, B)** Crystal structure of *E. coli* BcsC$^{707\text{-}1157}$ encompassing TPR^{19} and the outer membrane porin domain (Acheson, Derewenda and Zimmer 2019). The protein is shown in cartoon; the extracellular loops and luminal C-terminal tail are also shown as transparent surface. The lumen constriction proximal to the extracellular surface is seen in panel (B); the gating π-stacking residues Y^{1025} and Y^{1124} from extracellular loops EL6 and EL8 are shown as sticks (Acheson, Derewenda and Zimmer 2019). **(C)** Multiple sequence alignment of BcsC homologs from bacteria featuring Type I and Type II Bcs secretion systems, showing correlation between the luminal C-terminal tail conservation and pEtN-cellulose secretion. **(D)** BcsC domain architecture and thumbnail representation of the protein in the outer membrane. **(E)** Crystal structure of the N-terminal TPR modules from an *Enterobacter* sp. BcsC homolog showing multiple conformations between the five chains crystallized in the asymmetric unit (Nojima *et al.* 2017). TPRs are colored in alternating red and orange; the α_5-helix insertion proposed to mediate the conformational flexibility is colored in green.

PEPTIDOGLYCAN CROSSING AND FATE OF THE SECRETED POLYSACCHARIDE

An overarching challenge for envelope-spanning secretion machineries is overcoming the physical barrier presented by the peptidoglycan. The latter is made of linear glycan chains laterally crosslinked by short tetra- or pentapeptides that yield a fishing net-like structure with high porosity. Based on permeability to various-sized dextrans, the lateral diameter of the peptidoglycan pores has been determined as relatively homogeneous and in the range of 2–2.5 nanometers in both Gram-positive and Gram-negative species (Vollmer, Blanot and de Pedro 2008). In theory, this diameter is sufficiently larger than the ~15 Å-wide electronegative pore of the BcsC$^{E.coli}$ export module (Acheson, Derewenda and Zimmer 2019), so even chemically modified cellulose should be able to traverse the peptidoglycan layer without the need of a specific conduit. In practice, however, such transit is expected to be complicated by the intrinsic flexibility of the polysaccharide, non-specific interactions with the peptidoglycan chains and aggregation among the cellulose polymers prior to their secretion to the cell surface. As mentioned earlier, several dedicated proteins have been proposed to guide the nascent cellulose through the periplasm such as BcsB's carbohydrate binding domains and—in the case of enterobacterial pEtN-cellulose secretion—the supramolecular periplasmic crown lumen (Abidi et al. 2021; Morgan, Strumillo and Zimmer 2013); BcsD's independent polysaccharide conduits in the assembled barrel-shaped octamers (Hu *et al.* 2010); the TPR-rich periplasmic modules of BcsC and BcsK with functional counterparts in multiple synthase-dependent exopolysaccharide secretion systems (Low and Howell 2018); or the putative TolC-like cylindrical exporter in some cyanobacterial species (Maeda *et al.* 2018).

It is important to note, however, that despite recent progress in unraveling the structure and mechanisms of many of the abovementioned components, to date there is no *in situ* information about their actual localization relative to the peptidoglycan layer in the cell wall or periplasm. Recent cryo-ET and modeling studies on the AcrAB-TolC tripartite efflux pumps, which could share structural and functional similarities with some cyanobacterial cellulose secretion assemblies (Maeda *et al.* 2018), have reported that the peptidoglycan layer positions at the AcrA–TolC junction, likely stabilizing the formation of a continuous secretion channel between the inner and outer membrane components (Shi *et al.* 2019; Gumbart *et al.* 2021). This peptidoglycan localization is dependent on its covalent tethering to the outer membrane via the so-called Braun's lipoprotein, or Lpp—a 6 kDa, ~9 nanometer-long α-helical polypeptide that forms trimeric coiled-coils, anchored in the outer membrane via triacetylated N-termini and covalently bound to the peptidoglycan via the side chains of C-terminal lysines (Asmar and Collet 2018). Although similar positioning and stabilizing roles of the peptidoglycan cannot be excluded for at least some of the cellulose secretion systems, actual experimental investigations are yet to be reported. One indication that peptidoglycan integrity could positively affect cellulose secretion comes from the observation that *G. xylinus* transposon mutants carrying disruptions in the lysine decarboxylase (Ldc) and alanine racemase (AlaR) enzymes for peptidoglycan precursor biosynthesis secrete cellulose with reduced degree of crystallinity (Deng *et al.* 2015). Nevertheless, the mutant strains also feature defects in their overall cell morphology with the appearance of very elongated curved

cells rather than the typical rod-shaped bacteria. It remains therefore to be determined whether the observed effects are due to specific roles of the enzymes and peptidoglycan in cellulose export and crystallinity, or any defect in cell morphology would have indirect negative influence on TC nanoarray assembly.

To our knowledge, there are similarly no reports of specific interactions between TPR-rich periplasmic proteins and their cognate exopolysaccharides from any EPS secretion system to date, at least not at concentrations consistent with the 1:1 polypeptide-to-polysaccharide ratio expected in the periplasm. As such, the proposed role of TPR-rich BcsC and BcsK modules as periplasmic guides for the nascent cellulose remains largely speculative. An alternative, or additional, role proposed for these extended subunits is that they could act as protein docking platforms for the recruitment of additional proteinaceous partners in the periplasm, such as the periplasmic modules of the BcsB co-polymerase, the crystallinity factors BcsD and BcsH, the cellulose modifying enzymes BcsZ and BcsG, or as-yet uncharacterized BcsK partners for outer membrane cellulose export. Although such interactions are yet to be experimentally tested for the cellulose secretion system, it is important to note that in the *P. aeruginosa* Pel biosynthetic machinery, activity of the PelA hydrolase (a BcsZ functional homolog) is indeed enhanced by direct binding to the TPR-rich modules of PelB (a BcsC counterpart) (Marmont *et al.* 2017). Another related but unexplored possibility is that the periplasmic TPR modules recruit additional factors, such as peptidoglycan-remodeling enzymes, to facilitate extrusion of the nascent cellulose across the periplasm. Such a strategy has been recently characterized for the TPR-rich, OM-anchored lipoprotein NlpI, which recruits multiple peptidoglycan-specific hydrolases and biosynthetic enzymes on behalf of the peptidoglycan biogenesis machinery (Banzhaf *et al.* 2020) and shares limited sequence homology with $BcsC^{NTD}$.

Following peptidoglycan crossing and—in the case of Gram-negatives—outer membrane extrusion, bacterial cellulose is generally considered a secreted and not a capsular exopolysaccharide, presumably retaining only loose association, if any, with the bacterial cell surface. Possible mechanisms for cellulose release from the surface could involve spontaneous outward translocation, BcsZ-mediated periplasmic cleavage and/or significant pull forces from extracellular interactions with biotic or abiotic surfaces. In practice, however, the fate of the secreted polymer can vary greatly across species. In *G. xylinus*, for example, the crystalline cellulose ribbon can serve both as a floatation device and a propulsive organelle for cell movement and thus requires the stable anchoring of the linear TC nanoarray and nascent cellulose chains in the bacterial cell envelope. As mentioned earlier, such anchoring is likely achieved via the recently observed cortical belt cytoskeleton (Nicolas *et al.* 2021); however, its composition remains to be characterized. Studies on the pEtN-cellulose secretion systems of *Salmonella* and *E. coli*, on the other hand, have shown that the chemically modified polymer interacts with extracellular curli, that are typically assembled onto the cell surface-bound CsgB amyloid (Serra, Richter and Hengge 2013; Hollenbeck *et al.* 2018; Bhoite *et al.* 2019). The curli-cellulose network thus forms a dense extracellular matrix that entraps and protects the bacterial cells close to the surface of the biofilm macrocolonies, whereas cells in the bottom are stabilized primarily by an intercellular mesh of presumably static flagella (Serra, Richter and Hengge 2013). Similar interactions with surface amyloids have also been proposed for the *P. fluorescens* SBW25 acetylated polysaccharide (Spiers *et al.* 2003), as well as the cellulose of Gram-positive streptomycetes (de Jong *et al.* 2009).

It is highly likely that additional mechanisms for cell surface attachment of secreted cellulose exist in nature. For example, many bacteria exhibit lectin-like cell surface proteins that could interact with extracellular polysaccharides, such as the Wzi outer membrane lectin that has been shown to organize group I capsular polysaccharides in *E. coli* and other Gram-negative species (Bushell *et al.* 2013). Interestingly, some Gram-positive streptomycetes, such as *Streptomyces reticuli*, feature a surface-exposed, coiled-coil-rich, cellulose-binding protein, AbpS (Walter, Wellmann and Schrempf 1998); however, its high affinity for crystalline versus amorphous cellulose suggests it might be involved in substrate cellulose degradation (Schrempf and Walter 1995), rather than structural cellulose accumulation. Instead, it has been recently proposed that the *Streptomyces* cell wall is composed of layers of both peptidoglycan and extracellular glycans, including cellulose, that are structurally anchored to the surface by cell wall teichoic acids (Ultee *et al.* 2020). Therefore, extracellular cellulose can likely associate not only with proteins, but also with other envelope glycoconjugates for its surface retention in cells and biofilms.

Finally, it is possible that not all Gram-negative bacteria extrude all of their synthesized cellulose extracellularly. Early studies on the *Rhizobium* cell wall report the microscopic observation of cellulose microfibrils associated with purified peptidoglycan sacculi, as well as the detection of covalent linkages between the peptidoglycan and cellodextrans (Drozański *et al.* 1981; Drozański 1983). A more recent work on the cyanobacterium *Synechococcus* sp. PCC 7002 similarly proposes that in addition to secretion of extracellular cellulose, the bacterium assembles a laminated cellulosic layer between the inner and outer membranes (Zhao *et al.* 2015), thus further highlighting a putative role for nanocellulose as a bacterial cell wall component.

CROSS-KINGDOM CELLULOSE SYNTHASE CONSERVATION

Similarly to bacteria, plants produce and secrete cellulose through a processive and conjugated process of glucose polymerization and polysaccharide extrusion. Plant cellulose synthases are encoded by genes from the *cesA* gene superfamily, which encodes glycosyl transferase 2 (GT2) enzymes spread over the cellulose synthase (CesA) lineage, as well as multiple cellulose synthase-like clades (Csl) proposed to mediate hemicellulose biosynthesis (Little *et al.* 2018). CesA homologs have been long visualized in freeze-fracture transmission electron microscopy (FF-TEM) experiments to assemble in six-lobed, hexagon-shaped terminal complexes termed 'rosettes' (Giddings, Brower and Staehelin 1980; Mueller and Brown 1980; Herth 1983; Kimura *et al.* 1999), previously thought to accommodate up to 36 CesA protomers that together secure the secretion of a crystalline microfibril (Perrin 2001). A more recent study using FF-TEM in combination with single-particle processing and homology modeling concluded that the 20–25 nanometer-wide rosettes accommodates 6 CesA trimers, each of which occupying a triangular lobe within the rosette (Nixon *et al.* 2016) (Fig. 8C). The proximity of the 18 CesA protomers in each terminal complex will thus secure the parallel packing of the secreted glucan chains into cellulose I microfibrils in a mechanism similar to the crystalline cellulose ribbon secretion by linear TC arrays in *G. xylinus*.

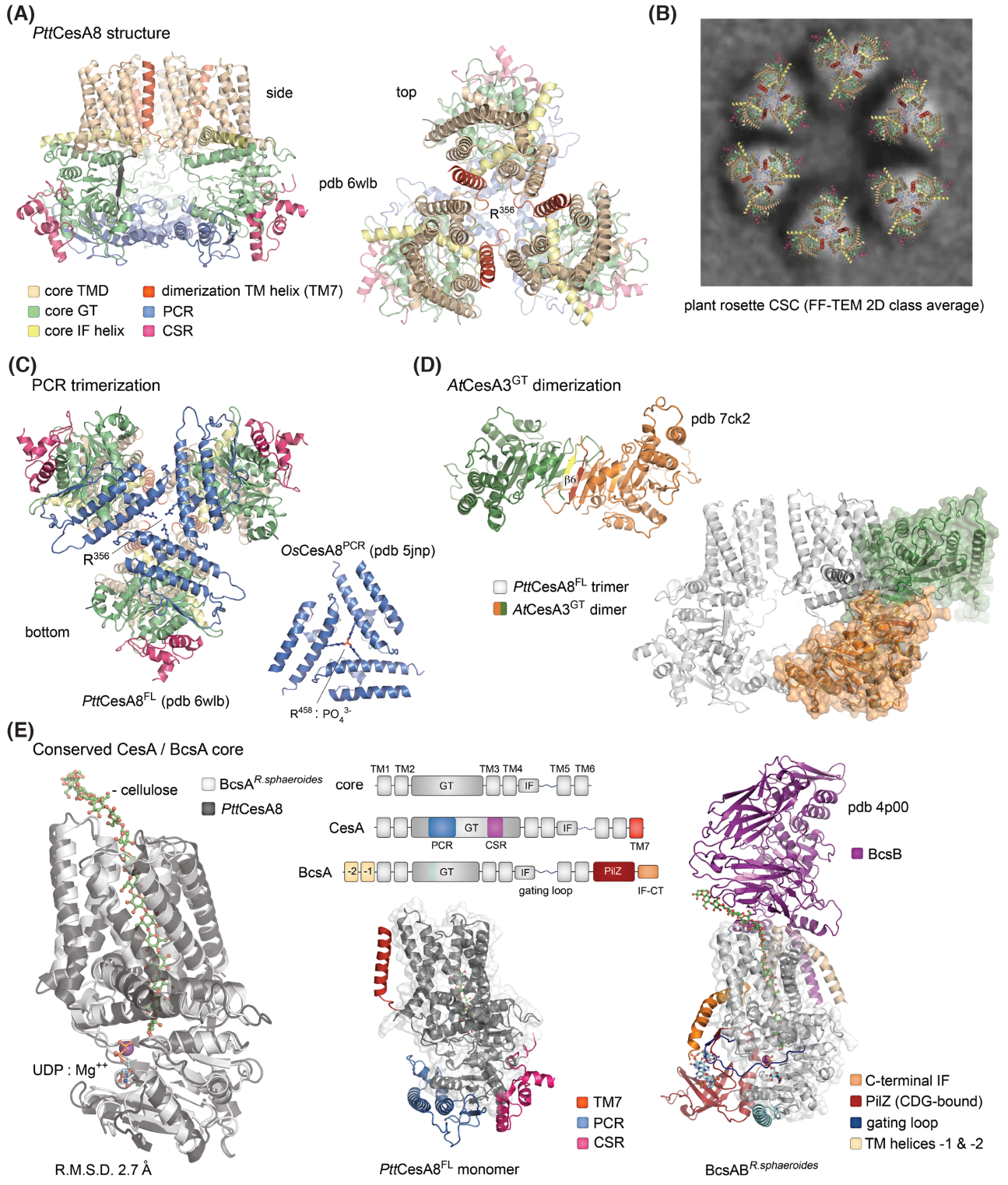

Figure 8. Eukaryotic CesA synthases are structurally conserved Bcs homologs. **(A)** Cryo-EM structure of the aspen PttCesA8 trimer shown in two different views (Purushotham, Ho and Zimmer 2020). The N-terminal domain is not modeled in the structure. PCR: plant-conserved region; CSR: class-specific region. **(B)** Proposed structure of the plant CesA rosette complexes based on Nixon *et al.* (2016) and Purushotham, Ho and Zimmer (2020). The FF-TEM 2D representative view is reproduced under the CC BY 4.0 license (https://creativecommons.org/licenses/by/4.0/legalcode). **(C)** PCR trimerization in the full-length PttCesA8 protein is virtually identical to that of the isolated PCR domains from rice OsCesA8 (Rushton *et al.* 2017). Arginine residues partaking in anion/phosphate-based stabilization are shown as sticks. **(D)** Crystal structure of a dimeric AtCesA3 glycosyl transferase domain based on Qiao *et al.* (2021). The dimerization β_6-strands from each protomer are colored in yellow and red. Bottom right, overlay of the $AtCesA^{GT}$ dimer with the full-length PttCesA8 protein. **(E)** Conservation of the BcsA/CesA core. Left, overlay of the core transmembrane and glycosyl transferase regions from PttCesA8 and *R. sphaeroides* BcsA showing virtually identical conformations. Cellulose, UDP and Mg^{++} are shown as observed in BcsA. Middle top, schematic representation of the conserved synthase core, CesA and BcsA. Middle bottom, structure of the PttCesA8 monomer with the core colored in dark gray and plant-specific insertions in color. Right, structure of the *R. sphaeroides* BcsAB tandem with the core colored in light gray and bacteria-specific regions in color.

Another parallel between bacterial and plant cellulose secretion is that plant cellulose synthase complexes (CSCs) also harbor many additional components to assist CesA in TC trafficking, assembly, subcellular localization, enzymatic activity and cellulose secretion. Indeed, mutations in the genes encoding proteins like Stello 1 and 2 (STL), Cellulose Synthase Interactive protein 1 (CSI1), Korrigan (KOR), Cobra (COB) and Kobito (KOB) result in severely impaired CSC functionality (Lampugnani *et al.* 2019); however, the specific roles and structure–function relationships for most of these components remain to be experimentally determined.

As mentioned earlier, plant cellulose synthases are thought to have been hijacked and evolved from cyanobacterial endosymbionts (Nobles, Romanovicz and Brown 2001; Nobles and Brown 2004; Little *et al.* 2018), and were in fact identified by sequence homology after the discovery of their prokaryotic counterparts (Pear *et al.* 1996; Arioli *et al.* 1998). Both plant and bacterial cellulose synthases share an overall similar architecture, consisting mainly of a canonical glycosyltransferase domain flanked on its N- and C-termini by the α-helical transmembrane segments of the membrane transport domain. However, some important differences were quickly identified such as the lack of a C-terminal PilZ domain in plant CesA homologs, as well as the presence of three distinct modules likely involved in oligomerization. The first one, or NTD, includes an N-terminal RING-like zinc-finger domain followed by an extended variable region that leads into the first transmembrane helix of the transport domain. The second is a plant-conserved region, or PCR, which is inserted into the membrane-distal region of the catalytic GT module and is found in plant CesA homologs, as well as some fungi (e.g. *Phytophthora infestans* CesA1, or PiCesA1). The third is a class-specific region, or CSR, which is inserted between conserved substrate-binding motifs near the enzyme's active site (Vergara and Carpita 2001; Somerville 2006; Purushotham, Ho and Zimmer 2020).

A recent cryo-EM structure of a purified plant cellulose synthase—the aspen synthase homolog CesA (*Populus tremula* × *tremuloides* CesA8 or *Ptt*CesA8)—revealed a remarkably conserved cellulose synthase core across kingdoms (Purushotham, Ho and Zimmer 2020) (Fig. 8). Albeit some of the plant-specific modules (such as the N-terminal domain and the complete CSR) and functionally important motifs (such as the active-site gating loop) were not well resolved in the structure, the study puts previously characterized structural modules in the context of a full-length protein and supports the recent model for hexamer-of-trimers rosette assembly (Nixon *et al.* 2016; Purushotham, Ho and Zimmer 2020) (Fig. 8A–C). The cryo-EM structure of the full-length protein and retention of the isolated soluble NTD on CSI1-coated beads suggest that the N-terminal domains of *Ptt*CesA8 protomers in each trimer form an extended coiled-coil stalk that protrudes into the cytosol to bind microtubule-interacting CSI1 and thus connect the terminal synthase complexes to the cortical cytoskeleton (Purushotham, Ho and Zimmer 2020). *Ptt*CesA8 oligomerization is further mediated by anion-dependent trimerization of the PCRs, which pack in a conformation identical to the one observed previously in the crystal structure of the isolated PCR from rice *Os*CesA8 (Rushton *et al.* 2017; Purushotham, Ho and Zimmer 2020) (Fig. 8C). Finally, the membrane transport domain in *Ptt*CesA8 is extended by an additional α-helix at its C-terminus relative to BcsA–TM7 that packs into a groove between TM4 and TM6 from a neighboring protomer, thus completing the trimerization interface at the membrane level (Purushotham, Ho and Zimmer 2020) (Fig. 8A). The CSR is not fully resolved in the structure but three short α-helices and connecting loops were modeled in the electron densities at the tips of the roughly triangular CesA trimer. The CSRs contain several cysteine residues that have been proposed to undergo acylation necessary for CesA trafficking to the plasma membrane (Kumar *et al.* 2016) and the apical position of these modules in each CesA trimer may provide a multimerization interface in the context of rosette assembly (Fig. 8B). Similar to the mechanism of cellulose extrusion by BcsA, *Ptt*CesA8 features a narrow channel for non-hydrated polysaccharide lined with both aromatic and hydrophilic residues for facilitated glucan translocation. The transmembrane channel of each protomer is curved toward the 3-fold symmetry axis of the *Ptt*CesA8 trimer, which would bring closer the exiting glucan chains and can thus facilitate polymer bundling (Purushotham, Ho and Zimmer 2020).

The 3D organization of the catalytic GT domain of *Ptt*CesA8 is in overall agreement with a separate structural study presenting the isolated GT domain from *Arabidopsis thaliana* CesA3 (*At*CesA3^{GT}) in apo- and UDP-bound forms at 2.05–2.35Å resolution (Qiao *et al.* 2021). A peculiar feature of *At*CesA3^{GT} is the identification of a potential dimerization interface, which was functionally assayed *in vitro*, *in cellulo* and *in planta* and is mediated mainly by antiparallel interactions between the β6 strands of neighboring protomers at the periphery of the core catalytic domain in the crystals (Qiao *et al.* 2021) (Fig. 8D). In addition, several modeling discrepancies between the crystal and cryo-EM structures from the two studies are observed, including conserved and functionally crucial elements such as the finger helix involved in catalysis, as well as modeling of separate β-strands including the abovementioned β6 region (Qiao *et al.* 2021). Such modeling discrepancies could be due to isoform-specific fold differences, conformational changes in the context of the full-length proteins or errors in the primary sequence assignment to the resolved electron densities, and will be hopefully settled by future high-resolution studies on assembled CesA isoforms. Indeed, overlay of the *At*CesA3^{GT} dimer with the full-length *Ptt*CesA8 structure indicates that significant conformational rearrangements between the CesA domains would be required if the putative β6-dimerization interface is indeed preserved in the context of the full length *At*CesA3 protein (Fig. 8D).

Comparison of the available bacterial and plant cellulose synthase structures provides the opportunity to propose a minimal synthase core architecture based on the conserved structural features between the resolved BcsA$^{R.sphaeroides}$, BcsA$^{E.coli}$ and *Ptt*CesA8 enzymes, namely the two TM α-helices preceding the glycosyltransferase domain, the GT domain core including the TM and interface helices preceding the gating loop, and finally the two TM α-helices following the gating loop, for a total of 6 TM α-helices (TM1-TM6) and cytosol-exposed GT regions excluding the PCR and CSR modules (Fig. 8E). Not only additional TM helices can be observed at the C- or N-terminal ends of this minimal core, but also larger structural modules such as the PilZ domain in most bacteria, the N-terminal BcsA$^{E.coli}$ extension proposed to mediate interactions with the pEtN-transferase BcsG, the C-terminal genetic fusion of the BcsB partner subunit in some bacterial homologs, the glycosyl hydrolase domain reported in ascidian synthases, etc. (Matthysse *et al.* 2004; Römling and Galperin 2015; Krasteva *et al.* 2017). The structural overlay also reveals that although occupying distinct regions in the proteins' primary structures, the bacterial PilZ domain and the plant PCR module occupy spatially overlapping regions in the tertiary protein folds. Interestingly, some cyanobacteria such as *Synechococcus* sp. and *Roseiflexus castenholzii* encode

BcsA homologs with a predicted domain architecture lacking a C-terminal PilZ domain but featuring a distinct structural module in lieu of the PCR (e.g. *Synechococcus* sp. and *Roseiflexus castenholzii* BcsA). Together, these observations highlight both the evolutionary conservation of BcsA/CesA enzymatic core, as well as the remarkable modularity of the enzymes in the species-specific context of cellulose secretion regulation.

CELLULOSE SECRETION AMID BACTERIAL EPS-PRODUCING PATHWAYS

Bacteria produce a remarkable variety of surface-attached or secreted polysaccharides that require an even greater diversity of protein subunits and accessory cofactors, such as energy sources, signaling molecules, lipid carriers and monomeric sugars. Nevertheless, polysaccharide-producing pathways can be generally viewed as variations of four major mechanisms that encompass EPS and glycoconjugate biogenesis in both Gram-negative and Gram-positive bacterial species (Fig. 9). The ensemble of these has been recently reviewed in more detail elsewhere (e.g. Schmid 2018; Caffalette *et al*. 2020; Moradali and Rehm 2020; Whitfield, Wear and Sande 2020), so here we will provide only a brief overview to put cellulose secretion into a broader context.

Extracellular sucrases

The simplest biosynthetic pathway relies on extracellular enzymes—sucrases—to generate dextrans (α-linked glucans) or levans (β-linked fructans) using monosaccharide precursors from the hydrolysis of extracellular sucrose (Fig. 9). The resulting polymers can be linear or branched, can be built onto different acceptor molecules, and often play a role in surface adhesion and colonization, such as dental plaque build-up by lactic acid bacteria (Schmid 2018; Whitfield, Wear and Sande 2020). Glucansucrases are relatively well-studied, large, multidomain members of the glycosyl hydrolase 70 (GH70) family of enzymes and are likely secreted in a Sec-dependent manner using an N-terminal signal peptide. The mature proteins carry a variable noncatalytic N-terminal region that might play a role in cell surface association, and a conserved catalytic core that folds into five separate domains (A, B, C, IV and V). Four of these are formed from noncontinuous polypeptide stretches from the proteins' amino acid sequence and catalyze the transglycosylation reaction (domain A), complete the active site pocket and contribute to substrate specificity (domain B), or participate in glycan binding and elongation (modules IV and V), whereas the fifth folds into a non-interrupted β-strand-rich module whose function remains elusive (domain C) (Meng *et al*. 2016). The modularity, extracellular activity and overall simplicity of these biosynthetic enzymes present a great potential for tailored polysaccharide production with applications in the biomedical, food and cosmetics industries.

The remaining three biosynthetic pathways for EPS and glycoconjugate production rely on intracellular precursor polymerization and as such require much more complex assembly and regulation mechanisms for polysaccharide export through the complex bacterial envelope.

Synthase-dependent exopolysaccharide secretion systems

The Bcs systems reviewed here belong to the larger group of synthase-dependent systems for exopolysaccharide secretion, which include but are not limited to the biosynthesis of *P. aeruginosa* alginate, PNAG and Pel exopolysaccharides in diverse Gram-positive and Gram-negative species, bacterial hyaluronic acid in certain *Streptococcus* and *Pasteurella* strains, and various β-linked glucans in plant-associated bacteria (Low and Howell 2018; Bundalovic-Torma *et al*. 2020; Whitfield, Wear and Sande 2020) (Fig. 9). With the exception of few atypical synthases, which act in capsular biogenesis in some *Streptococcus pneumoniae* serotypes and use phosphatidylglycerol as initial acceptor (Yother 2011), EPS synthases do not require a lipid carrier and are highly processive enzymes that couple linear glycan polymerization and export. The glycosyl transferase and inner-membrane translocation activities can be carried out by separate subunits (e.g. the PelF and PelG components of the Pel systems), or be incorporated in a single polypeptide as is the case for the cellulose, alginate and PNAG-producing pathways (e.g. BcsA, Alg8 and PgaC, respectively) (Low and Howell 2018). Common traits among synthase systems include the presence of an inner-membrane co-polymerase subunit that is necessary for the activation and/or stability of the synthase (e.g. BcsB, Alg44, PelE and PgaD), c-di-GMP-dependent activation through one or more dinucleotide-sensing protein modules (e.g. BcsA^{PilZ} and BcsE$^{REC*\text{-}GGDEF*}$ domains, Alg44^{PilZ}, PelD^{GGDEF*}, and a composite binding site at the PgaC–PgaD interface), TPR-rich periplasmic scaffolding components (e.g. AlgK and periplasmic modules of BcsC, PelE, PelB and PgaA), and the presence of a periplasmic hydrolase/lyase enzymes (e.g. BcsZ, AlgL, PelA and PgaB) (Low and Howell 2018) (Fig. 9). Some systems contain additional subunits for covalent modifications of the secreted polysaccharides, such as the alginate and cellulose acetylation complexes or the BcsG subunit for pEtN addition, whereas others utilize pre-acetylated monosaccharide precursors, such as the Pel and PNAG secretion pathways. Over the last decade, an impressive catalog of resolved structural modules from the above has been contributed to the literature, whereas comparative genomics studies have identified homologous system over a vast range of bacteria (Low and Howell 2018; Bundalovic-Torma *et al*. 2020). It remains to be determined, however, how the various individual components assemble into highly cooperative nanomachines to secure biofilm matrix secretion.

ABC transporter-dependent pathways

ATP-binding cassette transporters are a large and evolutionary ancient protein superfamily, representatives of which can be found in all three domains of life where they couple ATP binding, hydrolysis and nucleotide recycling to the inward or outward translocation of diverse substrates across the plasma membrane (Thomas and Tampé 2020). In bacteria, they mediate the transport of undecaprenyl-diphosphate (Und-PP)-linked glycans for the synthesis of N-glycosylated proteins, some LPS O-antigens in Gram-negatives and wall teichoic acids (WTA) in Gram-positives, as well as phosphatidylglycerol-linked capsular polysaccharides (CPS) in diderm mucosal pathogens (Whitfield, Wear and Sande 2020).

ABC transporter-dependent O-antigen biogenesis starts with the synthesis of cytosol-facing Und-PP-linked hexosamine primers by inner-membrane polyprenol-phosphate phosphoglycosyl transferases (PGT), such as enterobacterial WecA homologs that use UDP-*N*-acetylglucosamine (UDP-GlcNAc) as a substrate. A multicomponent complex of conventional mono- or multidomain Leloir glycosyl transferases is proposed to then extend the polysaccharide chain using a variety of NDP–linked sugars as substrates (Caffalette *et al*. 2020). Export to the outer

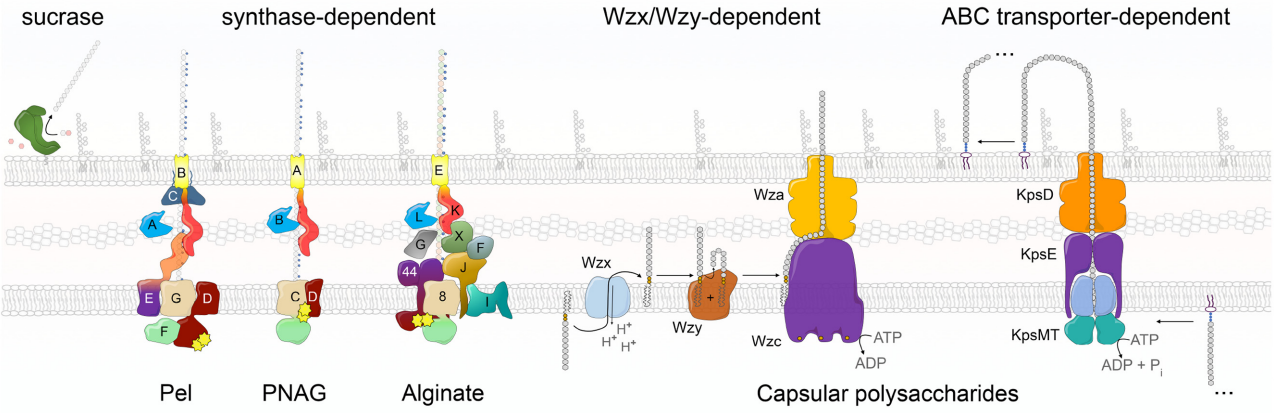

Figure 9. Bacterial exopolysaccharide secretion. Examples of the four major exopolysaccharide secretion pathways are shown as thumbnail representations. Summary models based on (Schmid 2018; Krasteva and Sondermann 2017; Low and Howell 2018; Caffalette *et al.* 2020; Whitfield, Wear and Sande 2020).

leaflet of the inner membrane can be coupled to chain elongation, as in the case of *K. pneumoniae* O2a LPS, where competition between the Wzm/Wzt ABC transporter and the glycosyltransferase complexes determines LPS chain length, or can occur after completion of the elongation process and capping of the polysaccharide by a covalent chemical modification (Schmid 2018; Caffalette *et al.* 2020). In *E. coli* O9a, for example, the LPS terminal sugar carries a phosphomethyl group added by the WbdD protein, a mushroom-shaped homotrimer with kinase and methyltransferase domains that are separated from the inner membrane by a coiled-coil 'stalk', the length of which likely dictates that of the O antigen's polysaccharidic chain (Hagelueken *et al.* 2015).

LPS O-antigens are long molecules and their export through the Wzm/Wzt ABC transporter requires a continuous transmembrane passage rather than a classical alternating access mechanism (Bi *et al.* 2018). Wzm is a dimeric, polytopic membrane protein that forms a single inner-membrane channel lined with aromatic residues for CH-π stacking interactions with the exported glycan, whereas Wzt homologs provide the nucleotide-binding domains (NBDs) and, in the case of chemically capped polymers, additional carbohydrate-binding modules (CBDs) (Bi *et al.* 2018). Polysaccharide translocation is thought to be energized by iterative cycles of coupled ATP hydrolysis, rigid-body NBD motion and stepwise outward extrusion of the polysaccharide moiety in a mechanism reminiscent of processive synthases rather than Wzx-like flippases (see below) (Whitfield, Wear and Sande 2020). Following translocation of the entire glycolipid to the outer leaflet of the inner membrane, the O-antigen is transferred onto the lipid A core by the polytopic glycosyltransferase WaaL, whose structure remains to be determined. The resulting mature LPS molecule is then extracted from the inner membrane by a second ABC transporter complex, namely the multicomponent $LptB_2FGC$ extractor (Thomas and Tampé 2020). In it an LptB dimer provides the energizing NBDs, whereas the LptFG subunits build up the force-transducing transmembrane domains and harbor additional periplasmic β-jellyrolls, which together with the membrane-anchored LptC subunit are thought to accept the acyl chains of the extracted LPS (Li, Orlando and Liao 2019; Owens *et al.* 2019). Successive cycles of extraction have been proposed to push the LPS molecules along a transperiplasmic LptA filament and toward an outer membrane LptED 'plug-and-barrel' complex responsible for LPS insertion and lateral diffusion in the outer membrane (Dong *et al.* 2014; Qiao *et al.* 2014; Sherman *et al.* 2018).

ABC transporter-dependent biosynthesis of capsular glycolipids (CPS) follows an overall similar mechanism of assembly and inner-membrane export. The lipid carrier is typically a phosphatidylglycerol moiety onto which a primer of ketodeoxyoctonic acid (Kdo) residues is first introduced by dedicated CMP-Kdo–dependent glycosyltransferases (e.g. *E. coli* KpsS and KpsC) and then elongated by a complex of various conventional Leloir GTs. The glycolipids are then exported by a two-component ABC transporter, such as the KpsM (TMDs)–KpsT (NBDs) tandem of *E. coli*, proposed to adopt similar structure and processive translocation mechanism as the Wzm-Wzt transporter discussed earlier (Caffalette *et al.* 2020; Whitfield, Wear and Sande 2020). CPS secretion to the cell surface is likely further dependent on the formation of a trans-envelope complex of an inner membrane-embedded, multimeric co-polymerase, as well as a cognate outer membrane translocon (e.g. *E. coli* KpsD and Wza-like KpsE, respectively) (Whitfield, Wear and Sande 2020) (Fig. 9). The emerging capsular glycolipids can then remain associated with the membrane via their priming lipid anchor or partake in ionic interactions with secreted LPS and other surface molecules (Whitfield, Wear and Sande 2020).

Finally, Gram-positive bacteria also employ ABC transporter-dependent mechanisms for assembly and export of their cell WTA. Teichoic acids are anionic co-polymers composed of phosphodiester-linked glycerol- or ribitol-phosphate moieties and carbohydrates, and can be either attached in the cell membrane via a diacylglycerol (DAG) anchor (lipoteichoic acids, or LTA) or covalently crosslinked to the peptidoglycan (WTA) (Brown, Santa Maria and Walker 2013). LTAs are synthesized extracellularly by two main actors: (i) the LtaA flippase, which is a polytopic Wzx-like member of the multidrug/oligosaccharidyl-lipid/polysaccharide (MOP) superfamily of transporters (see later) and flips the DAG anchor into the outer leaflet, as well as (ii) the membrane-anchored phosphoglycerol transferase LtaS (Lu *et al.* 2009), which shares structural homology with BcsG and catalyzes the lipid anchor-distal addition of monomeric building blocks for polymer extension (Reichmann and Gründling 2011). In contrast, peptidoglycan-crosslinked WTAs are synthesized intracellularly by homologs of TagF, a membrane-associated dual-domain glycosyl transferase (Lovering *et al.* 2010) that uses CDP-glycerol as a substrate to reiteratively transfer PG moieties

onto an Und-PP-GlcNAc anchor. Export of the TA is then mediated by homologs of the Wzm/Wzt-like TarGH ABC transporter. Following translocation, the polymer can be glycosylated with glucose or GlcNAc moieties by trimeric extracellular enzymes (e.g. TarM, TarS or TarP; Brown, Santa Maria and Walker 2013; Caffalette *et al*. 2020) or undergo D-alanylation by the DltABCD complex. First, DltC is posttranslationally modified in the cytosol with the addition of a phosphopantetheine (Ppant) moiety by an acyl carrier protein synthase (AcpS). DltA then catalyzes the attachment of D-alanine to pPant-DltC and the carrier protein interacts with the AlgI/WssH-like MBOAT enzyme DltB (Ma *et al*. 2018). The latter transfers the D-alanine moiety through the membrane and onto the TA polymer in a process that requires the membrane-anchored DltD subunit *in vivo*; however, its exact role remains to be experimentally determined.

Wzx/Wzy-dependent pathways

The fourth major pathway for exopolysaccharide and glycoconjugate production in bacteria is the Wzx/Wzy-dependent mechanism, responsible for the secretion of many LPS O-antigens, as well as capsular and biofilm polysaccharides in both Gram-positive and Gram-negative bacteria. Examples of these include important virulence and stress-protective factors, such as *Streptococcus pneumoniae* capsular polysaccharides, xanthan and fastidian gum of the *Xanthomonas campestris* and *Xylella fastidiosa* plant pathogens, Psl and Vps exopolysaccharides in *P. aeruginosa* and *V. cholerae*, respectively, and enterobacterial colanic acids among many others (Whitfield, Wear and Sande 2020). Essentially, the Wzx/Wzy-dependent pathways involve the cytosolic synthesis of modular oligosaccharides onto membrane-embedded Und-PP carrier moieties, which are then flipped to accept a nascent polysaccharide onto the opposite side of the plasma membrane. As opposed to the above-mentioned synthase-dependent pathways, these are flippase-dependent, non-processive mechanisms for exopolysaccharide production (Fig. 9).

Similarly to the ABC transporter pathway described earlier, glycan synthesis is initiated by mono- or polytopic inner-membrane PGT enzymes, which generate Und-PP-linked hexose or N-acetylhexosamine residues to be used as primers for subsequent extension by a complex of structure-specific glycosyl transferases (Whitfield, Wear and Sande 2020). The resulting Und-PP-anchored oligosaccharidic modules are then exported by Wzx homologs from the larger MOP superfamily of transporters, in a mechanism that is likely coupled to the countermovement of protons (Islam *et al*. 2013) (Fig. 9). Wzx flippases are expected to harbor twelve transmembrane helices distributed in two pseudodimeric six-helix bundles around a central hydrophilic lumen for glycan binding and export. Although no Wzx structures have been reported to date, a putative alternating-access translocation mechanism can be proposed based on structural and functional insights into the peptidoglycan lipid II flippase MurJ, where dynamic changes in the lumen's accessibility and shape have been proposed to drive the transporter from its resting state, through its inward opening and substrate entry, to extracellular substrate release via counterion-dependent transition to an outward open conformation (Kuk, Mashalidis and Lee 2017; Kuk *et al*. 2019; Kumar *et al*. 2019; Caffalette *et al*. 2020).

Following its translocation to the periplasm or cell surface, the Und-PP-linked oligosaccharide then serves as an acceptor for a nascent glycan chain in a reaction catalyzed by a non-processive Wzy polymerase (Fig. 9). Wzy homologs are polytopic membrane proteins with conserved periplasmic loop motifs implicated in catalysis; however, no Wzy structure is currently available to reveal the mechanism of modular glycan chain elongation (Whitfield, Wear and Sande 2020). The product chain length is controlled by additional polysaccharide co-polymerase proteins (PCP), which can be markedly diverse across biosynthetic pathways. In O-antigen biogenesis, for example, this role is taken by the Wzz protein, which forms α-helical, membrane-anchored, bell-shaped oligomers (Collins *et al*. 2017). The latter have been proposed to recruit Wzy partners at the interface between adjacent Wzz^{TMD} protomers, whereas the nascent glycan chains could wrap around the inner or outer surface of the Wzz periplasmic bell-like structure (Collins *et al*. 2017), before being transferred to the lipid A core and extracted for outer membrane sorting (see above).

Synthesis of capsular polysaccharides, in contrast, typically involves PCPs with additional cytosolic tyrosine kinase modules, whose activity is thought to affect the oligomeric state of the co-polymerase, as well as the stability and/or activity of other pathway-specific enzymes (Whitfield, Wear and Sande 2020). An early negative-stain electron microscopy reconstruction of the *E. coli* Wzc co-polymerase in complex with the outer membrane translocon Wza revealed an envelope-spanning, ~180 Å-long multimeric assembly, in which Wzc adopted a tetrameric organization with dome-like periplasmic architecture and spatially separated kinase domains (Collins *et al*. 2007); however, further work is necessary to provide mechanistic insights into Wzy recruitment and regulation, or the role of Wzc in polysaccharide protection and guidance (Fig. 9).

In Gram-positive bacteria, capsular polysaccharides, as well as wall teichoic acids, can be covalently attached to the peptidoglycan via enzymes belonging to the LytR-CpsA-Psr (LCP) family of enzymes. In Gram-negatives, cell export is secured by outer membrane export proteins, the best characterized representative of which is the *E. coli* Wza lipoprotein. Wza forms an octamer with an ~100 Å-long, cylindrical periplasmic architecture, the lumen of which is lined with polar residues thought to facilitate glycan export, whereas an atypical barrel of amphipathic α-helices secures transport through the hydrophobic lipid bilayer (Dong *et al*. 2006). Such outer membrane export is in stark contrast with the general organization of synthase-dependent systems, where the extended TPR-rich periplasmic modules are unlikely to provide physical exclusion from the periplasm and where outer membrane crossing is typically secured by monomeric β-barrel modules.

USE AND APPLICATIONS OF BACTERIAL CELLULOSE

Cellulose in bacterial physiology and virulence

Bacterial colonization, survival and fitness in different environmental niches or eukaryotic hosts are largely dependent on efficient intercellular communication and formation of multicellular biofilm communities. The latter can be aerobic, microaerophilic or anaerobic and can grow on a variety of biotic and abiotic surfaces including solid substrates, host tissues, air–liquid interfaces or, even—as in the fungus-like mycelia of streptomycetes—develop extensive aerial networks of multicellular hyphae (O'Toole, Kaplan and Kolter 2000; Hall-Stoodley, Costerton and Stoodley 2004; Flemming *et al*. 2016; Jones and Elliot 2018). In most cases, initial surface attachment is typically mediated by c-di-GMP-mediated inhibition of flagellar motility

and expression of proteinaceous extracellular adherence factors such as pili, cell surface adhesins or amyloid fimbriae. The progressive secretion of exopolysaccharides and release of extracellular DNA then further inhibits flagellar motility and serves as mortar in the complex biofilm architecture (O'Toole, Kaplan and Kolter 2000; Hall-Stoodley, Costerton and Stoodley 2004; Flemming *et al.* 2016; Krasteva and Sondermann 2017). The biofilm matrix is thus an extremely complex and differentiated habitat that needs to simultaneously provide hydration, osmotic and pH-balance, nutrient and oxygen sorption and distribution, clearance of toxic metabolites, mechanical strength and resistance to external factors (e.g. UV radiation, temperature variations, desiccation) or host immune response, as well as to enable synergistic relationships between harbored bacteria such as metabolic complementation, coordinated secretion of extracellular substrate-digesting enzymes or virulence factors, and acquisition of new traits by horizontal gene transfer events (Flemming *et al.* 2016). The unique physical properties of cellulose as a polymer alone, including its high wettability, rigidity, microporosity and biocompatibility, respond to most of the abovementioned requirements and make it a preferred biofilm matrix component.

Perhaps counterintuitively, especially in light of the prevalent role of the polymer in sessile biofilm development, cellulose can also stimulate bacterial motility. In *Gluconacetobacter xylinus* and related species devoid of cellular flagella, synthesis and crystallization of the longitudinal cellulose ribbon generate a push force resulting in propulsion of the cell by ∼2 microns per minute in a direction opposite to that of cellulose ribbon elongation (Brown, Willison and Richardson 1976). This motility is directly linked to bacterial chemotaxis and substrate utilization (Basu, Vadanan and Lim 2018) and is likely mediated by both the tethering of synthase terminal complexes by the cytoskeletal cortical belt (Nicolas *et al.* 2021), and interactions of the cellulose ribbon with the nanoscale architecture of the growth substrate itself (Tomita and Kondo 2009). A similar motility mechanism dependent on directional polysaccharidic slime extrusion is also observed in some cyanobacteria (e.g. from the *Nostoc*, *Synechocystis* and *Scytonema* lineages), where cellulose, additional polysaccharides and Type IV pili could cooperate to provide gliding motility to the cells or multicellular filaments (Nobles, Romanovicz and Brown 2001; Khayatan, Meeks and Risser 2015). Apart from motility, cellulose secretion in *G. xylinus* can also confer floatability to the air–liquid interface by trapping gas bubbles expelled in metabolism (Schramm and Hestrin 1954), or can help the colonization and microaerophilic growth on decaying solid substrates while inhibiting the growth of competitors and facilitating nutrient diffusion (Williams and Cannon 1989). When secreted onto plant-derived substrates, bacterial cellulose suffers structural modifications through its interaction with components of the plant cell wall such as pectin, lignin or hemicelluloses (Hackney, Atalla and VanderHart 1994; Uhlin, Atalla and Thompson 1995). This can significantly disrupt microfibril formation and the crystallinity of the secreted cellulose mat and thus reduce its transparency and confer UV resistance to the bacterial biofilm (Williams and Cannon 1989; Hackney, Atalla and VanderHart 1994). Such interactions of bacterial cellulose with plant or fungal cell wall polysaccharides are also important for efficient tissue colonization in symbiotic or pathogenic relationships. For example, in the symbiotic bacteria *Rhizobium leguminosarum* and *Pseudomonas fluorescens*, cellulose secretion is necessary for efficient rhizosphere and phyllosphere colonization and nutrient exchange, whereas in pathogenic bacteria such as *A. tumefaciens* and *Erwinia amylovora* similar interactions are crucial for irreversible attachment and host tissue invasion (Gal *et al.* 2003; Spiers *et al.* 2003; Matthysse *et al.* 2005; Castiblanco and Sundin 2018). Importantly, many cellulose secreting bacteria can use cellulose to adhere to agricultural plants and then exhibit pathogenic effects in humans when the contaminated plants are consumed as food sources (e.g. Shaw *et al.* 2011; Yaron and Römling 2014).

Regarding interactions of cellulose-secreting pathogens with mammalian hosts, the effects of cellulose secretion on bacterial virulence likely depend on the specific bacterial species or strain, the targeted tissues and organs, the co-expression of additional adherence factors, as well as the stage of infection. As mentioned earlier, cellulose secretion by *M. tuberculosis* has been shown to facilitate the establishment of infection in the host and to confer resistance to antimicrobial treatment (Chakraborty *et al.* 2021). In the case of uropathogenic *E. coli* UTI89, recent work has shown that coproduction of cellulose and curli stimulates bacterial adhesion to bladder cells in culture by enhancing bacterial surface association of amyloid fimbriae (Hollenbeck *et al.* 2018). In contrast, cellulose secretion by the commensal *E. coli* TOB-1 isolate was shown to inhibit curli-mediated adhesion and internalization by gastrointestinal epithelial cells, while at the same time counteracting the production of immunostimulatory interleukin-8 (Wang *et al.* 2006). In addition, research on *S. typhimurium* has shown that cellulose secretion inhibits intracellular growth within macrophages and that disruption of the *bcsA* gene increases the pathogen's virulence *in vivo* (Pontes *et al.* 2015). Taken together, these observations suggest that bacterial cellulose secretion in the mammalian hosts likely enhances persistence and establishment of chronic infections on one hand, while preventing acute virulence-associated proinflammatory effects on the other (Pontes *et al.* 2015; Römling and Galperin 2015).

Finally, bacterial cellulose secretion can also influence animal–microsymbiont interactions. In *Aliivibrio fischeri*, which establishes a unique symbiotic relationship with the Hawaiian bobtail squid to confer nighttime bioluminescence to its light organ, secretion of cellulose alternates with that of a separate 'symbiosis' polysaccharide, or SYP. In the early stages of light organ colonization and symbiosis initiation, cellulose secretion is proposed to be inhibited and bacterial adhesion to be mediated by SYP polysaccharide induction (Bassis and Visick 2010). Cellulose is proposed to be secreted in the later stages of biofilm growth within the light organ's crypts, whose overpopulation is controlled by a daily venting event expulsing ∼95% of the crypt contents at dawn (Lee and Ruby 1994). Cellulose secretion can thus contribute to maintenance of the symbiosis in the squid, confer resistance to the bacterium upon expulsion from the host and facilitate bacteria–plant interactions with seaweed in the aquatic environment (Augimeri, Varley and Strap 2015).

Biotechnological applications

Bacterial cellulose, and in particular crystalline cellulose I produced by the *Gluconacetobacter* lineage, has multiple advantages over plant-sourced polymers that are making it a preferred material for a large variety of medical and biotechnological applications. Such properties include the polymer's exceptional purity due to the lack of hemicelluloses and lignin, its excellent water retention capacity, microporosity, high crystallinity, transparency, tensile strength and elasticity, thermal and chemical stability allowing efficient non-denaturing sterilization, biodegradability, possibilities for chemical functionalization, and low antigenicity and implantability (Rajwade, Paknikar and

Kumbhar 2015; Li *et al.* 2021b). Examples of specific industrial and biomedical applications of the polymer include its use in tissue engineering as a scaffold for small blood vessel replacement or in wound dressing materials (Czaja *et al.* 2006; Scherner *et al.* 2014; Zheng *et al.* 2020), in drug-delivery applications (Sun *et al.* 2019; Islam *et al.* 2021) or as an immobilization matrix for enzymes or microbial cultures (Yao *et al.* 2011; Akduman *et al.* 2013; Drachuk *et al.* 2017); in the food industry as thickening, gelling, stabilizing, emulsifying or active packaging agent (Shi *et al.* 2014; Ludwicka, Kaczmarek and Białkowska 2020); in the paper industry for paper with improved quality and flame-retardation properties (Basta and El-Saied 2009; Fillat *et al.* 2018); in the electronics industry for the development of electronic paper displays (Shah and Brown 2005), electroacoustic membranes (Ciechańska *et al.* 2002) or organic light emitting diodes (Pinto *et al.* 2015); in the cosmetics industry as a carrier of active ingredients or as a texturing agent (Almeida *et al.* 2021); and in the development of aerogels and polymer foams with specific adsorption, filtration, insulation, compound-release, antibacterial or fire-resistance properties (Haimer *et al.* 2010; Olsson *et al.* 2010; Wu *et al.* 2013; Revin *et al.* 2020; Li *et al.* 2021a), among others. The main challenge in bacterial cellulose production on an industrial scale is the generally inverse relationship between culture cost versus quality and yield of the produced polymer, and there is a strong interest in the engineering of cellulose superproducer strains (Florea *et al.* 2016; Singh *et al.* 2020); utilization of alternative low-cost carbon sources (Molina-Ramírez *et al.* 2018), including CO_2-utilizing photosynthetic pathways in recombinant cyanobacteria (Zhao *et al.* 2015), and overall optimization of the cell culture conditions for each strain (Blanco Parte *et al.* 2020). A profound understanding of the molecular mechanisms governing cellulose biogenesis by the Bcs secretion systems in nature can thus not only shed light on the ways in which bacteria use the exopolysaccharide to thrive in the environment or their eukaryotic hosts, but also serve to overcome practical bottlenecks that currently hamper widespread use of the polymer as a sustainable and renewable industrial product.

Outlook

Bacteria produce a remarkable diversity of surface-attached and extracellular polysaccharides, many of which are released by multicomponent, c-di-GMP-sensing, synthase-dependent secretion machineries and can play important roles in bacterial biofilm formation, stress survival and virulence. In the last decades, many advances in understanding the underlying principles of glycan synthesis and export have been made, relying both on elegant genetic studies and multidisciplinary approaches to study the structure and function of key protein actors and cognate polysaccharide products. As a widespread biofilm exopolysaccharide and a polymer of particular biotechnological interest, bacterial cellulose has provided much of our current understanding of synthase-dependent exopolysaccharide secretion; however, it is evident from the preceding pages that many of the underlying molecular principles remain to be uncovered.

In our opinion, the most important step going forward is to move from a simplistic, BcsAB-dependent polymerization and export model to viewing Bcs assemblies as highly cooperative secretion nanomachines with multilevel control of their expression, assembly, cellular and biofilm localization, synthase activation and product modifications. A better understanding of the cellulose crystallinity determinants, for example—such as the composition and structure of the recently discovered cortical belt or the role of the BcsHD components—can not only lead to the engineering of strains or tailored chemi-enzymatic systems for the production of optimized bacterial cellulose, but also potentially yield molecular scaffolds for increased efficiency and metabolic flux in other bacterial biosynthetic pathways. Similarly, c-di-GMP-dependent activation should be examined in the bigger picture of diguanylate cyclase- and phosphodiesterase-dependent dinucleotide flux and synthase-proximal c-di-GMP-enrichment mechanisms—such as the ones reported for the enterobacterial pEtN-cellulose secretion systems—can be further harnessed for modifying cellulose production. The putative role of synthase-priming mechanisms and the molecular structure of synthase-interacting cellulose-modifying enzymes need to be further examined and can lead to optimized biosynthetic reactions and the engineering of enzymes with altered substrate specificities to yield custom-designed, chemically decorated polymers. More *in situ* studies are certainly needed to pinpoint the localization and dynamics of Bcs secretion system components in cells and biofilms, and deciphering the interactions of the secreted polymer with other extracellular matrix components can be of great interest not only from a biotechnological but also from a biomedical perspective.

ACKNOWLEDGMENTS

We are grateful to all current and former members of the SBB group and especially to Samira Zouhir and Marion Decossas for preliminary literature research and useful discussions on bacterial cellulose secretion. We apologize to authors with important contributions to the field who are not highlighted in this work or are cited indirectly.

FUNDING

This work received funding from the European Research Council (ERC) Executive Agency under grant agreement 757507-BioMatrix-ERC-2017-StG (to PVK) and was also supported by the European Institute of Chemistry and Biology (IECB), the Centre National de Recherche Scientifique (CNRS) and a Université de Bordeaux IDEX Junior Chair grant (to PVK).

AUTHOR CONTRIBUTIONS

WA, LTS, AS and PVK prepared preliminary drafts on sections of the manuscript, conducted literature and database mining and participated in stimulating discussions. PVK integrated and expanded upon the abovementioned contributions and prepared the final version of the manuscript.

Conflict of interest. None declared.

REFERENCES

Abidi W, Zouhir S, Caleechurn M *et al.* Architecture and regulation of an enterobacterial cellulose secretion system. *Sci Adv* 2021;**7**:eabd8049.

Acheson JF, Derewenda ZS, Zimmer J. Architecture of the cellulose synthase outer membrane channel and its association with the periplasmic TPR domain. *Structure* 2019;**27**:1855–61.

Acheson JF, Ho R, Goularte NF *et al.* Molecular organization of the *E. coli* cellulose synthase macrocomplex. *Nat Struct Mol Biol* 2021;**28**:310–8.

Ahmad I, Rouf SF, Sun L *et al.* BcsZ inhibits biofilm phenotypes and promotes virulence by blocking cellulose production in *Salmonella enterica* serovar Typhimurium. *Microb Cell Fact* 2016;**15**:177.

Akduman B, Uygun M, Coban EP *et al.* Reversible immobilization of urease by using bacterial cellulose nanofibers. *Appl Biochem Biotechnol* 2013;**171**:2285–94.

Almagro Armenteros JJ, Tsirigos KD, Sønderby CK *et al.* SignalP 5.0 improves signal peptide predictions using deep neural networks. *Nat Biotechnol* 2019;**37**:420–3.

Almeida T, Silvestre AJD, Vilela C *et al.* Bacterial nanocellulose toward green cosmetics: recent progresses and challenges. *Int J Mol Sci* 2021;**22**:2836.

Aloni Y, Cohen R, Benziman M *et al.* Solubilization of the UDP-glucose:1,4-beta-D-glucan 4-beta-D-glucosyltransferase (cellulose synthase) from *Acetobacter xylinum*. A comparison of regulatory properties with those of the membrane-bound form of the enzyme. *J Biol Chem* 1983;**258**:4419–23.

Aloni Y, Delmer DP, Benziman M. Achievement of high rates of *in vitro* synthesis of 1,4-beta-D-glucan: activation by cooperative interaction of the *Acetobacter xylinum* enzyme system with GTP, polyethylene glycol, and a protein factor. *Proc Natl Acad Sci USA* 1982;**79**:6448–52.

Anandan A, Evans GL, Condic-Jurkic K *et al.* Structure of a lipid A phosphoethanolamine transferase suggests how conformational changes govern substrate binding. *Proc Natl Acad Sci USA* 2017;**114**:2218–23.

Anderson AC, Burnett AJN, Hiscock L *et al.* The *Escherichia coli* cellulose synthase subunit G (BcsG) is a Zn^{2+}-dependent phosphoethanolamine transferase. *J Biol Chem* 2020;**295**:6225–35.

Arioli T, Peng L, Betzner AS *et al.* Molecular analysis of cellulose biosynthesis in *Arabidopsis*. *Science* 1998;**279**:717–20.

Asmar AT, Collet JF. Lpp, the Braun lipoprotein, turns 50-major achievements and remaining issues. *FEMS Microbiol Lett* 2018;**365**:fny199.

Augimeri RV, Varley AJ, Strap JL. Establishing a role for bacterial cellulose in environmental interactions: lessons learned from diverse biofilm-producing Proteobacteria. *Front Microbiol* 2015;**6**:1282.

Baker P, Hill PJ, Snarr BD *et al.* Exopolysaccharide biosynthetic glycoside hydrolases can be utilized to disrupt and prevent *Pseudomonas aeruginosa* biofilms. *Sci Adv* 2016;**2**:e1501632.

Baker P, Ricer T, Moynihan PJ *et al. P. aeruginosa* SGNH hydrolase-like proteins AlgJ and AlgX have similar topology but separate and distinct roles in alginate acetylation. *PLoS Pathog* 2014;**10**:e1004334.

Bange G, Sinning I. SIMIBI twins in protein targeting and localization. *Nat Struct Mol Biol* 2013;**20**:776–80.

Banzhaf M, Yau HC, Verheul J *et al.* Outer membrane lipoprotein NlpI scaffolds peptidoglycan hydrolases within multi-enzyme complexes in *Escherichia coli*. *EMBO J* 2020;**39**:e102246.

Bassis CM, Visick KL. The cyclic-di-GMP phosphodiesterase BinA negatively regulates cellulose-containing biofilms in *Vibrio fischeri*. *J Bacteriol* 2010;**192**:1269–78.

Basta AH, El-Saied H. Performance of improved bacterial cellulose application in the production of functional paper. *J Appl Microbiol* 2009;**107**:2098–107.

Basu A, Vadanan SV, Lim S. A novel platform for evaluating the environmental impacts on bacterial cellulose production. *Sci Rep* 2018;**8**:5780.

Basu S, Omadjela O, Gaddes D *et al.* Cellulose microfibril formation by surface-tethered cellulose synthase enzymes. *ACS Nano* 2016;**10**:1896–907.

Benziman M, Haigler CH, Brown RM *et al.* Cellulose biogenesis: polymerization and crystallization are coupled processes in *Acetobacter xylinum*. *Proc Natl Acad Sci USA* 1980;**77**:6678–82.

Bhoite S, van Gerven N, Chapman MR *et al.* Curli biogenesis: bacterial amyloid assembly by the type VIII secretion pathway. *EcoSal Plus* 2019;**8**:ecosalplus.ESP–0037-2018.

Bi Y, Mann E, Whitfield C *et al.* Architecture of a channel-forming O-antigen polysaccharide ABC transporter. *Nature* 2018;**553**:361–5.

Blackwell J. The macromolecular organization of cellulose and chitin. In: Brown RM (ed). *Cellulose and Other Natural Polymer Systems: Biogenesis, Structure, and Degradation*. Boston, MA: Springer US, 1982, 403–28.

Blanco Parte FG, Santoso SP, Chou CC *et al.* Current progress on the production, modification, and applications of bacterial cellulose. *Crit Rev Biotechnol* 2020;**40**:397–414.

Blanton RL, Fuller D, Iranfar N *et al.* The cellulose synthase gene of *Dictyostelium*. *Proc Natl Acad Sci USA* 2000;**97**:2391–6.

Bogdanov M, Pyrshev K, Yesylevskyy S *et al.* Phospholipid distribution in the cytoplasmic membrane of Gram-negative bacteria is highly asymmetric, dynamic, and cell shape-dependent. *Sci Adv* 2020;**6**:eaaz6333.

Brahim Belhaouari D, Baudoin JP, Gnankou F *et al.* Evidence of a cellulosic layer in *Pandoravirus massiliensis* tegument and the mystery of the genetic support of its biosynthesis. *Front Microbiol* 2019;**10**:2932.

Brown RM, Willison JH, Richardson CL. Cellulose biosynthesis in *Acetobacter xylinum*: visualization of the site of synthesis and direct measurement of the *in vivo* process. *Proc Natl Acad Sci USA* 1976;**73**:4565–9.

Brown RM. Cellulose structure and biosynthesis: what is in store for the 21st century? *J Polym Sci A Polym Chem* 2004;**42**:487–95.

Brown S, Santa Maria JP, Walker S. Wall teichoic acids of Gram-positive bacteria. *Annu Rev Microbiol* 2013;**67**:313–36.

Bundalovic-Torma C, Whitfield GB, Marmont LS *et al.* A systematic pipeline for classifying bacterial operons reveals the evolutionary landscape of biofilm machineries. *PLoS Comput Biol* 2020;**16**:e1007721.

Bushell SR, Mainprize IL, Wear MA *et al.* Wzi is an outer membrane lectin that underpins group 1 capsule assembly in *Escherichia coli*. *Structure* 2013;**21**:844–53.

Caffalette CA, Kuklewicz J, Spellmon N *et al.* Biosynthesis and export of bacterial glycolipids. *Annu Rev Biochem* 2020;**89**:741–68.

Campeotto I, Percy MG, MacDonald JT *et al.* Structural and mechanistic insight into the *Listeria monocytogenes* two-enzyme lipoteichoic acid synthesis system. *J Biol Chem* 2014;**289**:28054–69.

Canale-Parola E, Borasky R, Wolfe RS. Studies on *Sarcina ventriculi*. III. Localization of cellulose. *J Bacteriol* 1961;**81**:311–8.

Carrasco S, Mérida I. Diacylglycerol, when simplicity becomes complex. *Trends Biochem Sci* 2007;**32**:27–36.

Castiblanco LF, Sundin GW. Cellulose production, activated by cyclic di-GMP through BcsA and BcsZ, is a virulence factor and an essential determinant of the three-dimensional architectures of biofilms formed by *Erwinia amylovora* Ea1189. *Mol Plant Pathol* 2018;**19**:90–103.

Chakraborty P, Bajeli S, Kaushal D *et al.* Biofilm formation in the lung contributes to virulence and drug tolerance of *Mycobacterium tuberculosis*. *Nat Commun* 2021;**12**:1606.

Chan C, Paul R, Samoray D *et al.* Structural basis of activity and allosteric control of diguanylate cyclase. *Proc Natl Acad Sci USA* 2004;**101**:17084–9.

Chaplin AK, Petrus ML, Mangiameli G *et al.* GlxA is a new structural member of the radical copper oxidase family and is required for glycan deposition at hyphal tips and morphogenesis of *Streptomyces lividans*. *Biochem J* 2015;**469**:433–44.

Chiaradia L, Lefebvre C, Parra J *et al.* Dissecting the mycobacterial cell envelope and defining the composition of the native mycomembrane. *Sci Rep* 2017;**7**:12807.

Ciechańska D, Struszczyk H, Kazimierczak J *et al.* New electroacoustic transducers based on modified bacterial cellulose. *Fibres Text East Eur* 2002;**10**:27–30.

Clairfeuille T, Buchholz KR, Li Q *et al.* Structure of the essential inner membrane lipopolysaccharide–PbgA complex. *Nature* 2020;**584**:479–83.

Collins RF, Beis K, Dong C *et al.* The 3D structure of a periplasm-spanning platform required for assembly of group 1 capsular polysaccharides in *Escherichia coli*. *Proc Natl Acad Sci USA* 2007;**104**:2390–5.

Collins RF, Kargas V, Clarke BR *et al.* Full-length, oligomeric structure of Wzz determined by cryoelectron microscopy reveals insights into membrane-bound states. *Structure* 2017;**25**:806–15.

Couillerot O, Prigent-Combaret C, Caballero-Mellado J *et al.* *Pseudomonas fluorescens* and closely-related fluorescent pseudomonads as biocontrol agents of soil-borne phytopathogens. *Lett Appl Microbiol* 2009;**48**:505–12.

Czaja W, Krystynowicz A, Bielecki S *et al.* Microbial cellulose: the natural power to heal wounds. *Biomaterials* 2006;**27**:145–51.

Da Re S, Ghigo JM. A CsgD-independent pathway for cellulose production and biofilm formation in *Escherichia coli*. *J Bacteriol* 2006;**188**:3073–87.

Dalebroux ZD, Edrozo MB, Pfuetzner RA *et al.* Delivery of cardiolipins to the *Salmonella* outer membrane is necessary for survival within host tissues and virulence. *Cell Host Microbe* 2015;**17**:441–51.

Dannheim H, Will SE, Schomburg D *et al.* *Clostridioides difficile* 630Δerm *in silico* and *in vivo*: quantitative growth and extensive polysaccharide secretion. *FEBS Open Bio* 2017;**7**:602–15.

de Jong W, Wösten HA, Dijkhuizen L *et al.* Attachment of *Streptomyces coelicolor* is mediated by amyloidal fimbriae that are anchored to the cell surface via cellulose. *Mol Microbiol* 2009;**73**:1128–40.

De N, Pirruccello M, Krasteva PV *et al.* Phosphorylation-independent regulation of the diguanylate cyclase WspR. *PLoS Biol* 2008;**6**:601–17.

Deng X, Gonzalez Llamazares A, Wagstaff JM *et al.* The structure of bactofilin filaments reveals their mode of membrane binding and lack of polarity. *Nat Microbiol* 2019;**4**:2357–68.

Deng Y, Nagachar N, Fang L *et al.* Isolation and characterization of two cellulose morphology mutants of *Gluconacetobacter hansenii* ATCC23769 producing cellulose with lower crystallinity. *PLoS One* 2015;**10**:e0119504.

Deng Y, Nagachar N, Xiao C *et al.* Identification and characterization of non-cellulose-producing mutants of *Gluconacetobacter hansenii* generated by Tn5 transposon mutagenesis. *J Bacteriol* 2013;**195**:5072–83.

Domozych DS, Ciancia M, Fangel JU *et al.* The cell walls of green algae: a journey through evolution and diversity. *Front Plant Sci* 2012;**3**:82.

Dong C, Beis K, Nesper J *et al.* Wza the translocon for *E. coli* capsular polysaccharides defines a new class of membrane protein. *Nature* 2006;**444**:226–9.

Dong H, Xiang Q, Gu Y *et al.* Structural basis for outer membrane lipopolysaccharide insertion. *Nature* 2014;**511**:52–6.

Drachuk I, Harbaugh S, Geryak R *et al.* Immobilization of recombinant *E. coli* cells in a bacterial cellulose-silk composite matrix to preserve biological function. *ACS Biomater Sci Eng* 2017;**3**:2278–92.

Drozański W, Drozańska D, Lorkiewicz Z *et al.* Structure of the rigid-layer of *Rhizobium* cell wall. II. Evidence for a covalent bond between peptidoglycan and cellodextrins. *Acta Microbiol Pol* 1981;**30**:371–85.

Drozański W. Structure of the rigid-layer of *Rhizobium* cell wall. III. Electron microscopic evidence for the cellulose microfibrils association with peptidoglycan sacculi. *Acta Microbiol Pol* 1983;**32**:161–7.

Faham S, Watanabe A, Besserer GM *et al.* The crystal structure of a sodium galactose transporter reveals mechanistic insights into Na+/sugar symport. *Science* 2008;**321**:810–4.

Fan J, Petersen EM, Hinds TR *et al.* Structure of an inner membrane protein required for PhoPQ-regulated increases in outer membrane cardiolipin. *mBio* 2020;**11**:e03277–19.

Fang X, Ahmad I, Blanka A *et al.* GIL, a new c-di-GMP-binding protein domain involved in regulation of cellulose synthesis in enterobacteria. *Mol Microbiol* 2014;**93**:439–52.

Fillat A, Martínez J, Valls C *et al.* Bacterial cellulose for increasing barrier properties of paper products. *Cellulose* 2018;**25**:6093–105.

Flemming HC, Wingender J, Szewzyk U *et al.* Biofilms: an emergent form of bacterial life. *Nat Rev Microbiol* 2016;**14**:563–75.

Florea M, Hagemann H, Santosa G *et al.* Engineering control of bacterial cellulose production using a genetic toolkit and a new cellulose-producing strain. *Proc Natl Acad Sci USA* 2016;**113**:E3431–40.

Franklin MJ, Nivens DE, Weadge JT *et al.* Biosynthesis of the *Pseudomonas aeruginosa* Extracellular Polysaccharides, Alginate, Pel, and Psl. *Front Microbiol* 2011;**2**:167.

Gal M, Preston GM, Massey RC *et al.* Genes encoding a cellulosic polymer contribute toward the ecological success of *Pseudomonas fluorescens* SBW25 on plant surfaces. *Mol Ecol* 2003;**12**:3109–21.

Galperin MY, Nikolskaya AN, Koonin EV. Novel domains of the prokaryotic two-component signal transduction systems. *FEMS Microbiol Lett* 2001;**203**:11–21.

Giddings TH, Brower DL, Staehelin LA. Visualization of particle complexes in the plasma membrane of *Micrasterias denticulata* associated with the formation of cellulose fibrils in primary and secondary cell walls. *J Cell Biol* 1980;**84**:327–39.

Goyal P, Krasteva PV, Van Gerven N *et al.* Structural and mechanistic insights into the bacterial amyloid secretion channel CsgG. *Nature* 2014;**516**:250–3.

Grenville-Briggs LJ, Anderson VL, Fugelstad J *et al.* Cellulose synthesis in *Phytophthora infestans* is required for normal appressorium formation and successful infection of potato. *Plant Cell* 2008;**20**:720–38.

Grimson MJ, Haigler CH, Blanton RL. Cellulose microfibrils, cell motility, and plasma membrane protein organization change in parallel during culmination in *Dictyostelium discoideum*. *J Cell Sci* 1996;**109**:3079–87.

Gromet Z, Schramm M, Hestrin S. Synthesis of cellulose by *Acetobacter xylinum*. 4. Enzyme systems present in a crude extract of glucose-grown cells. *Biochem J* 1957;**67**:679–89.

Gumbart JC, Ferreira JL, Hwang H *et al.* Lpp positions peptidoglycan at the AcrA–TolC interface in the AcrAB–TolC multidrug efflux pump. *Biophys J* 2021;**120**:3973–82.

Hackney JM, Atalla RH, VanderHart DL. Modification of crystallinity and crystalline structure of *Acetobacter xylinum* cellulose in the presence of water-soluble beta-1,4-linked

polysaccharides: 13C-NMR evidence. *Int J Biol Macromol* 1994;**16**:215–8.
Hagelueken G, Clarke BR, Huang H *et al*. A coiled-coil domain acts as a molecular ruler to regulate O-antigen chain length in lipopolysaccharide. *Nat Struct Mol Biol* 2015;**22**:50–6.
Häggström L, Förberg C. Significance of an extracellular polymer for the energy metabolism in *Clostridium acetobutylicum*: a hypothesis. *Appl Microbiol Biotechnol* 1986;**23**:234–9.
Haimer E, Wendland M, Schlufter K *et al*. Loading of bacterial cellulose aerogels with bioactive compounds by antisolvent precipitation with supercritical carbon dioxide. *Macromol Symp* 2010;**294**:64–74.
Hall-Stoodley L, Costerton JW, Stoodley P. Bacterial biofilms: from the natural environment to infectious diseases. *Nat Rev Microbiol* 2004;**2**:95–108.
Herth W. Arrays of plasma-membrane "rosettes" involved in cellulose microfibril formation of Spirogyra. *Planta* 1983;**159**:347–56.
Hollenbeck EC, Antonoplis A, Chai C *et al*. Phosphoethanolamine cellulose enhances curli-mediated adhesion of uropathogenic *Escherichia coli* to bladder epithelial cells. *Proc Natl Acad Sci USA* 2018;**115**:10106–11.
Hu M, Guo J, Cheng Q *et al*. Crystal structure of *Escherichia coli* originated MCR-1, a phosphoethanolamine transferase for colistin resistance. *Sci Rep* 2016;**6**:38793.
Hu SQ, Gao YG, Tajima K *et al*. Structure of bacterial cellulose synthase subunit D octamer with four inner passageways. *Proc Natl Acad Sci USA* 2010;**107**:17957–61.
Huang LH, Liu QJ, Sun XW *et al*. Tailoring bacterial cellulose structure through CRISPR interference-mediated downregulation of galU in *Komagataeibacter xylinus* CGMCC 2955. *Biotechnol Bioeng* 2020;**117**:2165–76.
Hur DH, Choi WS, Kim TY *et al*. Enhanced production of bacterial cellulose in *Komagataeibacter xylinus* via tuning of biosynthesis genes with synthetic RBS. *J Microbiol Biotechnol* 2020;**30**:1430–5.
Ingerson-Mahar M, Briegel A, Werner JN *et al*. The metabolic enzyme CTP synthase forms cytoskeletal filaments. *Nat Cell Biol* 2010;**12**:739–46.
Islam ST, Eckford PD, Jones ML *et al*. Proton-dependent gating and proton uptake by Wzx support O-antigen-subunit antiport across the bacterial inner membrane. *mBio* 2013;**4**:e00678–13.
Islam SU, Ul-Islam M, Ahsan H *et al*. Potential applications of bacterial cellulose and its composites for cancer treatment. *Int J Biol Macromol* 2021;**168**:301–9.
Iyer PR, Catchmark J, Brown NR *et al*. Biochemical localization of a protein involved in synthesis of *Gluconacetobacter hansenii* cellulose. *Cellulose* 2011;**18**:739–47.
Jenal U, Reinders A, Lori C. Cyclic di-GMP: second messenger extraordinaire. *Nat Rev Microbiol* 2017;**15**:271–84.
Jones SE, Elliot MA. 'Exploring' the regulation of *Streptomyces* growth and development. *Curr Opin Microbiol* 2018;**42**:25–30.
Kawano S, Tajima K, Kono H *et al*. Effects of endogenous endo-beta-1,4-glucanase on cellulose biosynthesis in *Acetobacter xylinum* ATCC23769. *J Biosci Bioeng* 2002;**94**:275–81.
Keegstra K. Plant cell walls. *Plant Physiol* 2010;**154**:483–6.
Kelley LA, Mezulis S, Yates CM *et al*. The Phyre2 web portal for protein modeling, prediction and analysis. *Nat Protoc* 2015;**10**:845–58.
Khayatan B, Meeks JC, Risser DD. Evidence that a modified type IV pilus-like system powers gliding motility and polysaccharide secretion in filamentous cyanobacteria. *Mol Microbiol* 2015;**98**:1021–36.
Kim DE, Chivian D, Baker D. Protein structure prediction and analysis using the Robetta server. *Nucleic Acids Res* 2004;**32**:W526–531.
Kimura S, Laosinchai W, Itoh T *et al*. Immunogold labeling of rosette terminal cellulose-synthesizing complexes in the vascular plant *Vigna angularis*. *Plant Cell* 1999;**11**:2075–86.
Kimura S, Ohshima C, Hirose E *et al*. Cellulose in the house of the appendicularian *Oikopleura rufescens*. *Protoplasma* 2001;**216**:71–4.
Koo HM, Song SH, Pyun YR *et al*. Evidence that a beta-1,4-endoglucanase secreted by *Acetobacter xylinum* plays an essential role for the formation of cellulose fiber. *Biosci Biotechnol Biochem* 1998;**62**:2257–9.
Krasteva PV, Bernal-Bayard J, Travier L *et al*. Insights into the structure and assembly of a bacterial cellulose secretion system. *Nat Commun* 2017;**8**:2065.
Krasteva PV, Sondermann H. Versatile modes of cellular regulation via cyclic dinucleotides. *Nat Chem Biol* 2017;**13**:350–9.
Krissinel E, Henrick K. Inference of macromolecular assemblies from crystalline state. *J Mol Biol* 2007;**372**:774–97.
Krystynowicz A, Koziołkiewicz M, Wiktorowska-Jezierska A *et al*. Molecular basis of cellulose biosynthesis disappearance in submerged culture of *Acetobacter xylinum*. *Acta Biochim Pol* 2005;**52**:691–8.
Kühn J, Briegel A, Mörschel E *et al*. Bactofilins, a ubiquitous class of cytoskeletal proteins mediating polar localization of a cell wall synthase in *Caulobacter crescentus*. *EMBO J* 2010;**29**:327–39.
Kuk AC, Mashalidis EH, Lee SY. Crystal structure of the MOP flippase MurJ in an inward-facing conformation. *Nat Struct Mol Biol* 2017;**24**:171–6.
Kuk ACY, Hao A, Guan Z *et al*. Visualizing conformation transitions of the lipid II flippase MurJ. *Nat Commun* 2019;**10**:1736.
Kumar M, Wightman R, Atanassov I *et al*. S-acylation of the cellulose synthase complex is essential for its plasma membrane localization. *Science* 2016;**353**:166–9.
Kumar S, Rubino FA, Mendoza AG *et al*. The bacterial lipid II flippase MurJ functions by an alternating-access mechanism. *J Biol Chem* 2019;**294**:981–90.
Lampugnani ER, Flores-Sandoval E, Tan QW *et al*. Cellulose synthesis: central components and their evolutionary relationships. *Trends Plant Sci* 2019;**24**:402–12.
Le Quéré B, Ghigo JM. BcsQ is an essential component of the *Escherichia coli* cellulose biosynthesis apparatus that localizes at the bacterial cell pole. *Mol Microbiol* 2009;**72**:724–40.
Lee KH, Ruby EG. Effect of the squid host on the abundance and distribution of symbiotic *Vibrio fischeri* in nature. *Appl Environ Microbiol* 1994;**60**:1565–71.
Lee VT, Matewish JM, Kessler JL *et al*. A cyclic-di-GMP receptor required for bacterial exopolysaccharide production. *Mol Microbiol* 2007;**65**:1474–84.
Li H, Wang Y, Ye M *et al*. Hierarchically porous poly(amidoxime)/bacterial cellulose composite aerogel for highly efficient scavenging of heavy metals. *J Colloid Interface Sci* 2021a;**600**:752–63.
Li S, Lei L, Somerville CR *et al*. Cellulose synthase interactive protein 1 (CSI1) links microtubules and cellulose synthase complexes. *Proc Natl Acad Sci USA* 2012a;**109**:185–90.
Li T, Chen C, Brozena AH *et al*. Developing fibrillated cellulose as a sustainable technological material. *Nature* 2021b;**590**:47–56.
Li Y, Orlando BJ, Liao M. Structural basis of lipopolysaccharide extraction by the LptB2FGC complex. *Nature* 2019;**567**:486–90.

Li Z, Chen JH, Hao Y *et al.* Structures of the PelD cyclic diguanylate effector involved in pellicle formation in *Pseudomonas aeruginosa* PAO1. *J Biol Chem* 2012b;**287**:30191–204.

Liman R, Facey PD, van Keulen G *et al.* A laterally acquired galactose oxidase-like gene is required for aerial development during osmotic stress in *Streptomyces coelicolor*. *PLoS One* 2013;**8**:e54112.

Lindenberg S, Klauck G, Pesavento C *et al.* The EAL domain protein YciR acts as a trigger enzyme in a c-di-GMP signalling cascade in *E. coli* biofilm control. *EMBO J* 2013;**32**:2001–14.

Little A, Schwerdt JG, Shirley NJ *et al.* Revised phylogeny of the cellulose synthase gene superfamily: insights into cell wall evolution. *Plant Physiol* 2018;**177**:1124–41.

Lovering AL, Lin LY, Sewell EW *et al.* Structure of the bacterial teichoic acid polymerase TagF provides insights into membrane association and catalysis. *Nat Struct Mol Biol* 2010;**17**:582–9.

Low KE, Howell PL. Gram-negative synthase-dependent exopolysaccharide biosynthetic machines. *Curr Opin Struct Biol* 2018;**53**:32–44.

Lu D, Wörmann ME, Zhang X *et al.* Structure-based mechanism of lipoteichoic acid synthesis by *Staphylococcus aureus* LtaS. *Proc Natl Acad Sci USA* 2009;**106**:1584–9.

Ludwicka K, Kaczmarek M, Białkowska A. Bacterial nanocellulose: a biobased polymer for active and intelligent food packaging applications: recent advances and developments. *Polymers (Basel)* 2020;**12**:2209.

Ma D, Wang Z, Merrikh CN *et al.* Crystal structure of a membrane-bound O-acyltransferase. *Nature* 2018;**562**:286–90.

Ma T, Ji K, Wang W *et al.* Cellulose synthesized by *Enterobacter* sp. FY-07 under aerobic and anaerobic conditions. *Bioresour Technol* 2012;**126**:18–23.

Maeda K, Tamura J, Okuda Y *et al.* Genetic identification of factors for extracellular cellulose accumulation in the thermophilic cyanobacterium *Thermosynechococcus vulcanus*: proposal of a novel tripartite secretion system. *Mol Microbiol* 2018;**109**:121–34.

Mahasenan KV, Batuecas MT, De Benedetti S *et al.* Catalytic cycle of glycoside hydrolase BglX from *Pseudomonas aeruginosa* and its implications for biofilm formation. *ACS Chem Biol* 2020;**15**:189–96.

Marmont LS, Whitfield GB, Rich JD *et al.* PelA and PelB proteins form a modification and secretion complex essential for Pel polysaccharide-dependent biofilm formation in. *J Biol Chem* 2017;**292**:19411–22.

Matthysse AG, Deschet K, Williams M *et al.* A functional cellulose synthase from ascidian epidermis. *Proc Natl Acad Sci USA* 2004;**101**:986–91.

Matthysse AG, Marry M, Krall L *et al.* The effect of cellulose overproduction on binding and biofilm formation on roots by *Agrobacterium tumefaciens*. *Mol Plant Microbe Interact* 2005;**18**:1002–10.

Matthysse AG, Thomas DL, White AR. Mechanism of cellulose synthesis in *Agrobacterium tumefaciens J Bacteriol* 1995;**177**:1076–81.

Mazur O, Zimmer J. Apo- and cellopentaose-bound structures of the bacterial cellulose synthase subunit BcsZ. *J Biol Chem* 2011;**286**:17601–6.

McNamara JT, Morgan JL, Zimmer J. A molecular description of cellulose biosynthesis. *Annu Rev Biochem* 2015;**84**:895–921.

Meng X, Gangoiti J, Bai Y *et al.* Structure–function relationships of family GH70 glucansucrase and 4,6-α-glucanotransferase enzymes, and their evolutionary relationships with family GH13 enzymes. *Cell Mol Life Sci* 2016;**73**:2681–706.

Molina-Ramírez C, Castro C, Zuluaga R *et al.* Physical characterization of bacterial cellulose produced by *Komagataeibacter medellinensis* using food supply chain waste and agricultural by-products as alternative low-cost feedstocks. *J Polym Environ* 2018;**26**:830–7.

Moradali MF, Donati I, Sims IM *et al.* Alginate polymerization and modification are linked in *Pseudomonas aeruginosa*. *mBio* 2015;**6**:e00453–15.

Moradali MF, Rehm BHA. Bacterial biopolymers: from pathogenesis to advanced materials. *Nat Rev Microbiol* 2020;**18**:195–210.

Morgan JL, McNamara JT, Fischer M *et al.* Observing cellulose biosynthesis and membrane translocation *in crystallo*. *Nature* 2016;**531**:329–34.

Morgan JL, McNamara JT, Zimmer J. Mechanism of activation of bacterial cellulose synthase by cyclic di-GMP. *Nat Struct Mol Biol* 2014;**21**:489–96.

Morgan JL, Strumillo J, Zimmer J. Crystallographic snapshot of cellulose synthesis and membrane translocation. *Nature* 2013;**493**:181–6.

Mueller SC, Brown RM. Evidence for an intramembrane component associated with a cellulose microfibril-synthesizing complex in higher plants. *J Cell Biol* 1980;**84**:315–26.

Nakai T, Sugano Y, Shoda M *et al.* Formation of highly twisted ribbons in a carboxymethylcellulase gene-disrupted strain of a cellulose-producing bacterium. *J Bacteriol* 2013;**195**:958–64.

Naritomi T, Kouda T, Yano H *et al.* Effect of ethanol on bacterial cellulose production from fructose in continuous culture. *J Ferment Bioeng* 1998;**85**:598–603.

Nicol F, His I, Jauneau A *et al.* A plasma membrane-bound putative endo-1,4-beta-D-glucanase is required for normal wall assembly and cell elongation in *Arabidopsis*. *EMBO J* 1998;**17**:5563–76.

Nicolas WJ, Ghosal D, Tocheva EI *et al.* Structure of the bacterial cellulose ribbon and its assembly-guiding cytoskeleton by electron cryotomography. *J Bacteriol* 2021;**203**:e00371–20.

Nixon BT, Mansouri K, Singh A *et al.* Comparative structural and computational analysis supports eighteen cellulose synthases in the plant cellulose synthesis complex. *Sci Rep* 2016;**6**:28696.

Nobles DR, Brown RM. The pivotal role of cyanobacteria in the evolution of cellulose synthases and cellulose synthase-like proteins. *Cellulose* 2004;**11**:437–48.

Nobles DR, Romanovicz DK, Brown RM. Cellulose in cyanobacteria. Origin of vascular plant cellulose synthase? *Plant Physiol* 2001;**127**:529–42.

Nojima S, Fujishima A, Kato K *et al.* Crystal structure of the flexible tandem repeat domain of bacterial cellulose synthesis subunit C. *Sci Rep* 2017;**7**:13018.

Notley SM, Pettersson B, Wågberg L. Direct measurement of attractive van der Waals' forces between regenerated cellulose surfaces in an aqueous environment. *J Am Chem Soc* 2004;**126**:13930–1.

O'Toole G, Kaplan HB, Kolter R. Biofilm formation as microbial development. *Annu Rev Microbiol* 2000;**54**:49–79.

Olsson RT, Azizi Samir MA, Salazar-Alvarez G *et al.* Making flexible magnetic aerogels and stiff magnetic nanopaper using cellulose nanofibrils as templates. *Nat Nanotechnol* 2010;**5**:584–8.

Omadjela O, Narahari A, Strumillo J *et al.* BcsA and BcsB form the catalytically active core of bacterial cellulose synthase sufficient for *in vitro* cellulose synthesis. *Proc Natl Acad Sci USA* 2013;**110**:17856–61.

Owens TW, Taylor RJ, Pahil KS *et al.* Structural basis of unidirectional export of lipopolysaccharide to the cell surface. *Nature* 2019;**567**:550–3.

Paredez AR, Somerville CR, Ehrhardt DW. Visualization of cellulose synthase demonstrates functional association with microtubules. *Science* 2006;**312**:1491–5.

Pear JR, Kawagoe Y, Schreckengost WE *et al.* Higher plants contain homologs of the bacterial *celA* genes encoding the catalytic subunit of cellulose synthase. *Proc Natl Acad Sci USA* 1996;**93**:12637–42.

Peng L, Kawagoe Y, Hogan P *et al.* Sitosterol-beta-glucoside as primer for cellulose synthesis in plants. *Science* 2002;**295**:147–50.

Perrin RM. Cellulose: how many cellulose synthases to make a plant? *Curr Biol* 2001;**11**:R213–216.

Petrus ML, Vijgenboom E, Chaplin AK *et al.* The DyP-type peroxidase DtpA is a Tat-substrate required for GlxA maturation and morphogenesis in *Streptomyces*. *Open Biol* 2016;**6**:150149.

Pfiffer V, Sarenko O, Possling A *et al.* Genetic dissection of *Escherichia coli*'s master diguanylate cyclase DgcE: role of the N-terminal MASE1 domain and direct signal input from a GTPase partner system. *PLoS Genet* 2019;**15**:e1008059.

Pinto ERP, Barud HS, Silva RR *et al.* Transparent composites prepared from bacterial cellulose and castor oil based polyurethane as substrates for flexible OLEDs. *J Mater Chem C* 2015;**3**:11581–8.

Pontes MH, Lee EJ, Choi J *et al.* *Salmonella* promotes virulence by repressing cellulose production. *Proc Natl Acad Sci USA* 2015;**112**:5183–8.

Purushotham P, Ho R, Zimmer J. Architecture of a catalytically active homotrimeric plant cellulose synthase complex. *Science* 2020;**369**:1089–94.

Qiao S, Luo Q, Zhao Y *et al.* Structural basis for lipopolysaccharide insertion in the bacterial outer membrane. *Nature* 2014;**511**:108–11.

Qiao Z, Lampugnani ER, Yan XF *et al.* Structure of *Arabidopsis* CESA3 catalytic domain with its substrate UDP-glucose provides insight into the mechanism of cellulose synthesis. *Proc Natl Acad Sci USA* 2021;**118**:e2024015118.

Rajwade JM, Paknikar KM, Kumbhar JV. Applications of bacterial cellulose and its composites in biomedicine. *Appl Microbiol Biotechnol* 2015;**99**:2491–511.

Reichmann NT, Gründling A. Location, synthesis and function of glycolipids and polyglycerolphosphate lipoteichoic acid in Gram-positive bacteria of the phylum Firmicutes. *FEMS Microbiol Lett* 2011;**319**:97–105.

Revin VV, Nazarova NB, Tsareva EE *et al.* Production of bacterial cellulose aerogels with improved physico-mechanical properties and antibacterial effect. *Front Bioeng Biotechnol* 2020;**8**:1392.

Richter AM, Possling A, Malysheva N *et al.* Local c-di-GMP signaling in the control of synthesis of the *E. coli* biofilm exopolysaccharide pEtN-cellulose. *J Mol Biol* 2020;**432**:4576–95.

Riley LM, Weadge JT, Baker P *et al.* Structural and functional characterization of *Pseudomonas aeruginosa* AlgX: role of AlgX in alginate acetylation. *J Biol Chem* 2013;**288**:22299–314.

Robledo M, Jiménez-Zurdo JI, Velázquez E *et al.* *Rhizobium* cellulase CelC2 is essential for primary symbiotic infection of legume host roots. *Proc Natl Acad Sci USA* 2008;**105**:7064–9.

Römling U, Bian Z, Hammar M *et al.* Curli fibers are highly conserved between *Salmonella typhimurium* and *Escherichia coli* with respect to operon structure and regulation. *J Bacteriol* 1998;**180**:722–31.

Römling U, Galperin MY. Bacterial cellulose biosynthesis: diversity of operons, subunits, products, and functions. *Trends Microbiol* 2015;**23**:545–57.

Römling U, Rohde M, Olsén A *et al.* AgfD, the checkpoint of multicellular and aggregative behaviour in *Salmonella typhimurium* regulates at least two independent pathways. *Mol Microbiol* 2000;**36**:10–23.

Ross P, Aloni Y, Weinhouse C *et al.* An unusual guanyl oligonucleotide regulates cellulose synthesis in *Acetobacter xylinum*. *FEBS Lett* 1985;**186**:191–6.

Ross P, Mayer R, Benziman M. Cellulose biosynthesis and function in bacteria. *Microbiol Rev* 1991;**55**:35–58.

Ross P, Weinhouse H, Aloni Y *et al.* Regulation of cellulose synthesis in *Acetobacter xylinum* by cyclic diguanylic acid. *Nature* 1987;**325**:279–81.

Rushton PS, Olek AT, Makowski L *et al.* Rice cellulose synthaseA8 plant-conserved region is a coiled-coil at the catalytic core entrance. *Plant Physiol* 2017;**173**:482–94.

Ryjenkov DA, Simm R, Römling U *et al.* The PilZ domain is a receptor for the second messenger c-di-GMP: the PilZ domain protein YcgR controls motility in enterobacteria. *J Biol Chem* 2006;**281**:30310–4.

Sarenko O, Klauck G, Wilke FM *et al.* More than enzymes that make or break cyclic Di-GMP-local signaling in the interactome of GGDEF/EAL domain proteins of *Escherichia coli*. *mBio* 2017;**8**:e01639–17.

Saxena IM, Kudlicka K, Okuda K *et al.* Characterization of genes in the cellulose-synthesizing operon (acs operon) of *Acetobacter xylinum*: implications for cellulose crystallization. *J Bacteriol* 1994;**176**:5735–52.

Scherner M, Reutter S, Klemm D *et al.* *In vivo* application of tissue-engineered blood vessels of bacterial cellulose as small arterial substitutes: proof of concept? *J Surg Res* 2014;**189**:340–7.

Schirner K, Marles-Wright J, Lewis RJ *et al.* Distinct and essential morphogenic functions for wall- and lipo-teichoic acids in *Bacillus subtilis*. *EMBO J* 2009;**28**:830–42.

Schmid J. Recent insights in microbial exopolysaccharide biosynthesis and engineering strategies. *Curr Opin Biotechnol* 2018;**53**:130–6.

Schramm M, Hestrin S. Factors affecting production of cellulose at the air/liquid interface of a culture of *Acetobacter xylinum*. *J Gen Microbiol* 1954;**11**:123–9.

Schrempf H, Walter S. The cellulolytic system of *Streptomyces reticuli*. *Int J Biol Macromol* 1995;**17**:353–5.

Scott W, Lowrance B, Anderson AC *et al.* Identification of the Clostridial cellulose synthase and characterization of the cognate glycosyl hydrolase, CcsZ. *PLoS One* 2020;**15**:e0242686.

Serra DO, Richter AM, Hengge R. Cellulose as an architectural element in spatially structured *Escherichia coli* biofilms. *J Bacteriol* 2013;**195**:5540–54.

Shah J, Brown RM. Towards electronic paper displays made from microbial cellulose. *Appl Microbiol Biotechnol* 2005;**66**:352–5.

Shan SO. ATPase and GTPase tangos drive intracellular protein transport. *Trends Biochem Sci* 2016;**41**:1050–60.

Shaw RK, Lasa I, García BM *et al.* Cellulose mediates attachment of *Salmonella enterica* Serovar Typhimurium to tomatoes. *Environ Microbiol Rep* 2011;**3**:569–73.

Sherman DJ, Xie R, Taylor RJ *et al.* Lipopolysaccharide is transported to the cell surface by a membrane-to-membrane protein bridge. *Science* 2018;**359**:798–801.

Shi X, Chen M, Yu Z *et al.* *In situ* structure and assembly of the multidrug efflux pump AcrAB-TolC. *Nat Commun* 2019;**10**:2635.

Shi Z, Zhang Y, Phillips GO *et al*. Utilization of bacterial cellulose in food. *Food Hydrocoll* 2014;**35**:539–45.
Simm R, Morr M, Kader A *et al*. GGDEF and EAL domains inversely regulate cyclic di-GMP levels and transition from sessility to motility. *Mol Microbiol* 2004;**53**:1123–34.
Singh A, Walker KT, Ledesma-Amaro R *et al*. Engineering bacterial cellulose by synthetic biology. *Int J Mol Sci* 2020;**21**:9185.
Sohlenkamp C, Geiger O. Bacterial membrane lipids: diversity in structures and pathways. *FEMS Microbiol Rev* 2016;**40**:133–59.
Somerville C. Cellulose synthesis in higher plants. *Annu Rev Cell Dev Biol* 2006;**22**:53–78.
Spiers AJ, Bohannon J, Gehrig SM *et al*. Biofilm formation at the air–liquid interface by the *Pseudomonas fluorescens* SBW25 wrinkly spreader requires an acetylated form of cellulose. *Mol Microbiol* 2003;**50**:15–27.
Spiers AJ, Kahn SG, Bohannon J *et al*. Adaptive divergence in experimental populations of *Pseudomonas fluorescens*. I. Genetic and phenotypic bases of wrinkly spreader fitness. *Genetics* 2002;**161**:33–46.
Standal R, Iversen TG, Coucheron DH *et al*. A new gene required for cellulose production and a gene encoding cellulolytic activity in *Acetobacter xylinum* are colocalized with the bcs operon. *J Bacteriol* 1994;**176**:665–72.
Steiner S, Lori C, Boehm A *et al*. Allosteric activation of exopolysaccharide synthesis through cyclic di-GMP-stimulated protein–protein interaction. *EMBO J* 2013;**32**:354–68.
Stojanoski V, Sankaran B, Prasad BV *et al*. Structure of the catalytic domain of the colistin resistance enzyme MCR-1. *BMC Biol* 2016;**14**:81.
Sun B, Zhang M, Shen J *et al*. Applications of cellulose-based materials in sustained drug delivery systems. *Curr Med Chem* 2019;**26**:2485–501.
Sun L, Vella P, Schnell R *et al*. Structural and functional characterization of the BcsG subunit of the cellulose synthase in *Salmonella typhimurium*. *J Mol Biol* 2018;**430**:3170–89.
Sunagawa N, Fujiwara T, Yoda T *et al*. Cellulose complementing factor (Ccp) is a new member of the cellulose synthase complex (terminal complex) in *Acetobacter xylinum*. *J Biosci Bioeng* 2013;**115**:607–12.
Thomas C, Tampé R. Structural and mechanistic principles of ABC transporters. *Annu Rev Biochem* 2020;**89**:605–36.
Thongsomboon W, Serra DO, Possling A *et al*. Phosphoethanolamine cellulose: a naturally produced chemically modified cellulose. *Science* 2018;**359**:334–8.
Tomita Y, Kondo T. Influential factors to enhance the moving rate of *Acetobacter xylinum* due to its nanofiber secretion on oriented templates. *Carbohydr Polym* 2009;**77**:754–9.
Trivedi A, Mavi PS, Bhatt D *et al*. Thiol reductive stress induces cellulose-anchored biofilm formation in *Mycobacterium tuberculosis*. *Nat Commun* 2016;**7**:11392.
Uhlin KI, Atalla RH, Thompson NS. Influence of hemicelluloses on the aggregation patterns of bacterial cellulose. *Cellulose* 1995;**2**:129–44.
Ultee E, van der Aart LT, Zhang L *et al*. Teichoic acids anchor distinct cell wall lamellae in an apically growing bacterium. *Commun Biol* 2020;**3**:314.
Valla S, Coucheron DH, Fjaervik E *et al*. Cloning of a gene involved in cellulose biosynthesis in *Acetobacter xylinum*: complementation of cellulose-negative mutants by the UDPG pyrophosphorylase structural gene. *Mol Gen Genet* 1989;**217**:26–30.
Vergara CE, Carpita NC. Beta-D-glycan synthases and the CesA gene family: lessons to be learned from the mixed-linkage (1-3),(1-4)beta-D-glucan synthase. *Plant Mol Biol* 2001;**47**:145–60.
Vollmer W, Blanot D, de Pedro MA. Peptidoglycan structure and architecture. *FEMS Microbiol Rev* 2008;**32**:149–67.
Walter S, Wellmann E, Schrempf H. The cell wall-anchored *Streptomyces* reticuli Avicel-binding protein (AbpS) and its gene. *J Bacteriol* 1998;**180**:1647–54.
Wang X, Rochon M, Lamprokostopoulou A *et al*. Impact of biofilm matrix components on interaction of commensal *Escherichia coli* with the gastrointestinal cell line HT-29. *Cell Mol Life Sci* 2006;**63**:2352–63.
Weinhouse H, Sapir S, Amikam D *et al*. c-di-GMP-binding protein, a new factor regulating cellulose synthesis in *Acetobacter xylinum*. *FEBS Lett* 1997;**416**:207–11.
White AP, Weljie AM, Apel D *et al*. A global metabolic shift is linked to *Salmonella* multicellular development. *PLoS One* 2010;**5**:e11814.
Whitfield C, Wear SS, Sande C. Assembly of bacterial capsular polysaccharides and exopolysaccharides. *Annu Rev Microbiol* 2020;**74**:521–43.
Whitfield GB, Marmont LS, Ostaszewski A *et al*. Pel polysaccharide biosynthesis requires an inner membrane complex comprised of PelD, PelE, PelF, and PelG. *J Bacteriol* 2020;**202**:e00684–19.
Whitney JC, Colvin KM, Marmont LS *et al*. Structure of the cytoplasmic region of PelD, a degenerate diguanylate cyclase receptor that regulates exopolysaccharide production in *Pseudomonas aeruginosa*. *J Biol Chem* 2012;**287**:23582–93.
Whitney JC, Whitfield GB, Marmont LS *et al*. Dimeric c-di-GMP is required for post-translational regulation of alginate production in *Pseudomonas aeruginosa*. *J Biol Chem* 2015;**290**:12451–62.
Williams WS, Cannon RE. Alternative environmental roles for cellulose produced by *Acetobacter xylinum*. *Appl Environ Microbiol* 1989;**55**:2448–52.
Williamson MP. The structure and function of proline-rich regions in proteins. *Biochem J* 1994;**297**:249–60.
Wu TH, Huang CH, Ko TP *et al*. Diverse substrate recognition mechanism revealed by *Thermotoga maritima* Cel5A structures in complex with cellotetraose, cellobiose and mannotriose. *Biochim Biophys Acta* 2011;**1814**:1832–40.
Wu ZY, Li C, Liang HW *et al*. Ultralight, flexible, and fire-resistant carbon nanofiber aerogels from bacterial cellulose. *Angew Chem Int Ed* 2013;**52**:2925–9.
Xu H, Chater KF, Deng Z *et al*. A cellulose synthase-like protein involved in hyphal tip growth and morphological differentiation in streptomyces. *J Bacteriol* 2008;**190**:4971–8.
Yao W, Wu S, Zhu J *et al*. Bacterial cellulose membrane: a new support carrier for yeast immobilization for ethanol fermentation. *Process Biochem* 2011;**46**:2054–8.
Yaron S, Römling U. Biofilm formation by enteric pathogens and its role in plant colonization and persistence. *Microb Biotechnol* 2014;**7**:496–516.
Yasutake Y, Kawano S, Tajima K *et al*. Structural characterization of the *Acetobacter xylinum* endo-beta-1,4-glucanase CMCax required for cellulose biosynthesis. *Proteins* 2006;**64**:1069–77.
Yother J. Capsules of *Streptococcus pneumoniae* and other bacteria: paradigms for polysaccharide biosynthesis and regulation. *Annu Rev Microbiol* 2011;**65**:563–81.
Yu H, Rao X, Zhang K. Nucleoside diphosphate kinase (Ndk): a pleiotropic effector manipulating bacterial virulence and adaptive responses. *Microbiol Res* 2017;**205**:125–34.

Yunoki S, Osada Y, Kono H *et al*. Role of ethanol in improvement of bacterial cellulose production: analysis using ^{13}C-labeled carbon sources. *Food Sci Technol Res* 2004;**10**:307–13.

Zeytuni N, Zarivach R. Structural and functional discussion of the tetra-trico-peptide repeat, a protein interaction module. *Structure* 2012;**20**:397–405.

Zhao C, Li Z, Li T *et al*. High-yield production of extracellular type-I cellulose by the cyanobacterium *Synechococcus* sp. PCC 7002. *Cell Discov* 2015;**1**:15004.

Zheng L, Li S, Luo J *et al*. Latest advances on bacterial cellulose-based antibacterial materials as wound dressings. *Front Bioeng Biotechnol* 2020;**8**:593768.

Zhong C, Zhang GC, Liu M *et al*. Metabolic flux analysis of *Gluconacetobacter xylinus* for bacterial cellulose production. *Appl Microbiol Biotechnol* 2013;**97**:6189–99.

Zouhir S, Abidi W, Caleechurn M *et al*. Structure and multitasking of the c-di-GMP-sensing cellulose secretion regulator BcsE. *mBio* 2020;**11**:e01303–20.